Modeling the Reaction Transport of Synaptic Acetylcholine Released at High Frequency in Weakly Electric Fish

Elham Alkhammash

A thesis submitted In partial fulfillment of the requirements

for the Master's of Philosophy degree in Physics.

Supervised by

Prof. Béla Joós

Prof. Ivan L'Heureux

Ottawa- Carleton Institute for Physics

Department of Physics

Faculty of Science

University of Ottawa

Ottawa, Canada

Abstract

Studying the synaptic transmission in the neuromuscular junction (NMJ) is central to the understanding of firing electrical signals at high frequencies. In this work, we present the processes involving acetylcholine and its receptors in the synaptic transmission across the cleft.

A one-dimensional diffusion model is proposed to explain the behavior of the reaction - diffusion system with nonlinear reaction terms monitoring the interaction of acetylcholine with the enzyme and the receptors. A proper numerical method is applied to solve the one-dimensional diffusion equation along the symmetry axis of the cylindrically shaped cleft with Neumann boundary condition on the postsynaptic end.

We assumed a periodic release of ACh in the frequency range of 200Hz to 500Hz. The kinetics of receptors (particularly the open receptors) during the release of acetylcholine to changes in selected parameters are investigated. We chose typical values for the concentration of ACh, the flux of ACh, and the surface concentration of receptors. The effects of the varying parameters, enzyme concentration, input flux, and the receptor concentration on the emission of acetylcholine in the synaptic cleft and the subsequent impact on the dynamics of the receptors are studied and discussed.

As the firing rate is increased, the enzyme concentration also has to be increased to ensure that the ACh receptors (AChR) close in between two releases of ACh. Our study revealed that the enzyme reaction limits our model. The concentration of ACh reaching the receptors falls close to a threshold and the receptors do not close completely during firing at a high frequency, such as 500 Hz. Our model can be used to describe the neuronal transmission across the synaptic up to about 500Hz. This being close to the physiological limit of *Eigenmannia,* it suggests that the mechanism described in this thesis reflects reality.

Acknowledgments

Even though writing this thesis only happened in the last months, it was the culmination of years and years of work. This work would not have been possible without God. So, I will start at the beginning to thank God Almighty for giving me the strength to keep going. I sincerely thank a few people on the sidelines who supported and encouraged me along the way.

I was fortunate enough to be advised by Professor Béla Joós. I would thank him for his supervision efforts. He was at the exact right level of thought, paired with unwavering encouragement and support. He went out of his way to find research opportunities for me and gave me research on synaptic transmission machinery during high frequency in *Eigenmannia*, weakly electric fish, as evidenced by the topic in this thesis.

I am grateful for Professor Joós's frequent and invaluable feedbacks on my progress as a graduate student because I would not be where I am today without him. I would especially like to thank Professor Ivan L'Heureux, who offered guidance and always made time to meet with me regarding all research requirements and pretty much anything else I wanted to talk about.

I want to thank my parents, who started loving me from the beginning .My parents taught me to work hard, whether it was schoolwork or bargain shopping. Of course, both skills turn out to be essential for surviving graduate school — lots of love for my sisters and brothers, especially Abdulrahman, who truly inspired me. And finally, lots of thanks to my country, Saudi Arabia, for awarding me the scholarship and sponsoring distinguished academics to study at the University of Ottawa.

Contents

List of Figures

List of Abbreviations

Abbreviation	Definition
APs	Action Potential.
ACh	Acetylcholine.
AChE	Acetylcholineesterase.
ATP	Adenosine Triphosphate.
EOD	Electric Organ Discharge.
EO	Electric Organ.
NMJ	Neuromuscular Junction.
nAChR	Ionotropic Acetylcholine Receptors.
mAChR	Muscarine Acetylcholine Receptors.
MM	Michaelis-Menten.
RMP	Resting Membrane Potential.

Preface

The nervous system is central to cognition and communication within a biological organism. Passing an electrical or chemical signal to another neuron or the target cell is mainly due to regulating membrane potential and synaptic function for the brain. Also, it is a crucial function in neuronal development, synapse formation, and signal transmission.

Studying the synaptic transmission process needs detailed of understanding the dynamics within the neuromuscular junction (NMJ) of the acetylcholine diffusion-reaction mechanism in the synaptic cleft. We are interested in the aspects of the transmission process at the NMJ. This process comprises several events occurring in NMJ — vesicles containing acetylcholine (the neurotransmitter) fuse with the presynaptic membrane. Acetylcholine is released into the cleft, which is the space between neurons at a nerve synapse. The cleft is located between the presynaptic membrane where the vesicles are released and the end of the electrocytes. ACh reacts with acetylcholinesterase (the enzyme), and acetylcholine receptors (AChR). The acetylcholinesterase (AChE) is an enzyme that hydrolyzes ACh and limits its existence in the cleft. ACh can be bonded to the ACh receptors which are located at the postsynaptic membrane, which leads to the opening and closing of the ACh receptor channels (A_2R, A_2R_{op}). These channels permit the interchange of potassium and sodium ions, which creates a postsynaptic terminal current initiated in the postsynaptic membrane[27,37].

Analysis of such behavior leads to a description of the transmission process as a reaction-diffusion system (RD system) for the acetylcholine. The reaction-diffusion system is used for interpreting the characteristics of the electric signal generated by the electrocytes of different types of weakly electric fish, such as *Eigenmannia*.

The goal of this thesis is to explore the synaptic transmission machinery during high frequency firing in *Eigenmannia*. It is not immediately clear how rapid firing rate can be transmitted across a synaptic cleft. We developed a model considering the diffusion of acetylcholine across the synaptic cleft with enzyme reactions, and the subsequent effects on receptors channels in NMJ.

The results from this theory are used in chapter 4 to better understand the process of synaptic transmission across the cleft. We show how the distribution of acetylcholine could affect the dynamics of receptors. By increasing the concentration of the enzyme(AChE),the acetylcholine is eliminated more effectively over time, i.e., ACh is led to limit receptors opening to 2 - 5 ms.

CHAPTER 1

Introduction

In the following, we present a brief introduction to electric fields produced by electric organ discharges(EOD) in weakly electric fish with an emphasis on the synaptic release of acetylcholine at the posterior end of the electric organ cells (EO) , electrocytes , at high frequency.

The weakly electric fish, *Eigenmannia*, uses self-generated electric fields produced by the simultaneous action potentials of a thousand or more electrocytes. As such, this species' electric organ (EO) provides an ideal model system; the cells are large and located close to the skin(under the belly) , which makes them accessible for most voltage measurement techniques[1]. Furthermore, the persistent pacemaker and the posterior neuromuscular junction (NEJ) in *Eigenmannia*, electrocytes provide a robust system to study rapid repolarization/depolarization events [2,3].

1.1 Review of Weakly Electric Fish.

A weakly electric fish, *Eigenmannia*, possesses an electric organ (EO) with the capability of generating a three-dimensional electric dipole commanded by the brain. An electric organ produces the electrical discharges derived from the myogenic organ (muscular tissues) built-in superimposed disks(syncytial cells of 1 mm length). In other words, the electric organ is composed of tightly arranged groups of modified muscle cells known as electrocytes. Electrocytes are organized in two bundles (one left and one right) , each bundle has 5 -6 columns electrocytes [4].

Eigenmannia has been examined and studied due to its exceptional physiological capacities and ease detection of its EODs. In *Eigenmannia*, electric organs (EOs) emit a high-frequency EOD. EOD frequencies are regulated and transported to electrocytes at the posterior end by a cholinergic nerve region[5].

In *Eigenmannia*, the simultaneous activation of the action potentials (APs) inside the electrical organ contributes to the generation of EODs. More specifically, the primary responsibility of the ion channels with the Na^+ currents are to trigger the AP, restricted to the posterior region of the electrocytes. When Na^+ moves inside the cell via voltage-gated Na^+ channels, AP is generated by the activation of the cholinergic synapse. As a result of the simultaneous APs of all the electrocytes, a current flow toward the head then takes a return path through the water to the tail see Figure1.1 [5,6].

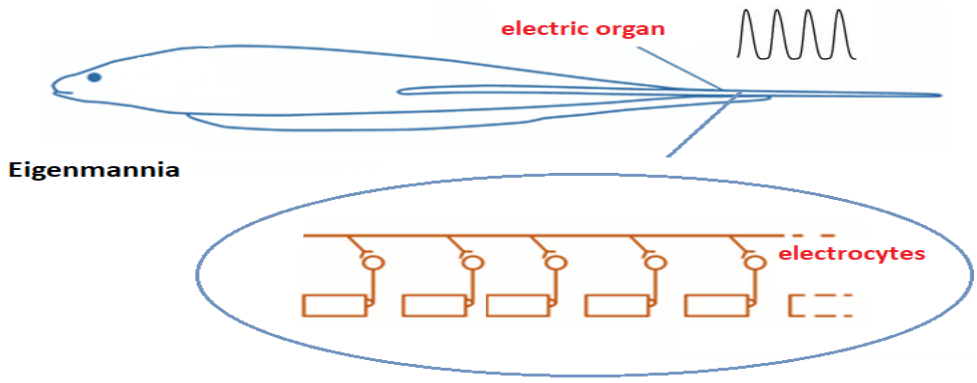

Figure1.1: This illustrates the electric organ in *Eigenmannia* which is made up of two bilateral cylindrical shapes with 5– 6 columns of electrocytes per side. Electrocytes are cylindrical cells ~800 – 1000 µm long and 100 –300 µm in diameter innervated on their posterior face which is stimulated by a cholinergic electromotor neuron synapse. *Eigenmannia* EODs are based on continuous APs at up to 600 Hz[4].

Continuous discharge of action potentials gives the overall resulting EOD a sinusoidal shape. Even though it was found that the wave shape is the result of the rhythmic evocation of head-positive action potentials, it is not fully understood what generates such a repetitive excitation in the first place. i.e., it is less clear how this rapid firing rate can be transmitted across a synaptic cleft [7].

Eigenmannia individuals produce a continuously oscillating-dipole-like EOD between 200 - 600Hz throughout their lifetime, which is a remarkable achievement. Importantly, APs are initiated at steady frequencies of 200–600 Hz with underlying Na^+ currents. Moreover, it has been measured that a single EOD waveform is compatible with one cycle of APs[8,9].

To understand cellular and sub-cellular mechanisms that mediate fast cholinergic pulses at the neuromuscular junction (NMJ) and the meaning of firing signal at high frequency, we must understand the properties of the cell membrane.

1.2 Nervous System and Cell Membrane.

Generally, electrical signals are driven by ions. The membrane is selectively permeable (or semipermeable), meaning that only particular molecules can pass through. Water, oxygen, and carbon dioxide can easily transport across the membrane. The cell membrane uses transient permeability to increase Na^+, K^+, and Ca^{++} ions across the membrane. The membrane is differentially permeable for the ions, with the highest permeability for potassium ions, see Figure 1.2 [10,11]. The permeability can be measured by:

$$\text{Flux} = \text{P}\,(C_{in} - C_{out}). \tag{1.1}$$

In this expression C is the concentration of ions either outside or inside the cell. P represents the permeability. The dynamic range of permeability has been measured [11], as shown below.

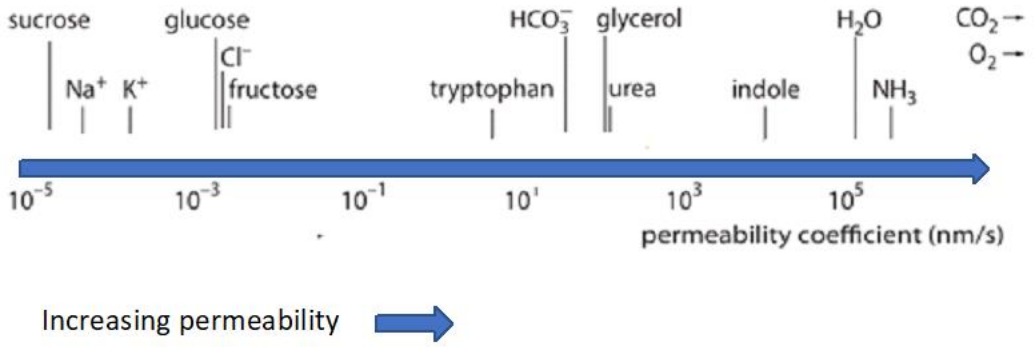

Figure 1.2: Illustrates the range of permeabilities of the membrane. Importantly Na^+ and K^+ are the least permeable to the membrane. Remarkably, the cell membrane has apparent permeability to uncharged compounds. The choice of units, nm/s, was based on the characteristics of the membrane [11].

Some ions (e.g., Na^+, K^+) and other polar molecules must be transported by specific channels or pumps that allow them to go through the layer of the membrane, as illustrated in Figure 1.3 Concentration differences between the cations (calcium, potassium, and sodium) and the anions (chloride) across the membrane generate a potential difference [10]. The cell membrane at rest has a very low permeability for Na^+. Even though a small amount of Na^+ can flow in the cell and a current of K^+ can flow out the cell via Na^+ and K^+ leak channels, the concentration gradients are maintained by the Na^+/ K^+ ATPase pump and different leak conductance. The pumps can transport two potassium ions inside and three sodium ions outside (3 Na^+/2 K^+) at the cost of 1 ATP molecule. Sodium-potassium pump operation generates steep gradients of concentration across the membrane for both sodium and potassium ions, but the potential difference across the membrane is very small. In the presence of an efficient sodium-potassium pump, the opening of the leak channel can have a dramatic impact on the membrane potential. The K^+ ions move down their concentration gradient when the leak channels are open, which tends to make the cell inside slightly more negative.

Regulated opening of sodium channels will cause the usually negative resting potential to turn to positive. In general, the identity of the open channels with maximum ion flux will determine the potential of the cell, where the ion with the highest permeability will drive the resting potential of the membrane toward its own preferred Nernst potential. Thus, the resting membrane potential (RMP), measured by using a reference point outside the cell, is negative and lies between -30 and -90 mV . It is -70 mV on average[10].

The resting potential is vital in the nervous system because the action potential is the basis for neural signaling. In brief, the RMP is based on ion gradients across the cell membrane, with excess potassium inside the cell - together with other anions, such as sulfate, carbonate and diverse proteins - and excess sodium and chloride outside the cell membrane [13,14].

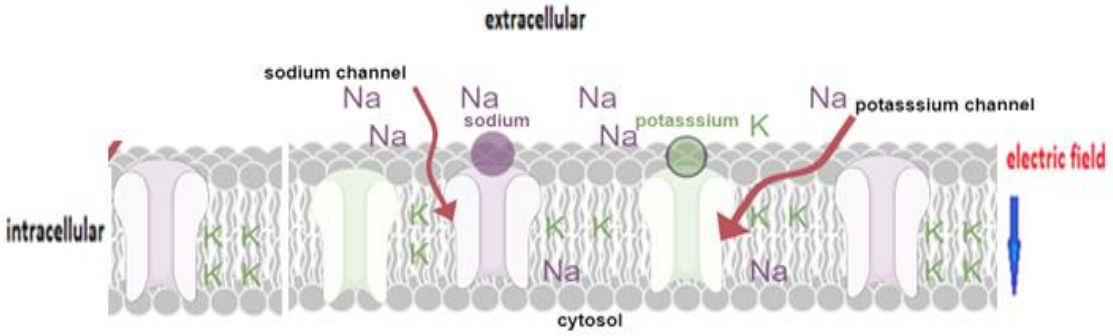

Figure 1.3 : Concentrations of potassium (K^+) are higher inside the cell compared to outside while concentrations of sodium (Na^+) are higher outside the cell. The sodium/potassium pump requires adenosine triphosphate (ATP) energy, so it is also referred to as ATPase. ATPase pump and selective membrane channels permit the concentration gradient difference, which removes 2 potassium ions inside and 3 sodium ions outside (3 Na^+ /2 K^+) at the cost of 1 ATP molecule . Na^+ permeability is much less than K^+ permeability. As a result, there are much more K^+ inside rather than outside, and much more Na^+ outside than inside.

Neurons must be able to send and receive signals to the nervous system to function. Such signals are possible because each neuron has a charged cellular membrane (a difference in voltage

between the inside and the outside), and this membrane's charging can change in response to neurotransmitter molecules released from other neurons and environmental stimuli.

1.3 Generation of Action Potentials.

The membrane potentials must shift to get an electrical signal going. A better way of considering this is to imagine a higher influx of positively charged sodium ions to change the negative charge inside the cell, which results in the reversal of the potential difference, such that the interior becomes slightly positively charged. At a point when a stimulus depolarizes the membrane potential to a threshold voltage of around - 50 to - 55 mV, sodium channels open, and an action potential of up to 40 mV results. After the sodium channels open , the potassium channels start opening then both sodium and potassium close again (after a period of only about 1 ms).This transient opening allows the outflow of potassium (K^+) which repolarizes or even hyperpolarizes the membrane. The flow of K^+ leads to restoring the potential difference. As a result, the membrane has a steady-state voltage difference from 40 mV down to - 70 mV or even - 90 mV [13].

Neuronal firing at 200 Hz corresponds to a period of 5 ms. As the frequency is increased, there is an overlap between consecutive APs. These fish can operate up to about 500 Hz [4,14,15].

The potassium ions can flow down an electrochemical gradient from high concentration (inside the cell) to low concentration (outside the cell). After a short delay of opening the voltage-gated potassium channels cause ‘delayed rectifier current’. The high rise of the K^+ concentration outside the cell would lead to uncontrolled membrane depolarization. Conversely, an excessive inflow K^+ would give rise membrane hyperpolarization[15].

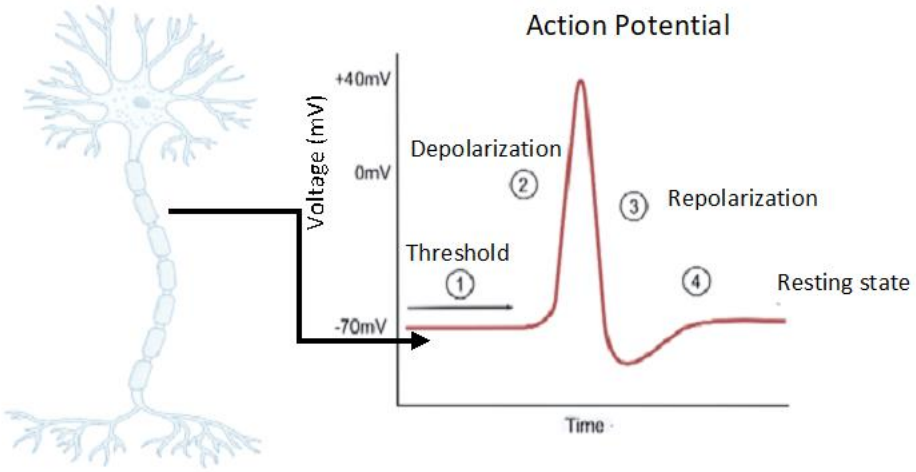

Figure 1.4: An action potential changes the polarity across the membrane. This results in a signal being sent to another neuron, causing open and closed (Na^+) and (K^+) gated ion channels, which allows the threshold potential to be attained in the membrane. Na^+ channels open and Na^+ flows into producing depolarization. When the K^+ channels start opening, the K^+ efflux outside of the membrane causes repolarization, creating a change in polarity between the outside of the cell and the inside.

To sum up, the shape of the action potential as illustrated in Figure 1.4 is stereotypical; 1) it starts when enough depolarization accumulates getting it to threshold for sodium channel activation, 2) it has a considerable rise to a positive membrane potential, due to the influx of sodium channels. This phase is known as the rising phase. 3) Then it has a rapid falling phase back down to below resting potential due to the closing of both sodium and potassium channels. However, 4) it returns to resting potential with the leaking currents.

The neuronal activity can be divided into two main parts: the generation of an action potential within a neuronal body, and the transmission of that potential to electrocytes, across gap-junctions and synapses. If we want to understand the synaptic transmission at high frequency, we must understand mechanisms that determine the release and distribution and concentration of ACh. This process will be discussed in Chapter 2 where we present a model of the synaptic transmission process. It is a one-dimensional model of the reaction-diffusion processes of ACh and its reaction with the receptor. The advantage of this model is that it not only explores the synaptic transmission of acetylcholine during high-frequency firing in a weakly electric fish but also it provides the numerical solution for the associated simple geometry.

In chapter 3, the simulation methodology will be discussed. Obtained results are discussed in chapter4.

CHAPTER 2

Principles of synaptic transmission

After this brief introduction to electric fields in a weakly electric fish in general, we focus on a more in-depth discussion of the dynamic behavior of the acetylcholine diffusing through the synaptic cleft.

2.1 Synapse.

Chemical synapses are made of filled vesicles in the presynaptic membrane, which is located on an axon and faces the synaptic cleft. As soon as the action potential reaches the presynaptic terminal, the vesicles fuse with the membrane, causing the release of their content into the synaptic cleft. The transmitter then diffuses across the cleft (around 20 - 50 nm) and binds to the postsynaptic receptors, which are at the posterior end of the electric organ cells [16]. Those receptors can belong to two different classes: ionotropic and metabotropic receptors. The ones relevant to this work are ionotropic receptors. They are coupled to a channel protein, which opens upon ligand binding, allowing Na^+ and K^+ ions to generate an action potential that then propagate towards the electric organ.

Importantly, once the neurotransmitters have been released into the synaptic cleft, they will stay available for continued signalling. As most signals only last for a limited time interval, they need to be deactivated or removed. One possibility is stimulating the reuptake by transmitter molecules through the presynaptic cell via endocytosis. The resulting vesicle can then be reused for the next round of neuronal transmission. Another possibility of deactivating the neural signal is by destroying the transmitter. In the case of acetylcholine, this is done by acetylcholine-esterase (AChE). This enzyme cleaves ACh into acetate and choline. The latter can be taken up by the presynaptic membrane and be turned into ACh again, using acetyl-CoA. The

deactivation of neurotransmitters is vital to the neuronal transmission and thus to the survival of the organism. AChE can be found in the vicinity of the postsynaptic membrane, and its block can lead to death through the overstimulation of neurons. Nerve gases such a sarin use AChE to degrade acetylcholine at NMJ. Regulating AChE is another possibility for the body to modulate neuronal transmission [20].

Usually, calcium ions trigger vesicle fusion; the action potential unlocks voltage gated Ca^{2+} channels in the presynaptic membrane. As the concentration of calcium is usually much larger outside than inside the cell, Ca^{2+} ions can speedily enter the cell through the channel, where they then bind to calmodulin[17]. Calmodulin, in turn, associates with calmodulin-dependent protein kinase II, which phosphorylates synapsin I. The latter protein binds to both vesicles and cytoskeletal actin, which surrounds the vesicles.

Upon phosphorylation, however, synapsin I changes its conformation and dissociates from the vesicle-actin connection, which then enables vesicles to dock to the plasma membrane, releasing its content into the synaptic cleft [17]. One example of neurotransmitters that bind to ionotropic receptors is acetylcholine (ACh). Importantly, the affinity of both receptors for acetylcholine can be modulated by other molecules. For example, ionotropic acetylcholine receptors are also called nicotinic (nAChR)**,** as the binding of nicotine can regulate them. On the other hand, metabotropic acetylcholine receptors are particularly sensitive to muscarine and are therefore called muscarinic (mAChR). The receptor composition of the postsynaptic membrane is another possible level for a cellular network to regulate neuronal transmission [18].

2.2 Acetylcholine

The foundation of synaptic transmission is tiny organelles (~ 30 nm diameter, see Ribrault et al., 2011) made of phospholipids, namely the synaptic vesicles that can be observed at different phases of a cycle backing the frequent release of neurotransmitters via a sequence of trafficking, exocytosis, and recycling [21]. ACh is indeed a molecule of central importance, integrating signals from multiple brain areas necessary for cognition, emotional acuity, and memory. Due to its multiple overlapping functions in different areas of the brain, it is difficult to define the precise function of ACh in the central nervous system (CNS). However, vital studies on muscarinic acetylcholine receptors (mAChR) in the mouse CNS suggest that ACh's roles modulate not only neuronal activity, but also plasticity, sensory, motor function, and cognition [22]. Taken together, we can say that acetylcholine functions at several crucial junctions, within, not only the central nervous system but also, the peripheral nervous system, where it mediates muscle contractions and relays impulses within the autonomic nervous system [23,24,25]. We consider the role of ACh release regime, diffusion, AChE, and binding to receptors (AChR) in defining the concentration of ACh at the neuromuscular junction (NMJ) see Figure 2.1**.**

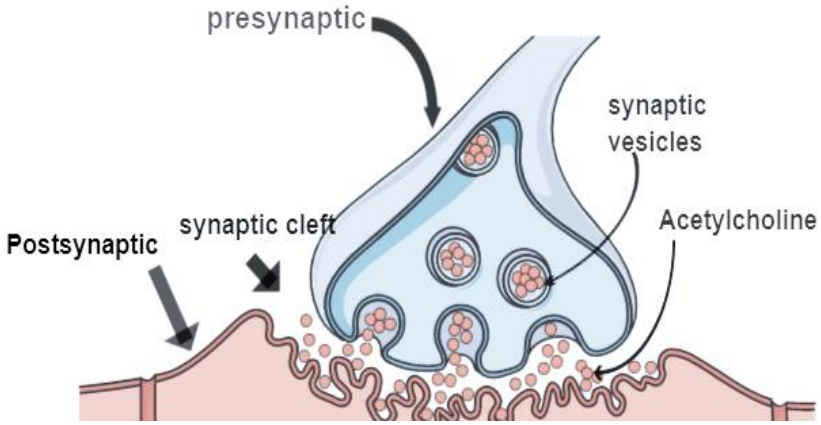

Figure 2.1 This synapse shows the junctions between two neurons, where signaling is passed from one presynaptic cell zone to the other postsynaptic zone, and vesicles release a neurotransmitter (acetylcholine) that diffuses into the synaptic cleft.

The release of one synaptic vesicle produces a measurable, subthreshold depolarization in the muscle cell. The arrival of an action potential, however, releases many vesicles at once. It is important to mention that not all action potentials will excite neurotransmitter exocytosis successfully. Thus, the neuromuscular connection occurs in two distinct phases: the presynaptic release of acetylcholine, followed by its postsynaptic activity [26].

Several factors and mechanisms can determine the distribution of the concentration of ACh in the synaptic cleft after it is released. These factors and mechanisms include the cleft geometry, the diffusion rate of ACh, the number of releasing vesicles, the transmitter diffusion coefficient, the availability of attaching sites on nicotinic ACh receptors (AChR), the enzyme reaction rate of AChE, and other factors, most of which may only be estimated[27]. A simple equation helps to approximate the time t that it takes for a specific molecule to diffuse through the mean distance L, in one dimension:

$$\mathrm{t} = \frac{\mathrm{L}^2}{\mathrm{D_A}} \qquad (2.1)$$

It rises with the square of diffusion distance. Diffusion time is inversely proportional to the diffusion coefficient (D_A).

A large number of ACh is released, but not all bond to receptors successfully because they are quickly removed by AChE, before activating AChR. Each receptor seeks two molecules to bond, which is necessary to activate the opening of the receptor channels. Generally, only a fifth of the ACh molecules is released into the cleft and then bound to AChR, to open the receptors channels. The influences that take control of the discharge of ACh into the synaptic cleft include the release of calcium, which is leading exocytosis and the process of releasing ACh from the synaptic vesicle [28]. It has been proven that the discharge of ACh from the synaptic vesicles takes place in the form of random events, with uniform release probability at the release site. The time evolution of release can be modeled as Gaussian function [29].

2.3 AChE hydrolysis

AChE permanently exists in the synaptic cleft, breaks down the neurotransmitter molecules (ACh). The principal biological role of impulse transmission is breaking down ACh to acetate and choline. Thus, a key component involved in impulse transmission, which causes the rapid hydrolysis of the neurotransmitter ACh. The hydrolysis of ACh leads to defining the profile of the concentration of ACh. This process is studied in the thesis and is significant part of our model. Researchers have proposed steady-state kinetic schemes[30.31]. Michealis-Menten(MM) is the classic, simple model of enzymatic action, and it models well the reaction pf AChE. It is given by:

$$\mathrm{A} + \mathrm{E} \underset{\mathrm{k}_{-\mathrm{AE}}}{\overset{\mathrm{k}_{\mathrm{AE}}}{\rightleftharpoons}} \mathrm{AE} \overset{\mathrm{k}}{\rightarrow} \mathrm{E} + \mathrm{B}. \tag{2.2}$$

Here, A is acetylcholine, Here, k_{AE} is the reaction rate for production of AE and $\mathrm{k}_{-\mathrm{AE}}$ is the reaction rate for the decomposition of AE into species A and E. Additionally, the AE may regenerate the enzyme E irreversibly while producing another products B with a rate k.

Enzyme kinetics take the form of an equation relating reaction velocity to ACh concentration for a system where A reacts with an enzyme E. This conforms to Michaelis-Menten kinetics, which demonstrates that a maximal reaction rate (V_{max}) is approached asymptotically[32,33]. The Michaelis-Menten equation for this system is

$$-\frac{d[A]}{dt} = \quad V = V_{max}\,\frac{[A]}{K_M + [A]}\,. \tag{2.3}$$

$$V = V_{max}\,\frac{1}{1 + \frac{K_M}{[A]}}\,. \tag{2.4}$$

Therefore, $\mathrm{V}_{\mathrm{max}}$ is the maximum velocity of the reaction reached by the system, as ACh concentration becomes much larger than the Michaelis constant K_{M} [12].

Subsequently, the MM equation describes the kinetics of saturation. At low ACh concentrations, the reaction velocity is proportional to$[\mathrm{A}]$. At higher concentrations, however, the additional delay in breaking out from the enzyme-substrate complex starts to change that result: the rate increases with $[\mathrm{A}]$,but never achieves V_{max} as seen in Figure 2.2. A derivation of the MM kinetics follows.

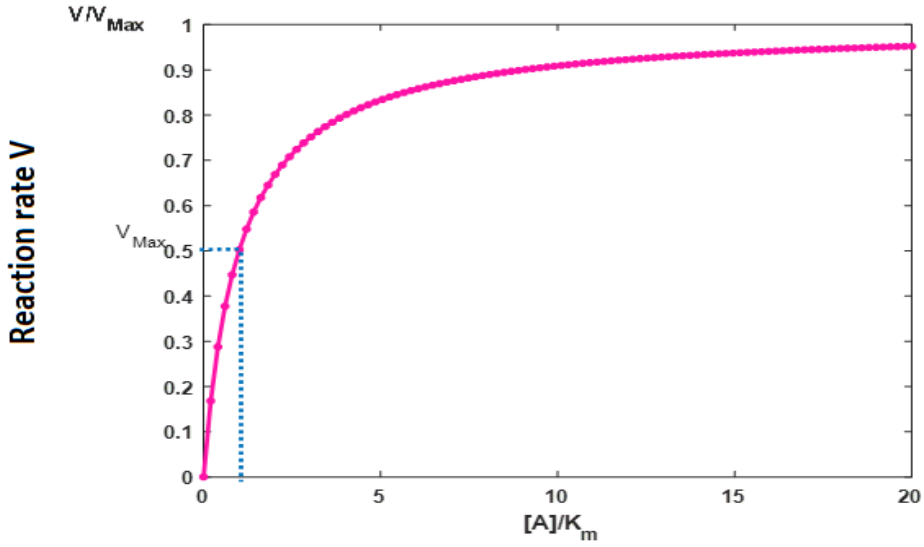

Figure 2.2 : A plot of Michaelis–Menten reaction rate as a function of the ACh concentration [A] for an enzyme displays the relationship between the substrate concentration and the rate of catalysis.

According to equation 2.2 , an enzyme E reacts with ACh to form an AE complex, with a rate constant k_{AE}. The AE complex has two likely events. It can break to E and A, with a rate constant k_{-AE}, or it can proceed to form a product B, with a rate constant k. Under these conditions, the enzyme concentration is much less than the concentration of ACh due to the complex's slow formation and its speedy consumption[32,33]. Therefore, a steady- state approximation for the net reaction rate of E and AE can be assumed. The kinetic for E and AE reacts as follows:

$$\frac{\mathrm{d}[\mathrm{E}]}{\mathrm{dt}} = -\mathrm{k}_{\mathrm{AE}}[\mathrm{A}]\,[\mathrm{E}] + \mathrm{k}_{-\mathrm{AE}}[\mathrm{AE}] + \mathrm{k}[\mathrm{AE}]. \tag{2.5}$$

$$\frac{\mathrm{d}[\mathrm{AE}]}{\mathrm{dt}} = \mathrm{k}_{\mathrm{AE}}[\mathrm{A}]\,[\mathrm{E}] - \mathrm{k}_{-\mathrm{AE}}[\mathrm{AE}] - \mathrm{k}[\mathrm{AE}]. \tag{2.6}$$

The effect of diffusion and spatial dependence will be discussed later in chapter 3.The total concentration of enzyme species is a constant:

$$[\mathrm{E}] + [\mathrm{AE}] = \text{constant} \equiv \mathrm{b}. \tag{2.7}$$

Setting Equation 2.6 approximately equal to zero (steady state approximation) and using 2.7 give:

$$[\mathrm{E}] = \frac{\mathrm{b}\,\mathrm{K_M}}{(\mathrm{K_M} + [\mathrm{A}])}. \tag{2.8}$$

$$[\mathrm{AE}] = \frac{\mathrm{b}\,[\mathrm{A}]}{(\mathrm{K_M} + [\mathrm{A}])}. \tag{2.9}$$

where $\mathrm{K_M} = \frac{(\mathrm{k_{-AE}} + \mathrm{k})}{\mathrm{k_{AE}}}$.

Substituting in the kinetic for [A] , we get:

$$\frac{\mathrm{d}[\mathrm{A}]}{\mathrm{dt}} = -\mathrm{k_{AE}}[\mathrm{A}]\,[\mathrm{E}] + \mathrm{k_{-AE}}[\mathrm{AE}] = -\mathrm{V_{max}}\,\frac{[\mathrm{A}]}{\mathrm{K_M} + [\mathrm{A}]}. \tag{2.9}$$

where $\mathrm{V_{max}} = \mathrm{k}\,\mathrm{b}$. Thus, we revealed equation (2.3).

CHAPTER 3

Simulation Methodology

Since the 1950s, there have been several experimental and theoretical studies on evaluating diffusion, the contribution of AChE hydrolysis, and reaction to AChR, to define the ACh concentration in the cleft. It is reported that there is no credible method that estimates both the spatial and temporal concentration of ACh in the synaptic cleft, directly [34]. Techniques have been suggested to measure and describe NMJ processes. These techniques are invasive and must be wisely applied to prevent any disturbance to the function of NMJ. Since NMJ processes are challenging to measure with direct experiments, mathematical models for NMJ events have been developed to analyze NMJ processes. Thus, diffusion-reaction kinetics are described by a system of coupled nonlinear partial differential equations (PDE). Some of the published research used numerical solutions to achieve a more complete description of the NMJ diffusion-reaction processes because analytical methods are not practical for complex systems.

In this way, interesting results have been published over the last thirty years and advanced our understanding of NMJ processes. Khaliq et al.[35] presented a three-dimensional (3D) model of reaction-diffusion processes taking place in the NMJ. They simplified the system as a right cylinder using cylindrical coordinates. In fact, NMJ occurs in a rather complicated geometry. In addition, in Liu et al.[36], a full three-dimensional model with complex geometry using a spectral nodal element method was presented. The system used a realistic geometry with a high order finite element method. Moreover, the Adioo et al. [27] model describes the release mechanism and the removal process, represented by the hydrolysis of acetylcholinesterase (AChE) and the rate of diffusion across the cleft and binding to nicotinic ACh receptor channels. It demonstrated by simulations that the distribution of ACh molecules in the cleft is influenced by diffusion, but the AChE hydrolysis dominates over diffusion in eliminating ACh molecules from the cleft. For a realistic neuromuscular system, the embodiment of activated enzyme reactions is imperative.

The present research presents a 1D model of the synaptic transmission across the cleft as a diffusion-reaction system. For simplicity, the model does not consider the full dynamics and interactions occurring at the synaptic cleft. We focus on the main processes that are fundamental to the production and transmission signal . Our model comprises the transport of acetylcholine A molecules through diffusion and its chemical reaction with neuron receptors R at the postsynaptic membrane and with acetylcholinesterase E in the cleft. we explore the sensitivity of receptors dynamics as key parameters are varied. In terms of numerical methods, we use a finite-difference discretization Crank- Nicholson method. The Crank- Nicholson method is a second order stable algorithm that is often used in reaction-diffusion systems.

3.1 Geometry of the system

To develop a 1D model, we first consider the neuromuscular junction (NMJ) to be a one-dimensional molecular transport-reaction system. The cylindrical geometry of the system consists of a volume bounded at the top by the presynaptic membrane and the bottom by the postsynaptic membrane, and open to the external environment. The cleft is assumed to have a thickness L and a radius r. Therefore, the coordinate z ranges from the presynaptic membrane ($z = 0$) down to the postsynaptic membrane ($z = L$), the cleft being at $0 < z < L$ and there is no r dependency on the values of the concentration. In other words, we assume homogeneity in the Z-plane of the system.

3.2 Boundary conditions

The role of presynaptic vesicles is to generate the acetylcholine A homogeneously across the system surface in a time-periodic fashion. This process is time-dependent and space independent (generation is homogeneous across the surface). Considering $f(t)$ input as the flux of A (in moles/ area per unit time), the boundary condition at the pre-synaptic vesicles is written as:

$$\mathrm{D_A}\frac{\partial[\mathrm{A}]}{\partial \mathrm{z}}\Big|_{\mathrm{z}=0} = -f(t) \tag{3.2}$$

where $\mathrm{D_A}$ is the diffusion coefficient of acetylcholine and $[\mathrm{A}]$ is the acetylcholine concentration (in moles/volume). Therefore, the problem includes a Neumann boundary condition at $z = 0$. The flux $f(t)$ of A is assumed to be a gaussian function, reproduced periodically through time. This periodic release can be mathematically represented by

$$f(t) = \frac{F}{\sqrt{2\pi w^2}}\sum_{i=1} \exp\left(-\frac{(t-iT)^2}{2w^2}\right). \tag{3.3}$$

where F is the total concentration of $[\mathrm{A}]$ released in one full cycle , T is the period of release and w is the temporal width of the distribution. An illustration of such a function is shown in Figure 3.1.

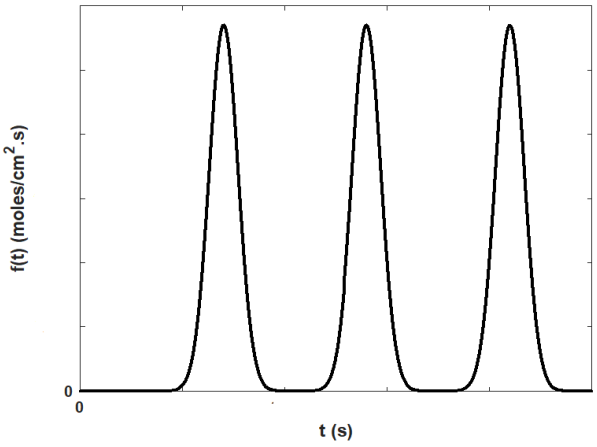

Figure 3.1: The illustrative shape of flux *f(t)* of Acetylcholine A on the presynaptic membrane.

It is assumed that there is no input of acetylcholinesterase E, as well as no input of species AE, formed through the binding of A and E. Therefore,

$$\left.\frac{\partial[\mathrm{E}]}{\partial \mathrm{z}}\right|_{\mathrm{z}=0} = \left.\frac{\partial[\mathrm{AE}]}{\partial \mathrm{z}}\right|_{\mathrm{z}=0} = 0. \qquad (3.4)$$

At the postsynaptic zone, the boundary condition of A consists of a heterogeneous reaction occurring between this species and receptors, which causes a decrease in the concentration of $[\mathrm{A}]$. These reactions are explained in detail later in this chapter. For the acetylcholinesterase E and the intermediary species AE, it is assumed that there is no flux at $z = L$.

$$\left.\frac{\partial[\mathrm{E}]}{\partial \mathrm{z}}\right|_{\mathrm{z}=\mathrm{L}} = \left.\frac{\partial[\mathrm{AE}]}{\partial \mathrm{z}}\right|_{\mathrm{z}=\mathrm{L}} = 0. \qquad (3.4)$$

3.3 Dynamics in the cleft

While being transported from the presynaptic to the postsynaptic species , A may react with E to produce another species AE. Additionally, the AE may regenerate irreversibly the enzyme E while producing other by products (B) with a rate k as mentioned in Equation 2.2

These reactions occur while these species are diffusing in the cleft $(0 < z < L)$. The equation describing the dynamics of the reaction-diffusion system is:

$$\frac{\partial[\mathrm{A}]}{\partial \mathrm{t}} = \mathrm{D_A}\frac{\partial^2[\mathrm{A}]}{\partial \mathrm{z}^2} + \mathrm{O_A}. \tag{3.5}$$

$$\frac{\partial[\mathrm{E}]}{\partial \mathrm{t}} = \mathrm{D_E}\frac{\partial^2[\mathrm{E}]}{\partial \mathrm{z}^2} + \mathrm{O_E}. \tag{3.6}$$

$$\frac{\partial[\mathrm{AE}]}{\partial \mathrm{t}} = \mathrm{D_{AE}}\frac{\partial^2[\mathrm{AE}]}{\partial \mathrm{z}^2} + \mathrm{O_{AE}}. \tag{3.7}$$

where $\mathrm{D_A}$, $\mathrm{D_E}$ and $\mathrm{D_{AE}}$ are the diffusion coefficients of A, E and AE respectively. The terms $\mathrm{O_A}$, $\mathrm{O_E}$ and $\mathrm{O_{AE}}$ are the net reaction rates and can be written as:

$$O_A = -k_{AE}[A][E] + k_{-AE}[AE]. \tag{3.8}$$

$$O_E = -k_{AE}[A]\,[E] + k_{-AE}[AE] + k[AE]. \tag{3.9}$$

$$O_{AE} = k_{AE}[A]\,[E] - k_{-AE}[AE] - \ k[AE]. \tag{3.10}$$

Note that $\mathrm{O_E} + \mathrm{O_{AE}} = 0$, so the reaction does not change the total concentration of the enzyme species E , $\mathrm{E_{tot}} = [\mathrm{E}] + [\mathrm{AE}] = \text{constant}.$

Initially, we will assume that there is no $[AE]$ present and that E is distributed uniformly, $[E(t=0)] = E_{tot}$.

It is important to notice that there is no effect of the receptors on the cleft. This effect is felt only on the boundary as A reaches the postsynaptic membrane and interacts with receptors R.

3.4 Dynamics with the receptors (boundary $z = L$)

The receptors interaction with A takes place only at the postsynaptic membrane. At this position, one receptor R may capture one or two molecules of ACh at two possible binding sites. These combinations may generate AR (one receptor coupled with ACh) or A_2R (one receptor coupled with two A's) according to the following schemes :

$$A + R \underset{k_{-R}}{\overset{2k_R}{\rightleftharpoons}} AR. \tag{3.11}$$

$$A + AR \underset{2k_{-AR}}{\overset{k_{AR}}{\rightleftharpoons}} A_2R. \tag{3.12}$$

Here, k_{AR} and k_{-AR} are the reaction rate for the direct/reverse reaction kinetics. Once case A_2R is activated, it may undergo opening of the channel, forming A_2R_{op}, which stays in equilibrium with its deactivated state A_2R. This equilibrium (activated/ deactivated form) can be chemically expressed as:

$$A_2R \underset{k_{cl}}{\overset{k_{op}}{\rightleftharpoons}} A_2R_{op}. \tag{3.13}$$

Here, k_{op} and k_{cl} are the rates corresponding to the opening and closing of the channels.

As described by the chemical reactions mentioned above, the kinetics of the receptor R, ACh and the combined species can be written mathematically according to the following differential equations, which incorporate the kinetics involved in the formation/ consumption of the species:

$$\frac{\mathrm{d}[\mathrm{R}]}{\mathrm{dt}} = -2\mathrm{k}_{\mathrm{R}}[\mathrm{A(L)}][\mathrm{R}] + \mathrm{k}_{-\mathrm{R}}[\mathrm{AR}]. \tag{3.14}$$

$$\frac{\mathrm{d}[\mathrm{AR}]}{\mathrm{dt}} = 2\mathrm{k}_{\mathrm{R}}[\mathrm{A(L)}][\mathrm{R}] - \mathrm{k}_{-\mathrm{R}}[\mathrm{AR}] - \mathrm{k}_{\mathrm{AR}}[\mathrm{A(L)}][\mathrm{AR}] + 2\mathrm{k}_{-\mathrm{AR}}[\mathrm{A_2R}]. \tag{3.15}$$

$$\frac{\mathrm{d}[\mathrm{A_2R}]}{\mathrm{dt}} = \mathrm{k}_{\mathrm{AR}}[\mathrm{A(L)}][\mathrm{AR}] - 2\mathrm{k}_{-\mathrm{AR}}[\mathrm{A_2R}] - \mathrm{k}_{\mathrm{op}}[\mathrm{A_2R}] + \mathrm{k}_{\mathrm{cl}}[\mathrm{A_2R_{op}}]. \tag{3.16}$$

$$\frac{\mathrm{d}[\mathrm{A_2R_{op}}]}{\mathrm{dt}} = \mathrm{k}_{\mathrm{op}}[\mathrm{A_2R}] - \mathrm{k}_{\mathrm{cl}}\,[\mathrm{A_2R_{op}}]. \tag{3.17}$$

where $[\mathrm{R}]$, $[\mathrm{AR}]$, $[\mathrm{A_2R}]$ and $\left[\mathrm{A_2R_{op}}\right]$ are the concentrations of the receptor species(moles/ area). The total amount of receptors is conserved, which means:

$$\mathrm{R_{tot}} = [\mathrm{R}] + [\mathrm{AR}] + [\mathrm{A_2R}] + \left[\mathrm{A_2R_{op}}\right] = \text{constant}. \tag{3.18}$$

Initially , we will assume that R is the only receptors present , $[\mathrm{R}](\mathrm{t}=0) = \mathrm{R_{tot}}$.

Due to the reaction with the acetylcholine, the differential equation for A should include an extra term localized at $z = L$ boundary by adding the term $\mathrm{S}\delta(\mathrm{z}-\mathrm{L})$, where $\delta(\mathrm{z}-\mathrm{L})$ is the delta-Dirac function and S is a sink term. Adding that to the reaction-diffusion differential equation of the acetylcholine. We get,

$$\frac{\partial[\mathrm{A}]}{\partial \mathrm{t}} = \mathrm{D_A}\frac{\partial^2[\mathrm{A}]}{\partial \mathrm{z}^2} + O_{\mathrm{A}} + \mathrm{S}\delta(\mathrm{z}-\mathrm{L}). \tag{3.19}$$

where S consists of the change of moles of acetylcholine per area per unit time due to the heterogeneous reaction. In mathematical terms,

$$\mathrm{S} = -2\mathrm{k_R}[\mathrm{A(L)}][\mathrm{R}] - \mathrm{k_{AR}}[\mathrm{A(L)}][\mathrm{AR}] + \mathrm{k_{-R}}[\mathrm{AR}] + 2\mathrm{k_{-AR}}[\mathrm{A_2R}]. \tag{3.20}$$

Integrate the differential equation across the boundary from $z = L - \frac{\epsilon}{2}$ to $z = L + \frac{\epsilon}{2}$ where ϵ is a small length and take the limit as ϵ goes to 0:

$$\lim_{\epsilon\to 0}\frac{\partial[\mathrm{A(L)}]}{\partial \mathrm{t}}\,\epsilon = -\lim_{\epsilon\to 0}\mathrm{D_A}\frac{\partial[\mathrm{A}]}{\partial \mathrm{z}}\Big|_{\mathrm{z=L}-\frac{\epsilon}{2}} + \lim_{\epsilon\to 0} O_{\mathrm{A}}(\mathrm{L})\epsilon + \mathrm{S}. \tag{3.21}$$

$$= -D_A\frac{\partial A}{\partial z}\Big|_{z=L} + S = 0. \tag{3.22}$$

The boundary condition for A at $z = L$ is thus expressed as:

$$0 = -\mathrm{D_A}\frac{\partial[\mathrm{A}]}{\partial \mathrm{z}}\Big|_{\mathrm{z=L}} - 2\mathrm{k_R}[\mathrm{A(L)}][\mathrm{R}] - \mathrm{k_{AR}}[\mathrm{A(L)}][\mathrm{AR}] + \mathrm{k_{-R}}[\mathrm{AR}] + 2\mathrm{k_{-AR}}[\mathrm{A_2R}]. \tag{3.23}$$

3.5 Simplified dimensionless diffusion-reaction system

The technique of scaling is an extremely powerful way of analyzing a model, so it is convenient to rescale the physical and chemical parameters of the problem. Thus, the complete model equations become dimensionless. Starting from the upper border $z = 0$, the flux f(t) [Moles/cm².s] can be rescaled by dividing it by the input flux of A, f_0 .

$$f_0 = \frac{F}{\tau}. \tag{3.24}$$

where F is the total release of A per cycle [Moles/cm²] and τ is the diffusive time:

$$\tau = \frac{L^2}{D_A}. \tag{3.25}$$

The running time t, the period of release T ,as well as the width of the release spike in the flux equation, are all scaled by τ. The position z is scaled with the thickness L of the cleft.
The concentration of acetylcholine [A] throughout the system can be transformed into dimensionless value by dividing it by a typical concentration scale C for A. We expressed it by the following equation.

$$C = \frac{F}{L}. \tag{3.26}$$

The concentration of [E] is converted into dimensionless unit through division of its value by the initial concentration E_{tot} of [E]:

$$[E](t = 0) = E_{tot}(0) = s. \tag{3.27}$$

We introduce the dimensionless initial concentration of [E] by dividing s by C:

$$\sigma = \frac{s}{C}. \tag{3.28}$$

The concentration of the receptors and other combined receptors species become dimensionless by dividing them by the initial concentration of R, namely

$$[\mathrm{R}](\mathrm{t} = 0) = \mathrm{R}_{\mathrm{tot}}(0) = \alpha. \tag{3.29}$$

We scale the receptor initial concentration with F and define the scale initial receptor concentration:

$$\gamma = \frac{\alpha}{F}. \tag{3.30}$$

The reaction rate constants are converted into dimensionless values through the cancellation of its units performing multiplication or division with the previously mentioned variables, diffusive time τ and concentration C. The following table summarizes this transformation.

$K_{AE} = k_{AE}\tau C$	$K_{AR} = k_{AR}\tau C$
$K_{-AE} = k_{-AE}\tau$	$K_{-AR} = k_{-AR}\tau$
$K = k\tau$	$K_{op} = k_{op}\tau$
$K_R = k_R\tau C$	$K_{cl} = k_{cl}\tau$
$K_{-R} = k_{-R}\tau$	

The following algebraic scaled relations between the receptors and enzyme concentrations is used:

$$[\mathrm{AE}] + [\mathrm{E}] = 1. \tag{3.31}$$

$$[\mathrm{A_2R_{op}}] + [\mathrm{A_2R}] + [\mathrm{AR}] + [\mathrm{R}] = 1. \tag{3.52}$$

$f(t)$ can be scaled by f_0, and t, T and w by τ. The scaled form of the flux becomes

$$\frac{f(t)}{f_0} = \frac{1}{\sqrt{2\pi(w/\tau)^2}} \sum_{i=1} \exp\left(-\frac{(t - iT/\tau)^2}{2(w/\tau)^2}\right). \tag{3.33}$$

The scaled boundary conditions would be written in a following:

$$\left.\frac{\partial[\mathrm{A}]}{\partial \mathrm{z}}\right|_{\mathrm{z}=0} = -\frac{f(t)}{f_0}. \tag{3.34}$$

$$\left.\frac{\partial \mathrm{A}}{\partial \mathrm{z}}\right|_{\mathrm{z}=1} = -2\mathrm{K_R}\gamma[\mathrm{A(L)}][\mathrm{R}] - \mathrm{K_{AR}}\gamma[\mathrm{A(L)}][\mathrm{AR}] + \mathrm{K_{-R}}[\mathrm{AR}]\gamma + 2\mathrm{K_{-AR}}\gamma[\mathrm{A_2R}]. \tag{3.35}$$

As far as the initial conditions are concerned ,we have:

$$[\mathrm{A}(0,\mathrm{z})] = 0.$$
$$[\mathrm{E}(0,\mathrm{z})] = 1.$$
$$[\mathrm{R}(0)] = 1.$$
$$[\mathrm{AR}(0)] = [\mathrm{A_2R}(0)] = [\mathrm{A_2R_{op}}(0)] = 0.$$

3.6 Fast equilibrium approximation

A simplification is assumed for the kinetics of the enzyme. Note that, $\mathrm{D_E} = 0$, and $\mathrm{D_{AE}} = 0$ because diffusion of the enzyme is considered negligible [35,36,37]. To a good approximation in most cases, it may be verified that its kinetics is appreciatively faster than the acetylcholine kinetics. The partial differential equation expressing E dynamics simplifies in scaled form:

$$\frac{\mathrm{d[E]}}{\mathrm{dt}} = -\mathrm{K_{AE}[A\,E]} + (\mathrm{K_{-AE}} + \mathrm{K})(1 - \mathrm{[E]}) \approx 0. \tag{3.36}$$

Using $[AE] = 1 - [E]$, this is rearranged to

$$\mathrm{[E]} = \frac{\mathrm{K_{-AE}} + \mathrm{K}}{\mathrm{K_{-AE}} + \mathrm{K} + \mathrm{K_{AE}[A]}}. \tag{3.37}$$

The equation above is rewritten as:

$$\mathrm{[E]} = \frac{\kappa}{\kappa + \mathrm{[A]}}. \tag{3.38}$$

where:

$$\kappa = \frac{\mathrm{K_{-AE}} + \mathrm{K}}{\mathrm{K_{AE}}}. \tag{3.39}$$

Therefore, enzyme kinetics follow a Michaelis-Menten form.

After all the assumptions and simplifications, the differential equation defining the evaluation of concentration of [A] in dimensionless units is:

$$\frac{\partial[\mathrm{A}]}{\partial \mathrm{t}} = \frac{\partial^2[\mathrm{A}]}{\partial \mathrm{z}^2} - \frac{\mathrm{K}\sigma[\mathrm{A}]}{\kappa + [\mathrm{A}]}. \tag{3.40}$$

In fact, one can verify that equation 3.40 is valid to a high degree of accuracy when the exact kinetics for E in considered with reaction rate coefficients(Liu et al.2013)[36]. The boundary conditions are given by equations 3.37 and 3.38. The receptors reactions are described by:

$$\frac{\mathrm{d}[\mathrm{R}]}{\mathrm{dt}} = -2\mathrm{K}_{\mathrm{R}}[\mathrm{A}(1)][\mathrm{R}] + \mathrm{K}_{-\mathrm{R}}[\mathrm{AR}] \tag{3.41}$$

$$\frac{\mathrm{d}[\mathrm{AR}]}{\mathrm{dt}} = 2\mathrm{K}_{\mathrm{R}}[\mathrm{A}(1)][\mathrm{R}] - \mathrm{K}_{-\mathrm{R}}[\mathrm{AR}] - \mathrm{K}_{\mathrm{AR}}[\mathrm{A}(1)][AR] + 2\mathrm{K}_{-\mathrm{AR}}[\mathrm{A}_2\mathrm{R}]. \tag{3.42}$$

$$\frac{\mathrm{d}[\mathrm{A}_2\mathrm{R}]}{\mathrm{dt}} = \mathrm{K}_{\mathrm{AR}}[\mathrm{A}(1)][\mathrm{AR}] - 2\mathrm{K}_{-\mathrm{AR}}[\mathrm{A}_2\mathrm{R}] - \mathrm{K}_{\mathrm{op}}[\mathrm{A}_2\mathrm{R}] + \mathrm{K}_{\mathrm{cl}}(1 - [\mathrm{A}_2\mathrm{R}] - [\mathrm{AR}] - [\mathrm{R}]). \tag{3.43}$$

To solve the system, three additional algebraic equations are incorporated, which are the conservation concentrations and the enzyme E kinetics, as shown below.

$$[\mathrm{E}] = \frac{\kappa}{\kappa + [\mathrm{A}]}. \tag{3.44}$$

$$[\mathrm{AE}] + [\mathrm{E}] = 1. \tag{3.45}$$

$$[\mathrm{R}] + [\mathrm{AR}] + [\mathrm{A}_2\mathrm{R}] + [\mathrm{A}_2\mathrm{R}_{\mathrm{op}}] = 1. \tag{3.46}$$

3.7 Numerical implementation

The numerical solution of the problem of reaction-diffusion through the cleft was obtained using the software MATLAB®. In general, it can be said that the following differential equation can describe the dynamics of the species involved in the process of reaction-diffusion through the cleft. To clarify, we revert to unscaled variables:

$$\frac{\partial[\mathrm{A}]}{\partial \mathrm{t}} = \mathrm{D_A}\frac{\partial^2[\mathrm{A}]}{\partial \mathrm{z}^2} + O_{\mathrm{A}}. \tag{3.47}$$

The boundary conditions for $[\mathrm{A}]$ take the following general form.

At $z = 0$,

$$\left.\frac{\partial[\mathrm{A}]}{\partial \mathrm{z}}\right|_{\mathrm{z=0}} = -\frac{f(t)}{f_0}. \tag{3.48}$$

at $z = L$,

$$-\mathrm{D_A}\left.\frac{\partial[\mathrm{A}]}{\partial \mathrm{z}}\right|_{\mathrm{z=L}} + \mathrm{r_{1A}(B)[A(L)]} + \mathrm{r_{2A}(B)} = 0. \tag{3.49}$$

where $r_{1A} = -2k_R[R] - k_{AR}[AR]$. $r_{2A} = k_{-R}[AR] + 2k_{-AR}[A_2R]$, and B stands for receptors type .

In our finite difference numerical scheme , we adopt the Crank-Nicholson method. We consider a spatial discretization of the length L in equally spaced points, generating $\mathrm{N}+1$ node separated by a distance $\Delta \mathrm{z}=\frac{L}{N}$. The state of a species at a spatial node can be indicated by a subscript i; each node is labelled as $\mathrm{i}=0,1,2,\ldots,\mathrm{N}$.

Similarly, time is discretized, generating $M+1$ node separated by a timestep $\Delta t=\frac{t_{tot}}{M}$. As it is done regarding the spatial index, the state of a species in a time node is indicated by a superscript n on the concentration variable, and $n=0,1,2,\ldots,M$. Coupling these two indexes, the state $\mathrm{A_i^n}$ indicates the concentration of A in the position $i\Delta z$ and time $n\Delta t$. It is important to highlight that the choice of proper Δz and Δt is crucial for the correct solution of the system dynamics. Generically, Δt must be much smaller than any physically significant time scales in the problem. Applying the Crank-Nicholson algorithm, the discretized version of the differential equations of A and E is written as follows.

$$\frac{[\mathrm{A_i^{n+1}}]-[\mathrm{A_i^n}]}{\Delta \mathrm{t}}=\frac{1}{2\Delta \mathrm{z}^2}\ D_A\left[([\mathrm{A_{i-1}^n}]-2[\mathrm{A_i^n}]+[\mathrm{A_{i+1}^n}])+([\mathrm{A_{i-1}^{n+1}}]-2[\mathrm{A_i^{n+1}}]+[\mathrm{A_{i+1}^{n+1}}])\right]+O_{\mathrm{Ai}}^{\mathrm{n+\frac{1}{2}}}. \qquad (3.50)$$

where, $\mathrm{O_{Ai}^{n+\frac{1}{2}}}=\frac{1}{2}\left(\mathrm{O_A^n}+\ \mathrm{O_A^{n+1}}\right)$.

Regarding the boundary conditions for each species, the following discretized version applies.

At $z\ =\ 0$:

$$\frac{[\mathrm{A_1^n}]-[\mathrm{A_{-1}^n}]}{2\Delta \mathrm{z}}=-\frac{f(t)}{D_A}. \qquad (3.51)$$

For the species A, an auxiliary ghost node -1 is placed above the discretization grid for the correct application of the method ($\mathrm{z}=-\Delta \mathrm{z}$). The value of A at this ghost node $\mathrm{A_{-1}^n}$ can be replaced by its definition as obtained by the application of the boundary condition above.

The discretized equation at the top boundary then becomes:

$$-\mathrm{D_A}\frac{\Delta \mathrm{t}}{\Delta \mathrm{z}^2}[\mathrm{A}_1^{\mathrm{n+1}}] + \left(1 + \frac{\mathrm{D_A}\Delta \mathrm{t}}{\Delta \mathrm{z}^2}\right)[\mathrm{A}_0^{\mathrm{n+1}}] = \frac{\mathrm{D_A}\Delta \mathrm{t}}{\Delta \mathrm{z}^2}[\mathrm{A}_1^{\mathrm{n+1}}] + \left(1 - \mathrm{D_A}\frac{\Delta \mathrm{t}}{\Delta \mathrm{z}^2}\right)[\mathrm{A}_0^{\mathrm{n}}] + \mathrm{O}_{\mathrm{A0}}^{\mathrm{n+\frac{1}{2}}}\Delta \mathrm{t} + \frac{2\Delta \mathrm{t}}{\Delta \mathrm{z}}\ f_{\cdot}^{n+\frac{1}{2}} \qquad (3.52)$$

where $f^{n+\frac{1}{2}} = f(t+\frac{1}{2})$.

At $z = L$:

$$0 = -D_A\frac{[A_{N+1}^n] - [A_{N-1}^n]}{2\Delta z} + r_{1A}[A_N^n] + r_{2A}^n. \qquad (3.53)$$

As mentioned above, we considered a ghost node slightly below L, at $z = N + \Delta z$. This allows us to use a more accurate centered scheme to treat this spatial derivative. Its definition can be obtained by setting the boundary condition at $i = N$ in the discretized reaction-diffusion equation:

$$\left(1 + \frac{\mathrm{D_A}\Delta \mathrm{t}}{\Delta \mathrm{z}^2} - \frac{\Delta \mathrm{t}\ \mathrm{r}_{1\mathrm{A}}^{\mathrm{n+\frac{1}{2}}}}{\Delta \mathrm{z}}\right)[\mathrm{A}_{\mathrm{N}}^{\mathrm{n+1}}] - \frac{\mathrm{D_A}\Delta \mathrm{t}}{\Delta \mathrm{z}^2}\ [\mathrm{A}_{\mathrm{N-1}}^{\mathrm{n+1}}] \qquad (3.54)$$

$$= \left(1 - \frac{\mathrm{D_A}\Delta \mathrm{t}}{\Delta \mathrm{z}^2} + \frac{\Delta \mathrm{t}\ \mathrm{r}_{1\mathrm{A}}^{\mathrm{n+\frac{1}{2}}}}{\Delta \mathrm{z}}\right)\mathrm{A}_{\mathrm{A}}^{\mathrm{n}} + \frac{\mathrm{D_A}\Delta \mathrm{t}}{\Delta \mathrm{z}^2}\ [\mathrm{A}_{\mathrm{N-1}}^{\mathrm{n}}]\ + O_{\mathrm{AN}}^{\mathrm{n+\frac{1}{2}}}\Delta \mathrm{t}\ + 2\ \frac{\Delta \mathrm{t}\ \mathrm{r}_{2\mathrm{A}}^{\mathrm{n+\frac{1}{2}}}}{\Delta \mathrm{z}}.$$

Let $\lambda = \frac{\mathrm{D_A}\Delta \mathrm{t}}{\Delta \mathrm{z}^2}$ be a dimensionless grid parameter. Then, the algorithm takes the form:

$$A \cdot C^{n+1} = B \cdot C^n + O^{n+\frac{1}{2}}. \qquad (3.55)$$

where C is the array of [A] concentrations at a given time and the matrices A and B are tridiagonal matrices expressed as follows:

$$A = \begin{bmatrix} 1+\lambda & -\lambda & 0 & \dots & 0 \\ -\frac{\lambda}{2} & 1+\lambda & -\frac{\lambda}{2} & \dots & 0 \\ 0 & -\frac{\lambda}{2} & 1+\lambda & -\frac{\lambda}{2}\dots & 0 \\ \dots & \dots & \dots & \dots & \dots \\ 0 & 0 & \dots & -\lambda & 1+\lambda-\frac{\Delta \mathrm{tr}_{1A}^{n+\frac{1}{2}}}{\Delta z} \end{bmatrix}. \quad (3.56)$$

$$B = \begin{bmatrix} 1-\lambda & \lambda & 0 & \dots & 0 \\ \frac{\lambda}{2} & 1-\lambda & \frac{\lambda}{2} & \dots & 0 \\ 0 & \frac{\lambda}{2} & 1-\lambda & \frac{\lambda}{2}\dots & 0 \\ \dots & \dots & \dots & \dots & \dots \\ 0 & 0 & \dots & \lambda & 1-\lambda+\frac{\Delta \mathrm{tr}_{2A}^{n+\frac{1}{2}}}{\Delta z} \end{bmatrix}. \quad (3.57)$$

The reaction array O is defined as below.

$$O = \begin{bmatrix} O_{A0}^{n+\frac{1}{2}}\Delta t + 2\frac{\Delta t}{\Delta z} f^{n+\frac{1}{2}} \\ O_{A1}^{n+\frac{1}{2}}\Delta t \\ O_{A2}^{n+\frac{1}{2}}\Delta t \\ \dots \\ O_{AN}^{n+\frac{1}{2}}\Delta t + \frac{2r_{2A}^{n+\frac{1}{2}}\Delta t}{\Delta z} \end{bmatrix}. \quad (3.58)$$

The solution is achieved by finding the concentrations updated at each time step according to the following equation:

$$C^{n+1} = A^{-1} \cdot B \cdot C^{n} + A^{-1} \cdot O^{n+\frac{1}{2}}. \tag{3.59}$$

Tridiagonal matrices are frequently used in computational physics as well as scientific investigations. The tridiagonal matrix algorithm inversion known as the Thomas algorithm, is used to solve the linear system numerically [38].

Finally, the nonlinear terms $O^{n+1/2}$, $r_{1A}^{n+\frac{1}{2}}, r_{2A}^{n+\frac{1}{2}}$ are treated by using the advanced projection method. These terms must be evaluated at the intermediate time (n+1/2) Δt. Using a Taylor expansion of all concentration fields, the concentration is written as follows:

$$[\mathrm{A_i}^{\mathrm{n}+\frac{1}{2}}] = [\mathrm{A_i^n}] + \frac{\Delta \mathrm{t}}{2}\frac{\partial [\mathrm{A_i^n}]}{\partial \mathrm{t}}. \tag{3.60}$$

Discretizing the partial derivative, one obtains:

$$[\mathrm{A_i}^{\mathrm{n}+\frac{1}{2}}] = [\mathrm{A_i^n}] + \frac{\Delta \mathrm{t}}{2}\frac{\mathrm{D_A}}{\Delta \mathrm{z}^2}([\mathrm{A_{i+1}^n}] - 2[\mathrm{A_i^n}] + [\mathrm{A_{i-1}^n}]) + \frac{\Delta \mathrm{t}}{2} O_{\mathrm{Ai}}^{\mathrm{n}}. \tag{3.61}$$

At $i = 0$, substitution of the boundary condition changes the above equation to the following:

$$[\mathrm{A_0}^{\mathrm{n}+\frac{1}{2}}] = [\mathrm{A_0^n}] + \frac{\Delta \mathrm{t}}{2}\frac{\mathrm{D_A}}{\Delta \mathrm{z}^2}([-\mathrm{A_0^n}] + [\mathrm{A_1^n}]) + \frac{\Delta \mathrm{t}}{2}\,\mathrm{O_{A0}^n} + \frac{\Delta \mathrm{t}}{\Delta \mathrm{z}}\;\; f^n. \tag{3.62}$$

At $i = N$,

$$[\mathrm{A_N}^{\mathrm{n}+\frac{1}{2}}] = \mathrm{A_N^n} + \frac{\Delta \mathrm{t}}{2}\frac{\mathrm{D_A}}{\Delta \mathrm{z}^2}([\mathrm{A_{N-1}^n}] - [\mathrm{A_N^n}]) + \frac{\Delta \mathrm{t}}{2}\,\mathrm{O_{AN}^n} + \frac{\Delta \mathrm{t}}{\Delta \mathrm{z}}\mathrm{r_{1A}^n}[\mathrm{A_N^n}] + \frac{\Delta \mathrm{t}}{\Delta \mathrm{z}}\mathrm{r_{2A}^n}. \tag{3.63}$$

The only thing left to find is to define the heterogeneous reaction terms r_{1A}^{n} and r_{2A}^{n} . Their values are determined by the concentration of the bound species B coupled to A(L) with the following dynamics:

$$\frac{\mathrm{d[B]}}{\mathrm{dt}} = O_{\mathrm{B}}([\mathrm{A(L)}], \mathrm{B}). \tag{3.64}$$

Here, B expresses any receptor species densities.

The discretized version of the solution is

$$\mathrm{B^{n+1}} = \mathrm{B^{n}} + \Delta \mathrm{t} O_{\mathrm{B}}[\mathrm{A}_{N}^{\mathrm{n+\frac{1}{2}}}], [\mathrm{B^{n+\frac{1}{2}}}]). \tag{3.67}$$

where $[\mathrm{B^{n+\frac{1}{2}}}]$ is obtained by projection method

$$[\mathrm{B^{n+\frac{1}{2}}}] = [\mathrm{B^{n}}] + \frac{\Delta \mathrm{t}}{2} O_{B}([A_{N}^{n}], [B^{n}]). \tag{3.68}$$

To investigate the dynamics of reaction-diffusion through the cleft, a reference study case was chosen, in terms of dimensionless parameters. Table 3.1 summarizes the parameters involved in the solution of the problem already described through this methodology section.

Variable	Value	Unit	Reference
Space z (L)	0.5×10^{-5}	cm	Khaliq et al., 2011
Diffusivity (D_A)	0.7×10^{-6}	cm²/s	Khaliq et al., 2011
Diffusive time (τ)	$\tau = \frac{L}{D_A^2} = 3.57 \times 10^{-5}$	s	calculated
Number of moles of A released/ cycle (F)	2.17×10^{-9}	moles/cm²	Aidoo et al., 2006
Scaled concentration [A](C)	$C = \frac{F}{L} = 0.434$	M	calculated
Initial concentration[E] (s)	4.5×10^{-4}	M	Aidoo et al., 2006
Initial concentration [R] (α)	3.3×10^{-12}	moles/cm²	Aidoo et al., 2006
Input flux of A (f_0)	$f_0 = \frac{F}{\tau} = 6.08 \times 10^{-5}$	moles/cm².s	calculated
Radius of the cleft *r*	0.5×10^{-5}	cm	Khaliq et al., 2011
k_R	3×10^7	$(M.s)^{-1}$	Khaliq et al., 2011
k_{-R}	1×10^4	s^{-1}	Khaliq et al., 2011
k_{AR}	3×10^7	$(M.s)^{-1}$	Khaliq et al., 2011
k_{-AR}	1×10^4	s^{-1}	Khaliq et al., 2011
k_{op}	2×10^4	s^{-1}	Khaliq et al., 2011
k_{cl}	5×10^3	s^{-1}	Khaliq et al., 2011
k_{AE}	2×10^8	$(M.s)^{-1}$	Liu et al., 2013
k_{-AE}	1×10^3	s^{-1}	Liu et al., 2013
k	1.1×10^5	s^{-1}	Liu et al., 2013
γ	1.52×10^{-3}	-	calculated
σ	10^{-3}	-	calculated
K_R	464.8	-	calculated
K_{-R}	0.357	-	calculated
K_{AR}	464.8	-	calculated
K_{-AR}	0.357	-	calculated
K_{op}	0.714	-	calculated
K_{cl}	0.178	-	calculated
K_{AE}	3.1×10^3	-	calculated
K_{-AE}	3.57×10^{-2}	-	calculated
K	3.93	-	calculated
κ	1.28×10^{-3}	-	calculated

Table 3.1: Parameters values that are used for simulations with their units, as well as the source.

In Table 3.1 the dimensionless parameters are not huge (except perhaps K_{AE}) which suggests that the scaling is a proper one. The large value of K_{AE} reflects the fast kinetics of the enzymes and is treated approximately in section 3.6. We will now implement our numerical techniques and illustrate some of the results in Chapter 4.

Chapter 4

Results and Discussion

In this chapter, the results of the simulations are presented and discussed to determine the influence of emission of acetylcholine at the posterior end of the electrocytes of weakly electric fish at high frequency. We use a Gaussian-shaped input flux of acetylcholine in the synaptic cleft and investigate the subsequent effects on the occupancy of different conformation receptor concentrations, especially the open receptors population. We will be using two frequencies: 200 Hz at the lower end and 500 Hz at the upper end. In order to test our code, we initially proceed with the kinetics of release without enzyme and with enzyme of a single load of ACh. Different parameter values are used in our study:

-The period of the input Gaussian function (T).

- The width of input Gaussian (w).

- The input concentration of acetylcholine (*F).*

- The ratio of initial receptors concentration to input acetylcholine concentration, $\gamma = \frac{\alpha}{F}$.

- The ratio of initial enzyme concentration$[\mathrm{E_{tot}}]$ to the [A]concentration scale, ($C = \frac{F}{L}$), $\sigma = \frac{s}{C}$.

The investigation of such parameters enabled a better understanding of the synaptic transmission dynamics. We find it is convenient to scale the problem by using dimensionless variables, see table 3.1. As such, parameters $\mathrm{D_A}$and L are equal to 1 (all present results are in reduced units).

4.1 Pure Diffusion of Acetylcholine

To verify the diffusion part of our numerical algorithm, we exclude the reactions with acetylcholinesterase enzyme and receptors for now. First, we compute $\frac{\partial[\mathrm{A}]}{\partial \mathrm{z}}\Big|_{\mathrm{z}=0}$ with no initial ACh $[\mathrm{A}](\mathrm{z},0) = 0$, with no homogeneous (enzyme interaction) heterogeneous (receptors interaction) reaction. The values shown in Table 3.1 are taken as reference for the results mentioned in this section.

The ACh release cycles are illustrated in Figure 4.1, which consists of three Gaussian pulses, all of them characterized by the same parameters (curve width and amplitude). We used three clearly separated input fluxes to avoid superposition of each curve and to have enough ACh to accumulate during its diffusion in the cleft. The input frequency was fixed at $200\ \mathrm{Hz}$ (i.e. with period of $5\ \mathrm{ms}$).

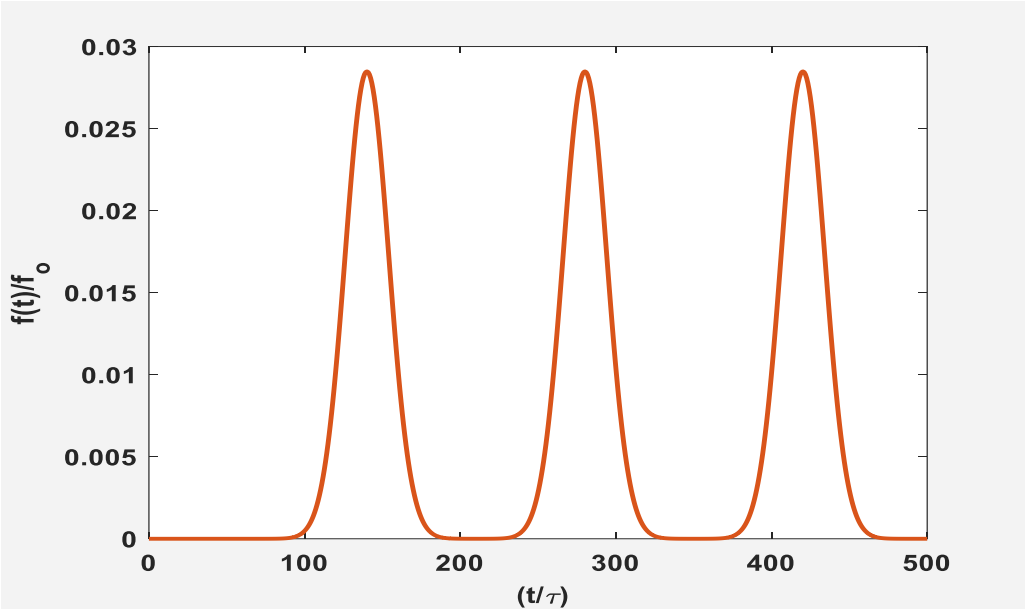

Figure 4.1 Three ACh release cycles for a frequency of 200 Hz. Three Gaussian shaped flux events are shown with a distribution width of 0.5ms. The time dimension showed on the x-axis above is in scaled unit τ. The values shown on the y-axis are scaled by f_o.

In Figure 4.1, It can be observed that the three peak inflows of acetylcholine fall on 140.8, 280.6 and 420.4, which corresponds to 5, 10 and 15 ms. Therefore, the total simulation time is 500τ (17.5 ms).

Figure 4.2 shows the results obtained for the concentration of ACh in the pure diffusion process across the cleft as a function of time at half space (in the middle of cleft) and the diffusion of acetylcholine profile as a function of space at time 150.4 τ(corresponding to the peak of the first release pulse).

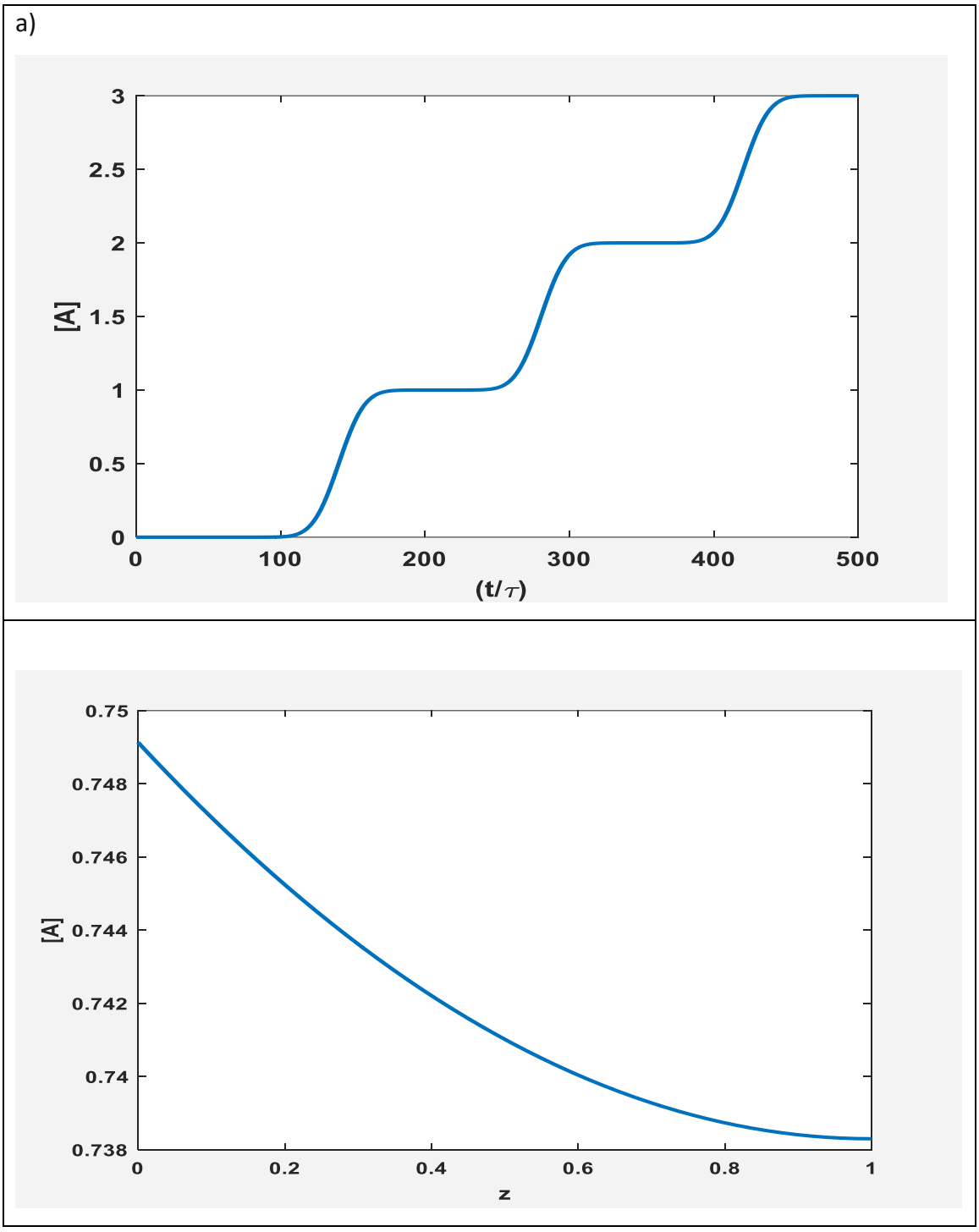

Figure 4.2: Pure diffusion of acetylcholine with three periodic releases of acetylcholine with respect to a) time at $z = \frac{1}{2}$ and b) space at time equals to 150.4 τ. There is a smooth increase in the concentration of acetylcholine with time, due to the three release cycles. By the end of each loading, the concentration of acetylcholine reaches a certain value with no variation.

The Figure 4.2 illustrates the diffusion (without reaction) of ACh with three periodic releases. The Figure 4.2 (a) illustrates the results obtained for the concentration of ACh in pure diffusion process across the cleft, as a function of the simulation time at half position. The Figure 4.2 (b) shows the concentration profile of ACh with position in the cleft at $t = 150.4\tau$ (from the pre-synaptic zone to the post-synaptic membrane). The space z represented in the Figure is dimensionless. Table 4.1 shows the time of start and end of each increase in ACh concentration, with the corresponding values in terms of real proportional units at $z = \frac{1}{2}$.

Table 4.1 – Time (scaled and real units) and concentration of ACh in pure diffusion process.

Time Unit	**Time (ms)**	**Concentration of Acetylcholine**
100.94 τ	3.5	0.00 (0 M)
205.3τ	7.3	1(0.434M)
264.7 τ	9.4	1.1(0.477M)
338.1 τ	12.0	2(0.868M)
402.6τ	14.3	2.1(0.911M)
468 τ	16.7	3(1.3M)

Since the simulation assumes homogeneous radial distribution of ACh, only the z-dependence is relevant. The concentration, though apparently decreasing along the z-axis, is almost the same because the scale on the y-axis has a small range starting value 0.7491 with an ending value of 0.7383. Therefore, the difference between these values is 0.0108 (1.08%). Thus, the diffusion of ACh is fast and [A] is almost homogeneous in space. In addition, we found the analytical solution for the pure diffusion problem (no reaction with E or R) for an arbitrary time-dependent boundary condition at $z = 0$,see Appendix I.

The investigation of pure diffusion transport is relatively simple when compared with the complete process (diffusion-reaction). This fact enables a better understanding of the dynamics of the process by isolation of one of the occurring phenomena. Firstly, we started the simulation model by defining the behavior of diffusion and blocking the enzyme reaction. Figure 4.2 shows that at each release cycle, the concentration of ACh at the cleft rises as expected. The non-

existence of a reaction causes the concentration in between the releases to be completely flat, as can be noted for instance at time instant surrounding $200\tau - 350\ \tau$ (7.14 or 12.4ms). This confirms that the mass balance is not violated. Since each cycle releases one dimensionless unit of ACh (which is equivalent to $0.434M$), after 3 cycles the concentration is equal to

$$3 \times 0.434 \approx 1.3M.$$

4.2 Single Loading Case - Diffusion-reaction of Acetylcholine in the cleft and a width of 0.5 ms

With the introduction of the reaction term in the pure diffusion model, a one-dimensional reaction-diffusion model is obtained. In such a model, four processes can be distinguished in the chemical transmission: the release of ACh, diffusion in the cleft and hydrolysis by E , and the bonding with R. The analysis of the dynamics in each process can assist in the understanding of the complete phenomena associated with chemical transmission and interaction.

In an initial approach, we chose to use a single release schedule event with a Gaussian-shaped flux, as illustrated in Figure 4.3. This single release flux enables the analysis of the process dynamics while avoiding the effect of accumulation due to the eventual occurrence of other releases. In this case, the frequency is $0\ \mathrm{Hz}$, because it consists of a single peak.

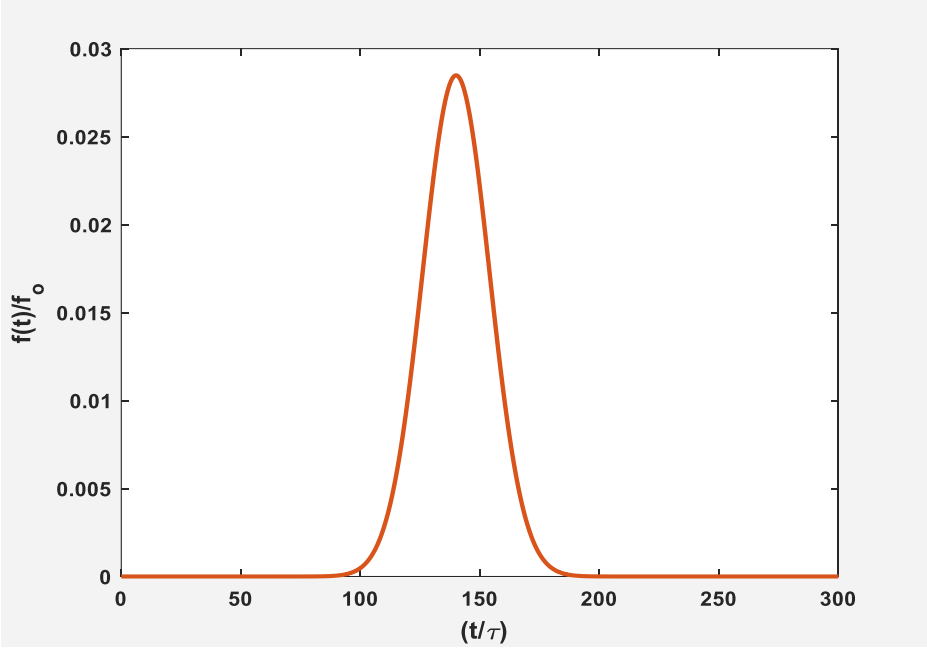

Figure 4.3: Single loading flux. As it is shown in the pure-diffusion case, the units in the plot are all scaled. The inflow of acetylcholine falls at 140τ, which corresponds to 5 ms in terms of real time units with a width of 0.5 ms.

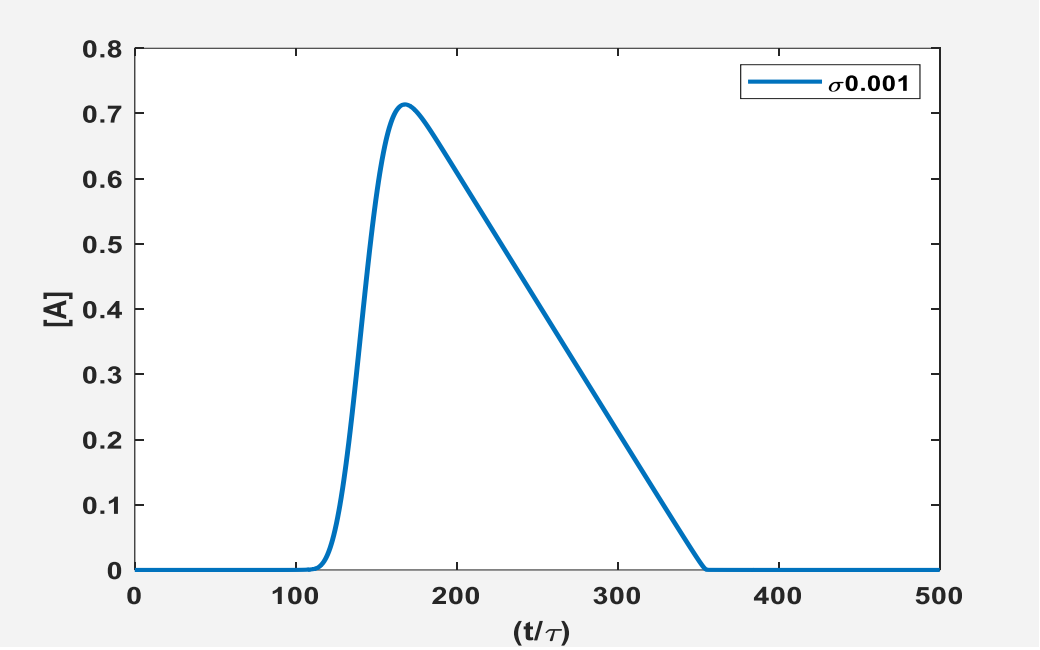

Figure 4.4: The effect of the AChE activity on the response of ACh concentration for a single loading with total simulation time 500 τ at $z = \frac{1}{2}$. Here, σ=0.001.

The concentration of ACh at one representative spatial node $z = \frac{1}{2}$ is shown in Figure 4.4. It can be observed that the concentration of acetylcholine in the cleft starts to increase at 113.3 τ simulation time with concentration approximately equals to 0.003 units ($1.302 \times 10^{-3} M$). It reaches a maximum of 0.7 units at 166.1 τ . The peak concentration of acetylcholine starts to decrease at 353.2 τ reaching a steady state with a concentration of around 0.004 units. As depicted in Figure 4.4, such a decay is linear in time, and its property is clarified in the stability analysis discussed below. We can obtain the value of that linear part analytically, as discussed in Appendix II. The value of the slope is $-\mathrm{K}\sigma$.

It is noticeable that reactions change significantly the concentration of ACh, with the appearance of a maximum and the monotonic decrease after the peak. Such observation can be inferred from Figure 4.2. in case of pure diffusion process, the ACh concentration increases to a level and maintains it, since it is not consumed. In the present case, the decay occurs because of the increase of the reaction kinetics associated with the consumption of ACh by AChE. The peak occurs at approximately 0.7 units at a time approximate by equal to 175τ.

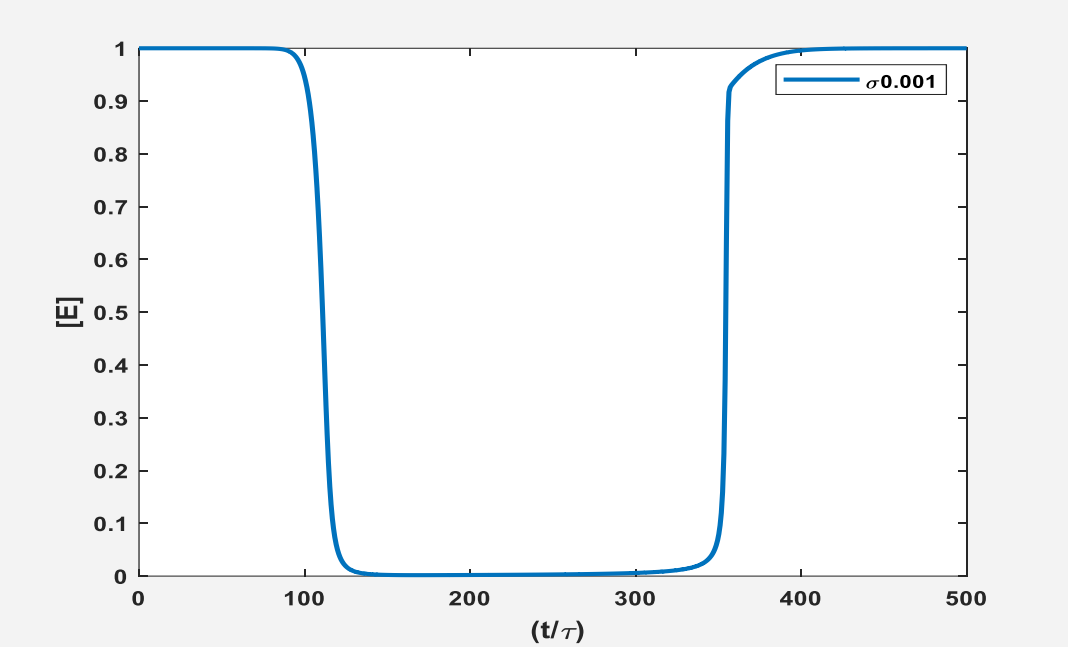

Figure 4.5: Illustrates the concentration of the enzyme [E] at a representative position $z = \frac{1}{2}$ with the simulation time. At the beginning of the simulation, the scaled enzyme concentration was fixed to one.

Figure 4.5 shows that the reaction process drastically consumes the enzyme, followed by its regeneration (at time 398 τ) due to reaction $\mathrm{AE} \xrightarrow{\mathrm{k}} \mathrm{E} + \mathrm{B}$ when $[\mathrm{A}]$ is close to zero.

Figure 4.6 shows the concentration of receptors states during the diffusion-reaction process. The behavior of the ACh receptors, especially their open conformational state, is the foundation of the characterization of NMJ [35]. Effectively almost all functional models of the NMJ revolve around relating the receptors conformational states to the other properties of interest.

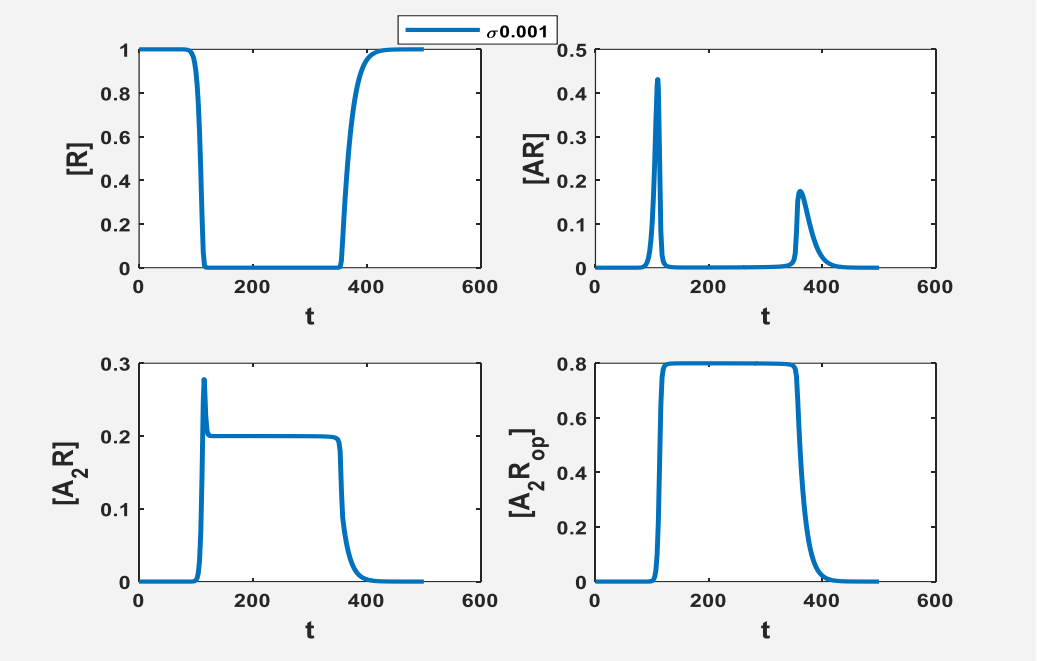

Figure 4.6: The concentration of ACh receptors during diffusion-reaction process in different states $[\mathrm{R}], [\mathrm{AR}], [\mathrm{A_2R}], [\mathrm{A_2R_{op}}]$ with $[\mathrm{R}]$ is initially fixed at one , corresponding to 3.3×10^{-12} M. An analysis of the dynamic process reveals that the steady state has one solution where the concentration of receptors $[\mathrm{R}] = 1, [\mathrm{AR}] = [\mathrm{A_2R}] = [\mathrm{A_2R_{op}}] = 0$.

The unbound receptors $[\mathrm{R}]$ starts to decrease at 85.37 τ , being almost completely bounded at time 114.8 τ . Relatively complete recovery of the receptors occurs at time 416.8 τ, raising its concentration back to its initial value.

The concentration of the first combination $[\mathrm{AR}]$ starts to rise at 91.23 τ , reaching a peak value at time 109.8 τ with scaled concentration value is equal to 0.434 which corresponds to 1.4×10^{-12} M. Due to the fast increase and subsequent decrease of such a peak, it is almost instantaneous, with a decline to nearly zero at 123.4 τ. This value is maintained until time 341.6 τ when it increases again and reaches a lower peak at 362 τ with scaled concentration 0.17 or 0.57×10^{-12} M. With a smoother slope than the previous peak, it decreases back to almost zero, reaching it by time 422.4 τ.

The concentration of the second combination $[A_2R]$ shows a sharp peak followed by a lower plateau which is maintained by a relatively long simulation time, returning to zero by the end of the simulation. The concentration initially raises at 101.9 τ , reaching the peak at 113.5 τ with scaled concentration 0.27, which corresponds to 0.89×10^{-12} M. Such values start to decrease at 113.7 τ , reaching a steady plateau with scaled concentration equal to 0.19 or 0.63×10^{-12} M. The plateau is kept stable for 234.7 τ, when it starts to decrease at 348.4 τ , reaching approximately zero at 403.7 τ.

Lastly, the activated form of the second combination $[A_2R_{op}]$ shows a concentration in which it starts at zero, reaches a plateau, and decreases back to zero by the end of the simulation. Specifically, the concentration starts to increase at 103.6 τ (3.6 ms) reaching the plateau at time 127.6 τ with concentration 0.79 units. This plateau is slightly declining until it reaches a concentration of 0.7 (2.3×10^{-12} M). when it drastically reduces to approximately zero at time 403.6 τ. Thus, the plateau duration is around 300 τ.

The model results corroborate with the known dynamics on the cleft for the receptors, as can be seen from Figure 4.6. When ACh approaches the post-synaptic terminal, it interacts with the receptor $[R]$, generating the intermediary species $[AR], [A_2R]$ and $[A_2R_{op}]$. $[AR]$ and $[A_2R]$, with attention to the first one, is rapidly consumed to generate $[A_2R_{op}]$, which at the end of the process regenerates $[R]$. A typical receptor concentration starts to decrease and goes to zero at about the same time when [A] starts to increase. In other words, ACh reaches receptors very fast. Consequently, the binding of ACh molecules to AChR has practically no effect on ACh concentration in the synaptic cleft in the long run.

4.3 Analytical Analysis of Pseudo-Steady-State

During the linear decay of $[A]$, the receptors species$[R , AR , A_2R , A_2R_{op}]$ reach a regime called “pseudo-steady state”. In such a situation, all-time derivatives of receptor concentrations are equal to zero.

$$\frac{d[R]}{dt} = 0 = -2K_R[A(1)][R] + K_{-R}[AR]. \tag{4.1}$$

$$\frac{d[AR]}{dt} = 0 = 2K_R[A(1)][R] - K_{-R}[AR] - K_{AR}[A(1)][AR] + 2K_{-AR}[A_2R]. \tag{4.2}$$

$$\frac{d[A_2R]}{dt} = 0 \tag{4.3}$$
$$= K_{AR}[A(1)][AR] - 2K_{-AR}[A_2R] - K_{op}[A_2R] + K_{cl}(1 - [A_2R] - [AR] - [R]).$$

By rearranging equation 4.1, it is found that the concentration of species $[AR]$ at steady-state condition is defined as,

$$[AR] = \frac{2K_R[A(1)]}{K_{-R}}[R]. \tag{4.4}$$

The concentration of $[A_2R]$ can be derived from Equation 4.2, in a similar fashion as it is done in the previous equation (4.4), thus obtaining Equation 4.5.

$$[A_2R] = \frac{K_R K_{AR}[A(1)^2]}{K_{-R}K_{-AR}}[R]. \tag{4.5}$$

As can be seen in both equations 4.4 and 4.5, the concentration of the acetylcholine-receptor species in the steady-state is dependent on the concentration of acetylcholine at the post-synaptic membrane and the concentration of receptor $[R]$. The latter one can be isolated from Equation 4.3, thus obtaining the following Equation.

$$[\mathrm{R}] = \frac{\mathrm{K_{-R}K_{-AR}}}{\mathrm{K_{-R}K_{-AR}} + 2\mathrm{K_R K_{-AR}}[\mathrm{A}(1)] + \mathrm{K_R K_{AR}}[\mathrm{A}(1)^2]\left(1 + \frac{\mathrm{K_{op}}}{\mathrm{K_{cl}}}\right)}. \tag{4.6}$$

Once the concentration of $[\mathrm{R}]$ is defined, back substitution of equations 4.4 and 4.5 gives.

$$[\mathrm{AR}] = \frac{2\mathrm{K_R}[\mathrm{A}(1)]\mathrm{K_{-AR}}}{\mathrm{K_{-R}K_{-AR}} + 2\mathrm{K_R K_{-AR}}[\mathrm{A}(1)] + \mathrm{K_R K_{AR}}[\mathrm{A}(1)^2]\left(1 + \frac{\mathrm{K_{op}}}{\mathrm{K_{cl}}}\right)}. \tag{4.7}$$

$$[\mathrm{A_2R}] = \frac{\mathrm{K_R K_{AR}}[\mathrm{A}(1)^2]}{\mathrm{K_{-R}K_{-AR}} + 2\mathrm{K_R K_{-AR}}[\mathrm{A}(1)] + \mathrm{K_R K_{AR}}[\mathrm{A}(1)^2]\left(1 + \frac{\mathrm{K_{op}}}{\mathrm{K_{cl}}}\right)}. \tag{4.8}$$

$$[\mathrm{A_2R_{op}}] = 1 - \frac{\mathrm{K_{-R}K_{-AR}} + 2\mathrm{K_{-R}K_{-AR}}\mathrm{A}(1) + \mathrm{K_R K_{AR}}[\mathrm{A}(1)^2]}{\mathrm{K_{-R}K_{-AR}} + 2\mathrm{K_R K_{-AR}}[\mathrm{A}(1)] + \mathrm{K_R K_{AR}}[\mathrm{A}(1)^2]\left(1 + \frac{\mathrm{K_{op}}}{\mathrm{K_{cl}}}\right)}. \tag{4.9}$$

By substitution of the parameter's values in the Equations 4.7, 4.8 and 4.9, we can obtain the values of the concentrations of the receptor and acetylcholine receptor species for different values of concentration of ACh in the steady state regime:

Table 4.2 – Calculated equilibrium point

Species	Concentration (dimensionless units)
R	1.5×10^{-7}
AR	3×10^{-4}
$\mathrm{A_2R}$	0.199
$\mathrm{A_2R_{op}}$	0.8

The values analytically obtained in Table 4.2 agree with the ones obtained from the simulation results shown in Figure 4.15. These are shown in Table 4.3. The numerical results validate the pseudo steady state approximation.

Table 4.3 – equilibrium point from the simulation.

Species	Concentration (dimensionless units)
R	1.6×10^{-7}
AR	3.5×10^{-4}
$\mathrm{A_2R}$	0.199
$\mathrm{A_2R_{op}}$	0.8

The states mentioned above are observed in the period 127τ until 334 τ.

The final values of steady state for the whole system are determined from the simulation as shown in Table 4.4.

Table 4.4 The final values of steady state from the simulation

Species	Concentration
$[\mathrm{A}]$	0
$[\mathrm{R}]$	1
$[\mathrm{AR}]$	0
$[\mathrm{A_2R}]$	0
$[\mathrm{A_2R_{op}}]$	0

To calculate the final values of steady state equilibrium point:

$$[\mathrm{A_2R_{oP}}] + [\mathrm{A_2R}] + [\mathrm{AR}] + [\mathrm{R}] = 1. \tag{4.10}$$

$$[\mathrm{E}] + [\mathrm{AE}] = 1. \tag{4.11}$$

At steady state:

$$\frac{\partial[\mathrm{A}]}{\partial \mathrm{t}} = 0. \tag{4.12}$$

Thus, from Eq. (3.40), $[\mathrm{A}] = 0$.

From Eq. (4.6-4.9), we get

$$[\mathrm{A_2R_{oP}}] = [\mathrm{A_2R}] = [\mathrm{AR}] = 0; [\mathrm{R}] = 1. \tag{4.13}$$

4.4 Single Loading Case - investigation of the effect of σ on [A] with a width of 0.5 ms

For a deeper understanding and analysis of the reaction-diffusion process on the cleft, some parameters were modified, and the effect of such changes was investigated. In the present case study, the impact of σ, which defines the ratio between acetylcholine concentration scale and the initial enzyme concentrations, is studied.

This parameter was manipulated by directly changing the value of s (the initial Enzyme concentration E_{tot}). According to Table 3.1, its reference value is $4.5 \times 10^{-4}\mathrm{M}$ corresponding to $\sigma = 0.001$. We consider the effect of the enzyme concentration with values of σ ranging from 0 to 0.012.

- 0
- $0.691 \text{ x } 10^{-3}$
- 10^{-3}(canonical values)
- $1.6 \text{ x } 10^{-3}$
- $2.1 \text{ x } 10^{-3}$
- $4.1\text{x}10^{-3}$
- $6.2\text{x}10^{-3}$
- $9\text{x}10^{-3}$
- $1\text{x}10^{-2}$
- $1.2\text{x}10^{-2}$

The selection of the schedule above took into consideration the fact that, for values of σ below 10^{-3} (canonical values – Table 3.1), it becomes difficult to observe the differences. Thus, the investigation was conducted starting from a value of σ equals to zero (0) (no reaction with enzymes) and increasing values. The obtained concentration for ACh is shown in Figure 4.7.

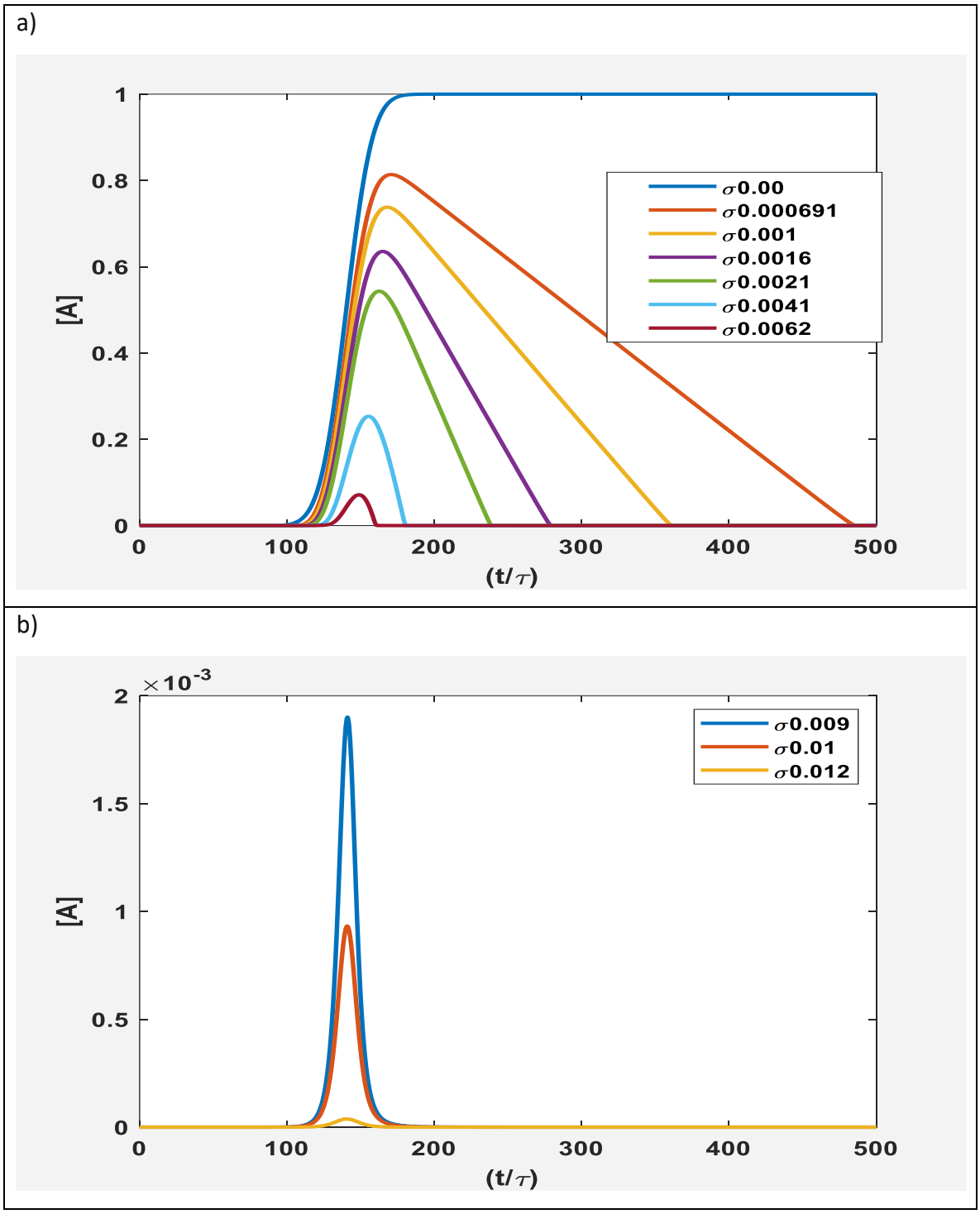

Figure 4.7: Concentration of acetylcholine as a function of time for different values of σ at representative position $z = \frac{1}{2}$. For a more consistent visualization of the concentration of acetylcholine, the results were split into two plots. The one at the top (Figure 4.7a) shows the concentrations for lower values of σ, while the one at the bottom (Figure 4.7b) shows the concentration for higher values.

We applied the determined range of parameters and constants available in the literature. In the following section, we discuss the key results of these experiments, which is the observation of increasing the initial enzyme concentration. This increases the hydrolysis reaction rate and, as a result, the Ach concentration is dramatically decreased.

From the results obtained for the concentration of acetylcholine[A], one can observe that there is a drastic difference in the concentration of acetylcholine. That is expected since the increase in the value of σ also indicates an increase in the concentration of enzyme, which reacts with ACh. Note that in the so-called pseudo-steady state regime, [A] decays linearly with a slope that changes as sigma is varied. Besides, the results show that linear decay extrapolates to $[\mathrm{A}] = 1$ at $t = \tau_D$, independently of σ (see the Appendix II).

Here τ_D is an initial time delay after which [A] has increased slightly from its initial value under the effect of the loading function. When the curves of [A] for different values of σ are extrapolated to [A]=1, they all converge at the same value of time. Extracting τ_D from Figure 4.7a, $\tau_D = 100\tau$.

From Figure 4.7, it can be clearly seen that there is a linear decay of $[\mathrm{A}]$after reaching the peak concentration level. Investigation of the slope of such decay as a function of the value of σ can be more clearly done by plotting it as shown in Figure 4.8. The decay slope obtained for each σ is shown in Table 4.5.

Table 4.5 Slope of linear decay of ACh for different values of σ.

$\boldsymbol{\sigma(\times 10^{-3})}$	**slope of ACh linear decay** $\boldsymbol{(\times 10^{-3})}$	$-\mathbf{K}\,\sigma$
0.000691	-2.0	-2.7×10^{-3}
1.0	-4.0	-3.9×10^{-3}
1.6	-6.0	-6.3×10^{-3}
2.1	-8.0	-8.3×10^{-3}
4.1	-14.0	-16.0×10^{-3}

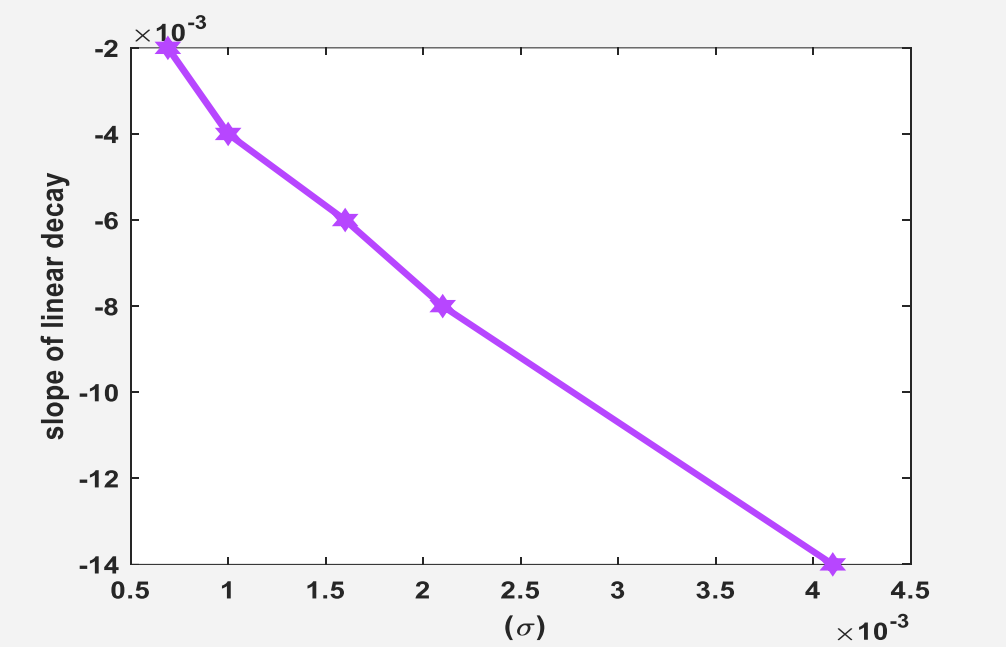

Figure 4.8: A plot of the relationship between varying σ and the slope of Linear decay of acetylcholine$[\mathrm{A}]$ which is a straight line.

From Figure 4.8, one may notice that there is a clear linear correlation between σ and the slope of ACh linear decay. When σ increases positively, the slope increases negatively, becoming steeper. This result agrees with the observations in Figure 4.7. Another point that can be mentioned related to Figure 4.7 is that extrapolation of σ to zero will show a slope equals to 0, thus a plateau. This is observed in the pure diffusion simulation.

The investigation of different σ values confirmed that the value of the slope of that linear part is $-\mathrm{K}\sigma$ where$\mathrm{K}$ is the regeneration rate of enzyme. Analytically, this value was obtained, as shown in the Appendix II. To illustrate, for $\sigma = 10^{-3}$, the observed slope of the linear decay is approximately equal to -0.004, whereas the value $-\mathrm{K}\sigma = -3.93 \times 10^{-3}$, which gives a relative deviation of 1.78% of the theoretical slope.

For $\sigma \geq 0.009$, the concentration resembles a Gaussian curve, with a similar increase and decay slopes. When reaching values superior to 0.012, the concentration peak of ACh is drastically lower than 0.1×10^{-3}, which makes analysis difficult.

Through observation of the concentration of ACh for larger σ, in Figure 4.7, it can be seen that an exponential decay follows the linear decay plotting the data for all large values of σ. For a comprehensive numerical analysis of such dynamics, the exponential decay of ACh is shown in Figures 4.9.

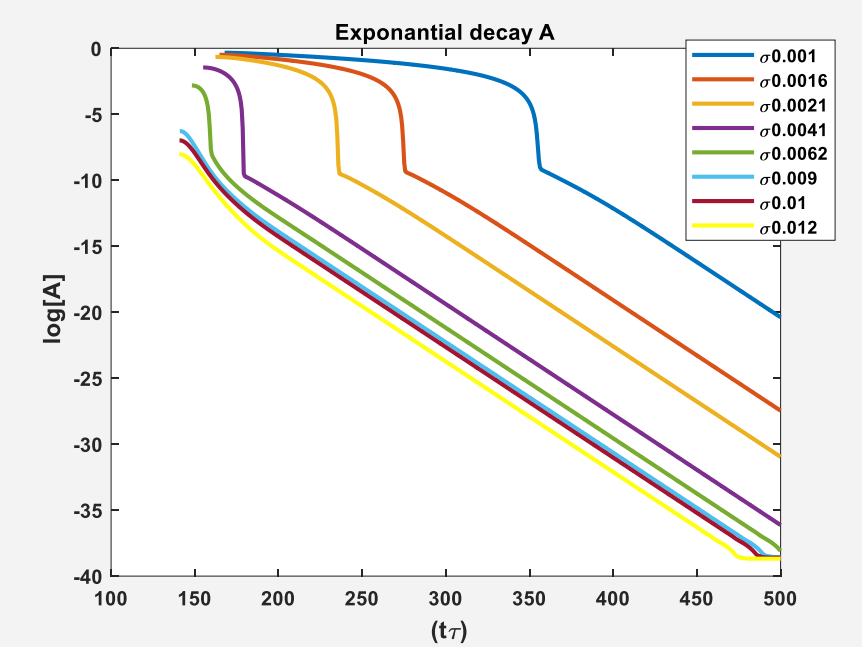

Figure 4.9: Semi-log plot plot of [A] versus time for different values of σ. The initial "non-linearity" on log scale derives from the linear decay after the peaks (from 150 τ to 437.5 τ) while the visible straight line in the semi-log plot indicates the exponential decay. It can be noticed that, for larger values of σ, the linear decay is shorter while the exponential decay is longer. Also, higher values of σ produce lower concentration values at the end of the simulation. For instance, when $\sigma = 0.001$, the final concentration of ACh is approximately 10^{-20}, while for $\sigma = 0.01$ (10 times higher) the final concentration is almost 10^{-40}.

Figure 4.9 show that the concentration of ACh decays exponentially when [A] approaches the steady state regime. The decay here is the sum of three exponentials. To calculate the slope, it is appropriate to perform a linear stability analysis involving full dynamic receptor kinetics. The Appendix III shows how the procedure works analytically. The result for the decaying modes [A]~exp(ωt) is

$$\omega = -\frac{K\sigma}{\kappa}.$$

$$\omega = \frac{-K_{cl}}{2} - K_{-AR} - \frac{K_{op}}{2} \pm [-2K_{cl}K_{-AR} + \left(\frac{K_{cl}}{2} + \frac{K_{op}}{2} + K_{-AR}\right)^2]^{\frac{1}{2}}. \quad (4.14)$$

Thus, for the reference state

$$\omega = -0.087;\ -1.519; -3.07.$$

This gives three exponentials decay; two are fast decaying (-3.07, -1.519). The mode at -0.087 (from Eq. (4.14)) is the only one remaining at large time and is the one seen in the Figure. 4.9.

Investigation of the slope of such exponential decay for different values of σ can be calculated numerically. The exponential decay slope obtained for each σ is shown in Table 4.6.

Table 4.6 - The exponential decay slope

$\sigma(\times 10^{-3})$	**slope of exponential decay** $(\times 10^{-2})$
1.0	-8.25
1.6	-8.23
2.1	-8.37
4.1	-8.38

It is noticed that the slope for each is almost the same as illustrated in table 4.6. This is consistent with Eq. 4.14.

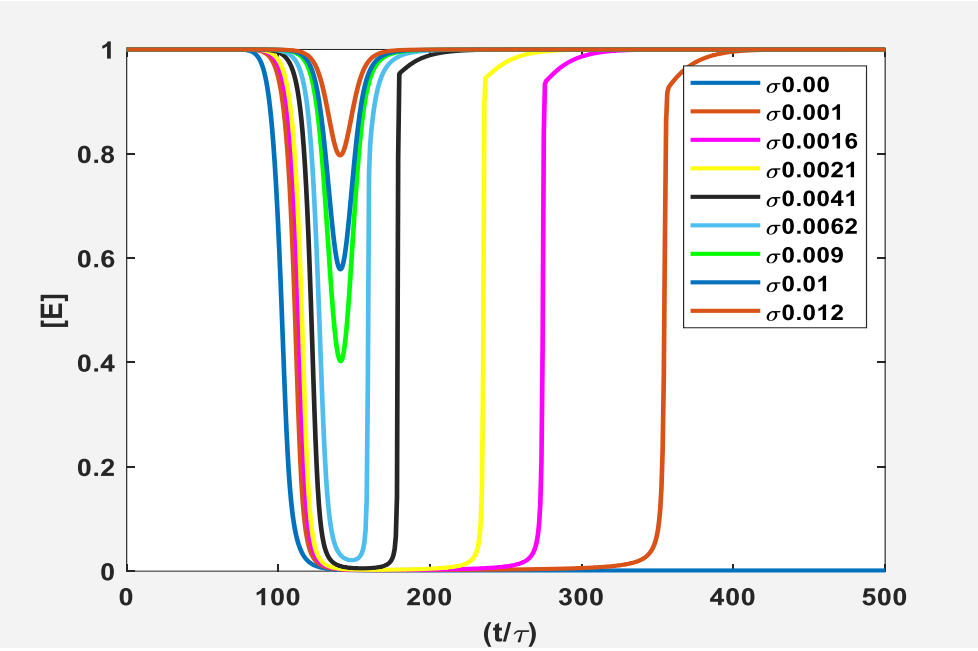

Figure 4.10: Enzyme concentrations for chosen values of σ at representative position $z = \frac{1}{2}$ .The concentration of the enzyme is similar to the one of ACh, though it starts with a concentration equal to 1, decreasing with the loading of ACh and recovering at the end of the simulation. $[\mathrm{E}]$ is regenerated by $\mathrm{AE} \xrightarrow{\mathrm{k}} \mathrm{E} + \mathrm{B}$. when $[\mathrm{A}]$ is close to 0.

In Figure 4.10, It is noticed that when σ increases, the enzyme concentration does not decrease directly to zero after the loading of acetylcholine, but it reaches low values. For $\sigma = 0.01$, the concentration of the enzyme decreases till it reaches 0.57 at time 140.9 τ. Thus, [E] decreases as low as 57%

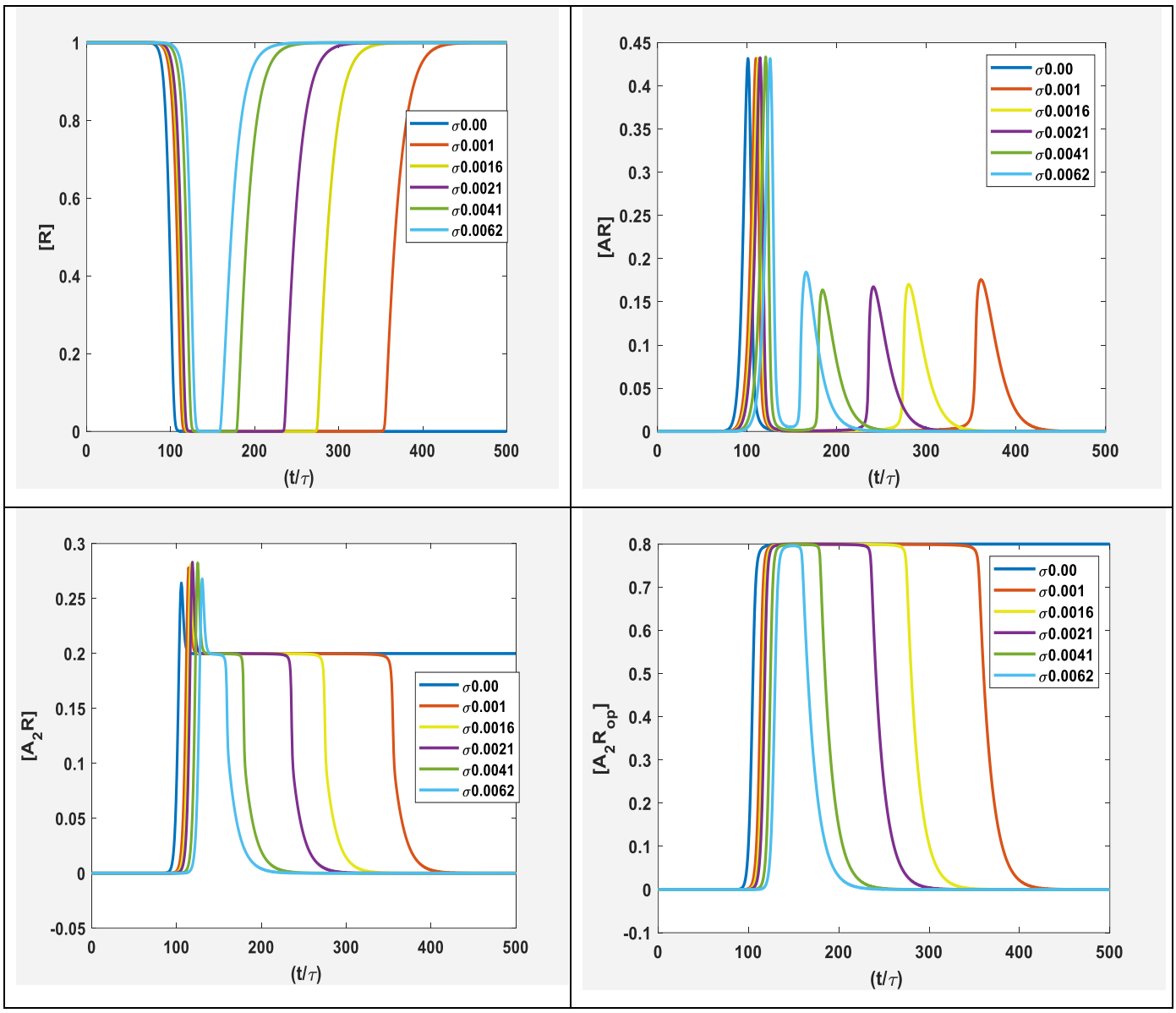

Figure 4.11: The concentration of receptors species $[\mathrm{AR}]$, $[\mathrm{A_2R}]$ and $[\mathrm{A_2R_{op}}]$ for different values of σ. The existence of a visible plateau can be seen between 100 τ and 430 τ of time.

Figure 4.11 shows that the concentrations of receptors $[\mathrm{R}]$ for different values of σ start to decrease at almost the same time (85.37 τ), being almost completely bounded between the time 114.8 τ (σ=0.001) and 131.7 τ(σ=0.0062). The complete recovery of the receptors occurs at a time between 354.2τ (σ=0.001) and 159τ (σ=0.0062) and raising its concentration back to its initial value (1).

$[\mathrm{AR}]$ concentrations start to rise at 91.23 τ , reaching peaks values at time 109.8 τ (σ=0.001) with scaled concentrations values are equal to 0.43. Due to the fast increase and subsequent decrease of such a peak, it is almost instantaneous, with a decline to nearly zero at 123.4 τ (σ=0.001) and 141 τ (σ=0.0062).These values are maintained until time 341.6 τ (σ=0.001) and 154.3 τ (σ=0.0062) when they increase again and reach a lower peak at 362 τ (σ=0.001) and 165 τ with scaled concentrations 0.17 and 0.18 respectively. With smoother slopes than the previous peaks, they decrease back to almost zero, reaching zero by time 422.4 τ (σ=0.001) and 230.3 τ(σ=0.0062). This gives a feature that is like a double-peak.

$[\mathrm{A_2R}]$ shows a sharp peak followed by a lower plateau which is maintained by a relatively long simulation time, returning to zero by the end of the simulation. The concentrations initially raise at 101.9 τ (σ=0.001) and 117.8 τ(σ=0.0062), reaching the peak at 113.5 τ (σ=0.001) with scaled concentration 0.28. When σ=0.0062, $[\mathrm{A_2R}]$ reaches a peak 130 τ with scaled concentration 0.26. Such values start to decrease at 113.7 τ , reaching a steady plateau with scaled concentration equal to 0.19. For σ=0.001, the plateau is kept stable for 234.7 τ while for σ=0.0062, the plateau is kept stable for 7 τ. After this ,$[\mathrm{A_2R}]$ starts to decrease again at 348.4 τ (σ=0.001), reaching approximately zero at 403.7 τ. For σ=0.0062, $[\mathrm{A_2R}]$ starts to decrease at 147 τ , reaching approximately zero at 197.8 τ.

Finally, $[\mathrm{A_2R_{op}}]$ starts at zero, reaches a plateau, and decreases back to zero by the end of the simulation. Specifically, the concentration starts to increase at 103.6 τ (σ=0.001) reaching

the plateau at time 127.6 τ with concentration 0.79. This plateau is slightly declining until it reaches a concentration of 0.8 when it drastically reduces to approximately zero at time 403.6 τ. Thus, the plateau duration is around 300 τ.Whereas for the case σ=0.0062, the concentration starts to increase at 117.3 τ, reaching the plateau at time 137.6 τ with concentration 0.79. This plateau decreases until it reaches a concentration of 0.8 when it drastically reduces to approximately zero at time 217.6. Thus, the plateau duration is around 2.7 τ .

Overall, changing σ affects not only the slope of the linear part of the $[\mathrm{A(t)}]$ decay in the pseudo-steady state regime as we mentioned before, but also generation of receptors species. Thus, changing σ affects the duration of the plateau in open receptors.

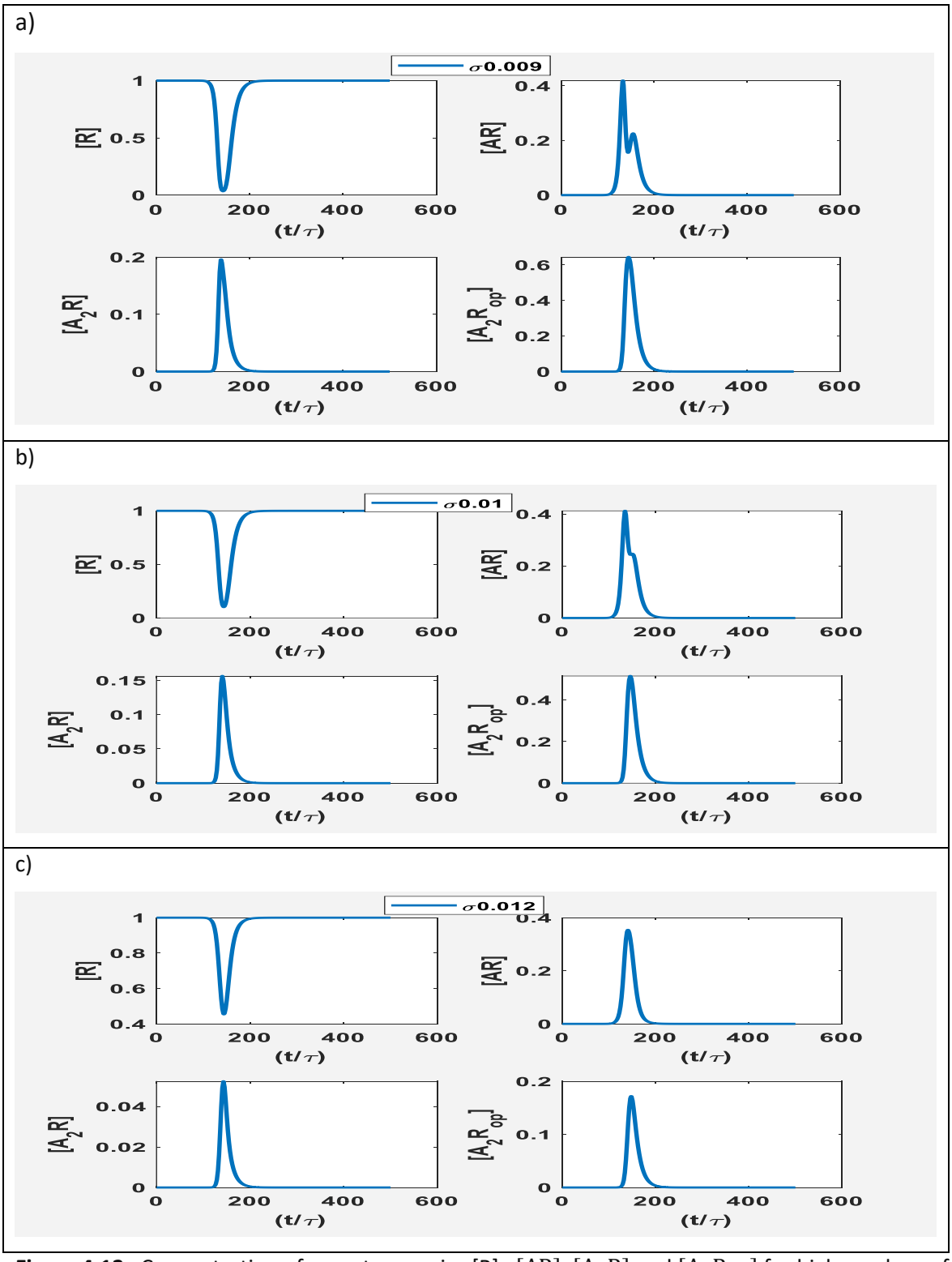

Figure 4.12: Concentration of receptor species [R], $[\mathrm{AR}]$, $[\mathrm{A_2R}]$ and $[\mathrm{A_2R_{op}}]$ for higher values of σ. The plateau on $[\mathrm{A_2R_{op}}]$ disappears for these values of σ. Results are shown above reveal that the bounded species [AR] and $[\mathrm{A_2R}]$ have distinctive features. These features are like a double-peak and a shoulder for [AR] and $[\mathrm{A_2R}]$respectively.

As we can see in Figure 4.12, increasing σ impacts on active and deactivated receptors species. $[\mathrm{R}]$ decreases very quickly but does not reach zero as σ increases. Regarding $[\mathrm{AR}]$, one can observe, in Figure 4.12(a) and (b) are the formation of two distinct peaks with increasing distance between them as σ increases. From $\sigma \geq 0.01$ only one peak can be observed. $[\mathrm{A_2R}]$ shows a very distinct concentration, with the visualization of a peak, followed by a shoulder for $0 \leq \sigma < 0.009$. For $\sigma \geq 0.009$, the shoulder vanishes and only a single peak can be observed.

For $[\mathrm{A_2R_{op}}]$, the existence of a visible plateau disappears for values of σ beyond 0.006 as seen in Figure 4.11. In addition, when σ is very large (larger than 0.012), because $\mathrm{K}\sigma$ is high, the plateau (at maximum concentration value) collapses to a point as seen in Figure 4.12. Those results are shown in Table 4.7, where the duration of the plateau Δt is compared for different values of σ. Additionally, the duration of the plateau is shown in Figure 4.13.

Table 4.7 Duration of concentration plateau on $[\mathrm{A_2R_{op}}]$ for different values of σ.

σ ($\times 10^{-3}$)	**Duration (τ)**
0.691	352.7
1.0	228.7
1.6	146.3
2.1	105.2
4.1	42.44
6.2	16.17

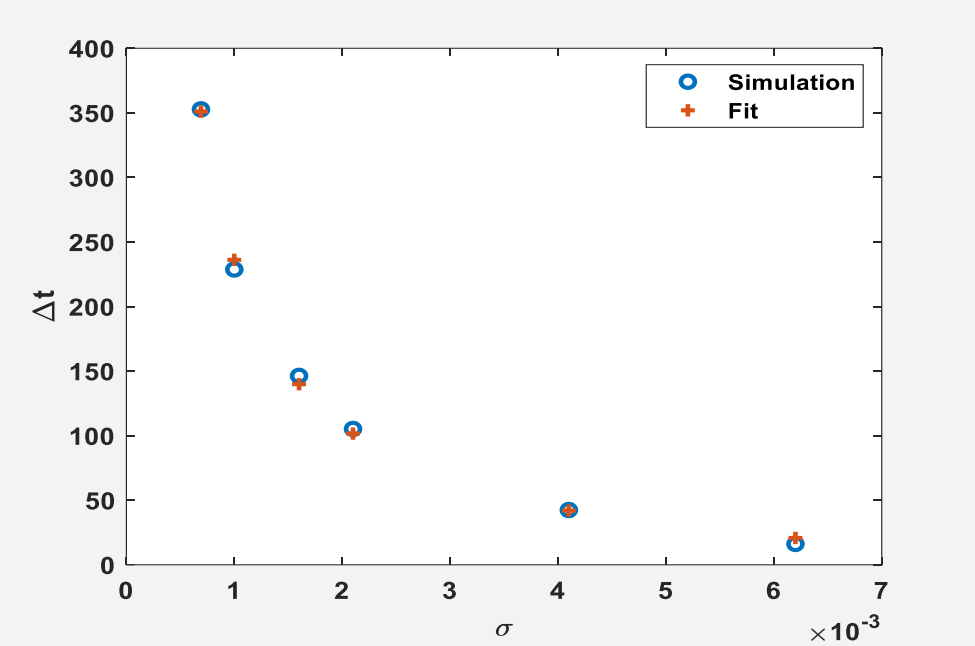

Figure 4.13: shows the duration of plateau in concentration of $[A_2R_{op}]$ for different values of σ as shown in table 4.6. The points obtained for the simulation is in blue and the ones obtained through the regression is in red. One can notice that there is good agreement between the two sets, with relatively low errors. Δt is inversely proportional to σ, i.e., it decreases when σ increases.

The duration of the plateau is inversely proportional to σ. It can be defined analytically as follows.

It was found that the relation between the duration of pseudo-steady state regime Δt (flat receptor concentrations) and σ is inversely proportional in character, which can be expressed as follows.

$$\Delta t = \frac{a}{\sigma} + b. \tag{4.15}$$

where a and b are constants (with respect to σ). This property is interesting because it allows for a very sensitive tuning of the dynamics with respect to σ. The Appendix II shows the procedure analytically, and the final results is shown below.

$$\Delta t = \frac{1}{K\sigma} - T + \sqrt{2}\, w \left[\log \frac{1}{k\sigma\sqrt{2\pi w^2}}\right]^{\frac{1}{2}} + \tau_D. \tag{4.16}$$

To prove that the above equation represents the relation between the duration of the plateau (Δt) and σ, a regression was performed on the data shown in Table 4.7. Equation 4.16 can be interpreted as a 1st order polynomial equation (line):

$$y = ax + b$$

where:

$y = \Delta t$ is the regression output.

$x = \frac{1}{\sigma}$ is the regression input.

$a = \frac{1}{K}$ is the slope of the line.

$b = -\mathrm{T} + \sqrt{2}\,\mathrm{w}\left[\log\frac{1}{\mathrm{k}\sigma\sqrt{2\pi\mathrm{w}^2}}\right]^{\frac{1}{2}} + \tau_{\mathrm{D}}$ is the intercept component of the regression.

We used MATLAB to perform the regression and calculate the optimum values of a and b. The Figure 4.13 shows the points obtained for the simulation and the ones obtained through the regression. One can notice that there is good agreement between the two sets, with relatively low errors.

We found it is convenient to calculate $\Delta\mathrm{t}$ by assuming $w \to 0$ which can be defined as the influx function approaches a delta function calculated at where it reaches a maximum at $\mathrm{t} = \mathrm{T}$:
From The Appendix II, Eq. (6.6), when w approaches 0 and $[A] \gg \kappa$:

$$\frac{f(t)}{f_0} \to \delta[\mathrm{t} - \mathrm{T}]. \tag{4.17}$$

$$\frac{\partial[A]}{\partial t} = \delta[\mathrm{t} - \mathrm{T}] - \mathrm{K}\sigma. \tag{4.18}$$

Integrating across T and using the initial condition $[\mathrm{A}] = 0$:
For $t < T$,

$$[A] = 0.$$

For $t = \mathrm{T}^{+}$, we get

$$[\mathrm{A}(\mathrm{T}^{+})] = 1. \tag{4.19}$$

For $t > T$, the evaluation is

$$[\mathrm{A}] = \ 1 - \mathrm{K}\sigma(\mathrm{t} - \mathrm{T}). \tag{4.20}$$

We define the plateau duration $\Delta \mathrm{t}$ as the time interval for [A] to reach zero

Thus,

$$\Delta \mathrm{t} = \frac{1}{\mathrm{K}\sigma}. \tag{4.21}$$

4.5 Single loading Case – modification of γ with a width of 0.5 ms

The parameter γ defines the ratio between initial receptors concentration α to input acetylcholine concentration scale F. As in the study of σ, different values of γ were used to evaluate its effect. This procedure required changing values of α at fixed $\sigma(0.001)$. The values of γ obtained for this investigation were:

- 1.5×10^{-3}.
- 2.0×10^{-3}.
- 3×10^{-3}.
- 6.1×10^{-3}.
- 9.5×10^{-3}.

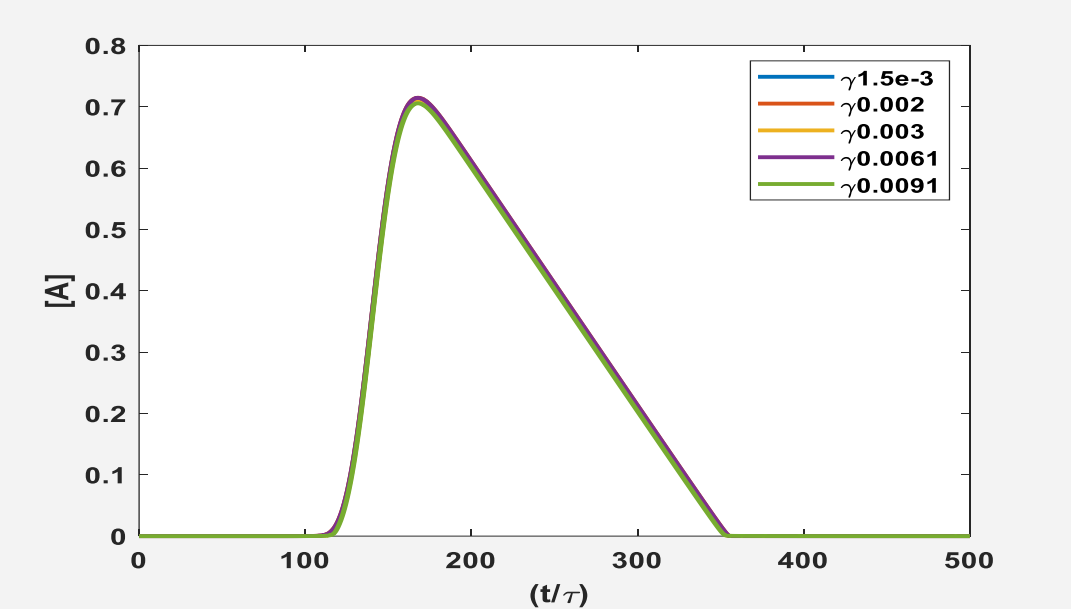

Figure 4.14: Concentration of acetylcholine for different values of γ at representative position $z = \frac{1}{2}$. The different is barely distinguishable from each other due to the superposition of the data. This indicates a relatively small effect of γ in the concentration of acetylcholine. Note $\sigma = 0.001$.

In general, it can be noticed that the curves are overlapping. Considering the role of γ in the process, it is expected that its increase would cause a decrease of ACh. As expected, the numerical simulation shows that when γ decreases, ACh becomes slightly higher than its canonical value when evaluated at the same time and spatial position. However, this effect is small, it can only be confirmed through an examination of the numerical results. Besides such effect, there is no major change in the simulation results, and it is difficult to see it on the plot.

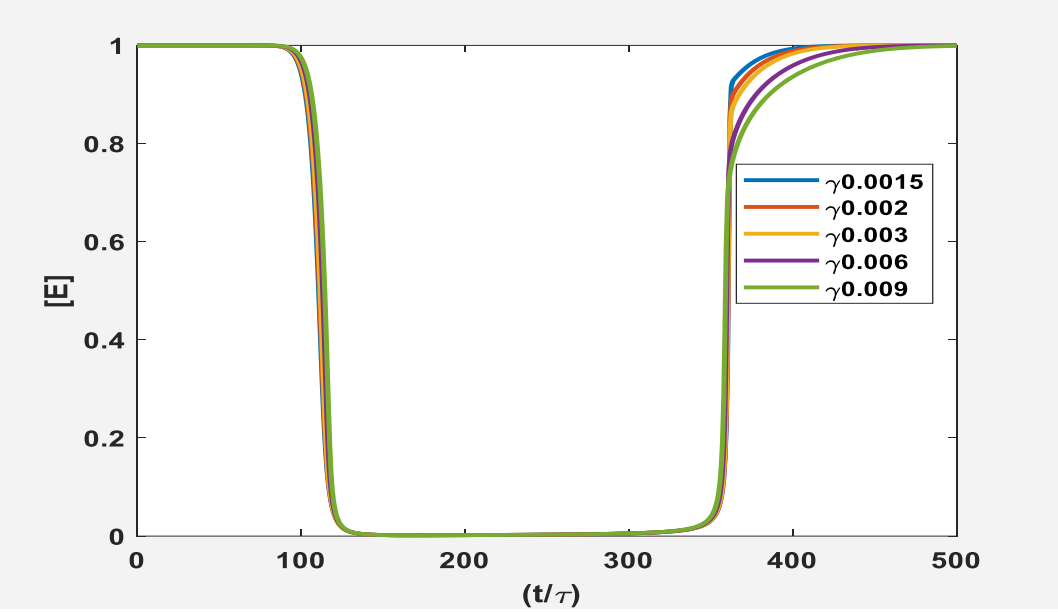

Figure 4.15: The enzyme concentration at representative position $z = \frac{1}{2}$ for all tested values of γ. In general, it can be noticed that the curves are overlapping, with slight differences in the recovery phase of the enzyme, where a faster recovery occurs for lower values of γ like 1.5×10^{-3}. Remember, $\sigma = 0.001$.

Figure 4.15 shows that the reaction process drastically consumes the enzyme concentrations as discussed before, followed by its regeneration at time 398 τ due to reaction AE. When $[A]$ is initially zero for these values of γ. Thus, changing γ (initial receptors concentrationα) would not have any major impact on the concentration of enzyme.

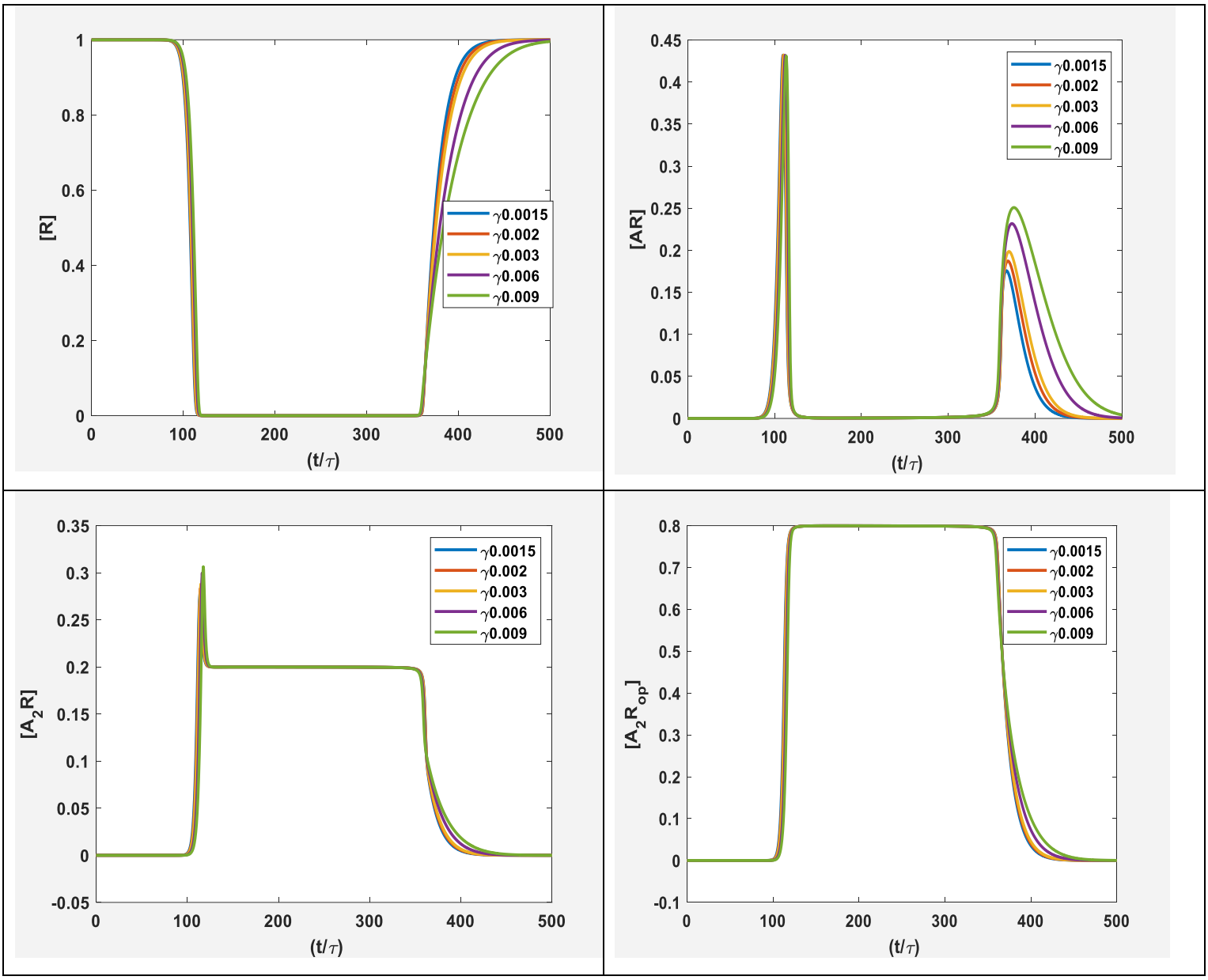

Figure 4.16: The concentration of receptor species for different values of γ from the range from 1.5×10^{-3} to 9.1×10^{-3}. Note $\sigma = 0.001$. There is almost no effect of this parameter on the dynamics of the receptor species.

Regarding the concentration of the receptors [R], it can be observed in Figure 4.16 that an increase in the value of γ causes a slight increase in the time for the complete recovery of receptors. Also, for the open and close receptors, the concentration for the different values of γ are almost identical, with the only distinguishable difference being the final slope after the plateau. In the reaction-diffusion process, the parameter γ changes the dynamics of the receptor-acetylcholine interaction, which is described in the boundary condition (at the base of the cleft). Changing this parameter changes the derivative of acetylcholine with space at position $z = 1$, with the effect propagating to the inner nodes of the simulation space. Still, it can be inferred from the concentration of the receptors in Figure 4.16 that the dynamics of this species is very fast, with a complete consumption of receptors. Also, the concentration of receptors for all evaluated scenarios (not scaled) is drastically lower than the concentration of acetylcholine. Therefore, changing γ causes no appreciable modification in acetylcholine concentration, as already stated.

Overall, the results show that changing γ does not change the concentrations significantly. Investigating the impact of γ in the concentration of acetylcholine reveals that, from the range 1.5×10^{-3} to 9.1×10^{-3}, there is almost no effect of this parameter changes on such species concentrations.

4.6 Single loading Case – investigation of the effect of Acetylcholine influx and a width of 0.5 ms

Due to the high impact of σ (the ratio of initial enzyme concentration [E_{tot}] the [A] scaled concentration)on the reaction-diffusion process, we evaluated the effect of another process parameter that has an effect on σ for a fixed initial enzyme concentration, which is the input flux parameter (F). According to the equations involved in the process it affects the following variables:

- σ
- γ
- $\mathrm{K_R}$
- $\mathrm{K_{AR}}$
- $\mathrm{K_{AE}}$
- κ

The value of flux F is inversely proportional to σ for a fixed initial enzyme concentration. For that reason, the schedule of investigated values consisted of lower values of F, to obtain higher values of σ. The following values were chosen:

- $2.17 \times 10^{-10}\mathrm{moles/cm^2}$
- $5.4 \times 10^{-10}\mathrm{moles/cm^2}$

They consist in a decrease from the base value from Table 3.1 of four times ($5.4 \times 10^{-10}\mathrm{moles/cm^2}$) and ten times ($2.17 \times 10^{-10}\mathrm{moles/cm^2}$).

Table 4.8- Reaction-diffusion properties for flux F.

Variable	**Values for F= $\mathbf{2.17 \times 10^{-10}}$ moles/cm²**	**Values for F= $\mathbf{5.4 \times 10^{-10}}$ moles/cm²**
Scaled concentration A (C)	$\mathrm{C} = \frac{\mathrm{F}}{\mathrm{L}} = 0.434 \times 10^{-3} M$	$\mathrm{C} = \frac{\mathrm{F}}{\mathrm{L}} = 0.108 \times 10^{-3} M$
σ	0.1	0.041
γ	0.152	0.06
$\mathrm{K_R}$	46.5	116.25
$\mathrm{K_{AR}}$	46.5	116.25
$\mathrm{K_{AE}}$	310	3.1×10^3
κ	0.0128	1.28×10^{-3}

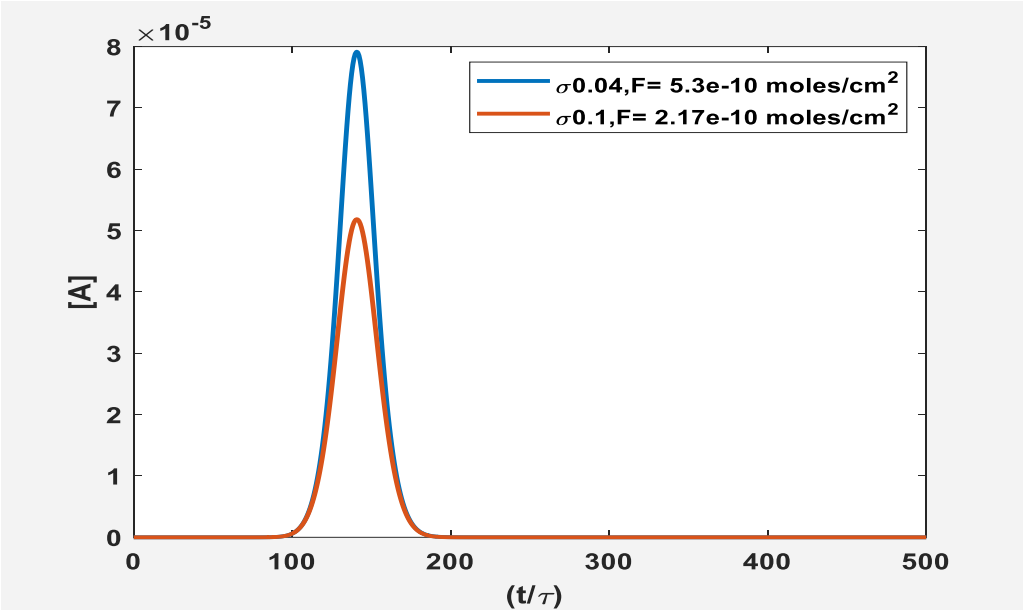

Figure 4.17: Concentration of acetylcholine at representative position $z = \frac{1}{2}$ for various values of F (5.4×10^{-10} and 2.17×10^{-10}). Note, when F =5.4×10^{-10}, $\sigma = 0.04$ and $\gamma = 0.06$ while when $F = 2.17 \times 10^{-10}$, $\sigma = 0.1$ and $\gamma = 0.152$.

It is noticed that the influx has a definite effect on the acetylcholine concentration, as already mentioned in the results in Figure 4.17. A decrease in the flux (F) causes a decrease in ACh concentration. Besides, Figure 4.17 shows the concentration scale of ACh is directly proportional to $C = \frac{F}{L}$. Importantly, decreasing F leads to an increase in the parameter σ (for a fixed initial enzyme concentration), which has a notable impact on hydrolysis ACh. Therefore, [A] is dramatically decreased as shown in Figure 4.17.

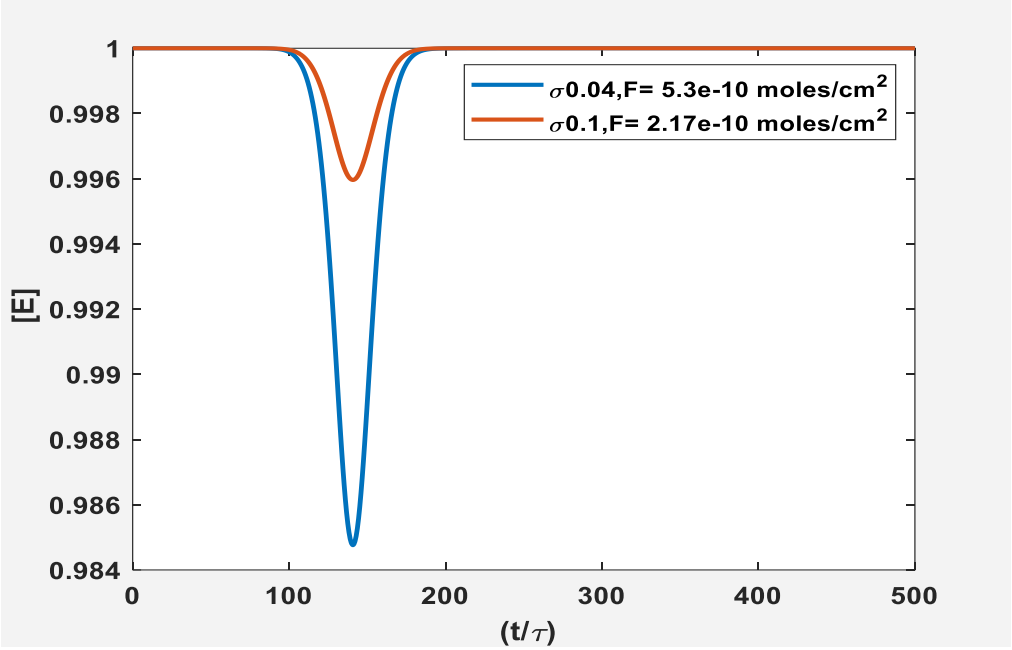

Figure 4.18: Enzyme concentration for various values of flux (F) previously mentioned at representative position $z = \frac{1}{2}$. Note, when $F = 5.4 \times 10^{-10}$, $\sigma = 0.04$ and $\gamma = 0.06$ while when $F = 2.17 \times 10^{-10}$, $\sigma = 0.1$ and $\gamma = 0.152$.

Figure 4.18 shows that the reaction process lightly consumes the enzyme concentrations due to the decrease in the flux *(F)* with the decrease in [A], followed by its regeneration. These low values are reflected in the concentration of enzyme, which decreases as low as 2.5% and 1.5% for 5.4×10^{-10} and 2.7×10^{-10},respectively. Thus, decreasing F impacts [E].

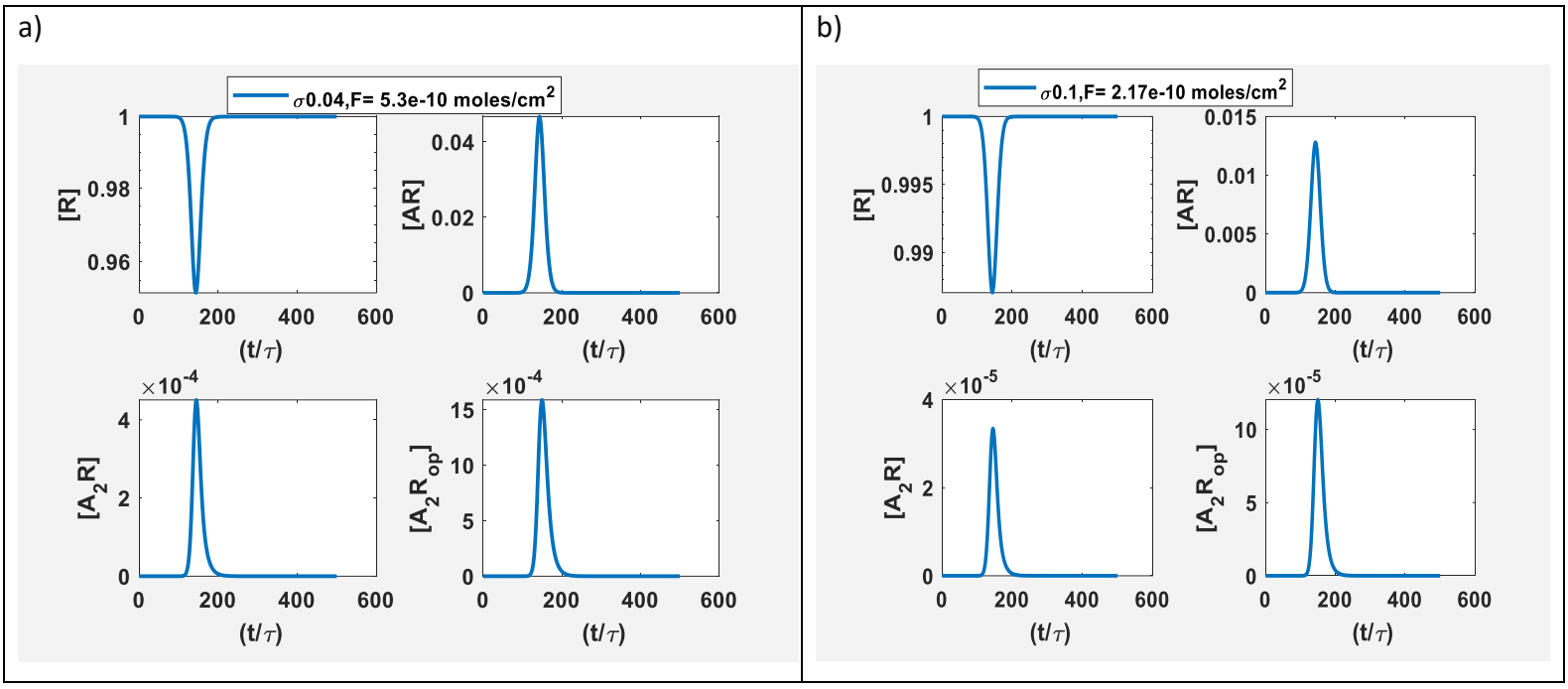

Figure 4.19: Concentration of receptor species for flux (F) a) 5.4×10^{-10} and b) 2.7×10^{-10}. Note that the peak concentration of open receptors $[\mathrm{A_2R_{op}}]$ for flux 2.7×10^{-10} lies slightly lower than 10^{-5}, while the same peak for flux 5.4×10^{-10} is approximately 10^{-4}. In both cases, such peak can reasonably be considered as negligible. A similar effect is observed for the species $[\mathrm{A_2R}]$. These low values are reflected in the concentration of receptors $[\mathrm{R}]$, which decreases as low as 4% and 1% for 5.4×10^{-10} and 2.7×10^{-10} respectively.

The magnitude of F has a direct effect on the reaction rate of ACh and receptors with reaction constant $\mathrm{K_R}$ and $\mathrm{K_{AR}}$. A low flux will necessarily cause a low consumption rate, with a low concentration of bounded species and relatively small changes in the concentration of receptors. Such change may not be enough to produce a significant number of open receptors. Such a behavior can be seen in Figure 4.19, where a substantial zoom was applied to the y-axis, so any difference in the concentration profiles can be noticed. Therefore, using such low values of F is not useful to obtain a quantitative estimate of open receptors.

4.7 200 Hz loading Case - Diffusion-reaction process with reference parameter values and a width of 0.5 ms

The reaction-diffusion process was investigated using a release cycle of three loading cycles at frequency 200 Hz, as shown in Figure 4.1.

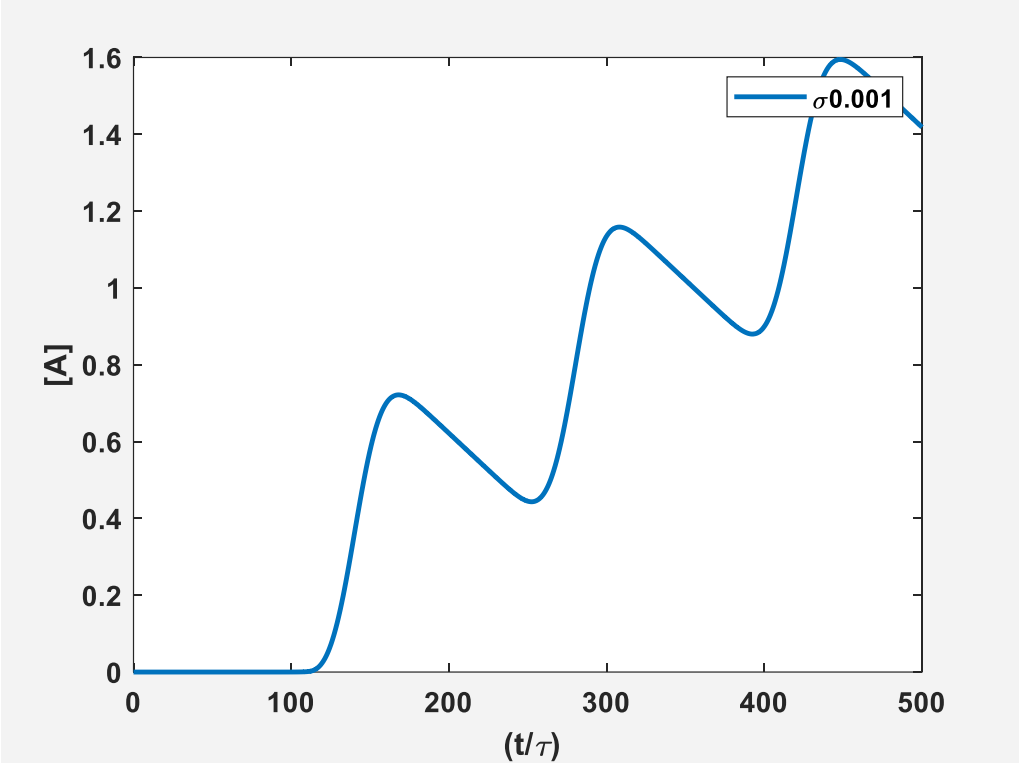

Figure 4.20: Concentration of acetylcholine at representative position $z = \frac{1}{2}$. A is consumed by the enzyme with three loading cycles with a frequency of 200 Hz (5ms) and a distribution width of 0.5ms. ACh concentration steadily increases and reaches a peak after the inflow. The concentration only significantly changes when another inflow peak is released, showing a steady increase in concentration. Therefore, there are three peaks due to these three loads.

Concentration peaks occur at the times indicates in table 4.9.

Table 4.9– Time and Concentration peaks form Figure 4.20.

Scaled Time	**Time (ms)**	**Concentration of Acetylcholine**
165.4τ	5.80	0.71(3.08x 10^{-4}M)
258 τ	9.03	0.45(1.95x 10^{-4}M)
308.2 τ	10.79	1.15(4.99x 10^{-4}M)
393.6 τ	13.78	0.88(3.819x 10^{-4}M)
448.8 τ	15.71	1.5 (6.51x 10^{-4}M)

Figure 4.20 illustrates the dynamics of acetylcholine with the reaction-diffusion process. Such dynamics are clearly distinguishable from the one shown in Figure 4.2, where no reaction takes place, and only diffusion occurs. The concentration initially increases steadily with the release, but as soon as this release decreases, the reaction process causes consumption of acetylcholine, with subsequent reduction of its concentration. Still, a new release causes an inflection on the concentration curve, with subsequent increase of the concentration. The same behavior is observed for the three release cycles.

From the reaction with the enzyme, one can observe that there is a short “delay” on the increase of acetylcholine concentration, which is attributed to the reaction with the enzyme. In the pure diffusion process, as soon as the loading takes place, the concentration starts to build up steadily. However, in the presence of the enzyme, such build- up is only noticeable after its complete consumption, thus the concentration of enzyme vanishes and free acetylcholine in the medium remains.

a)

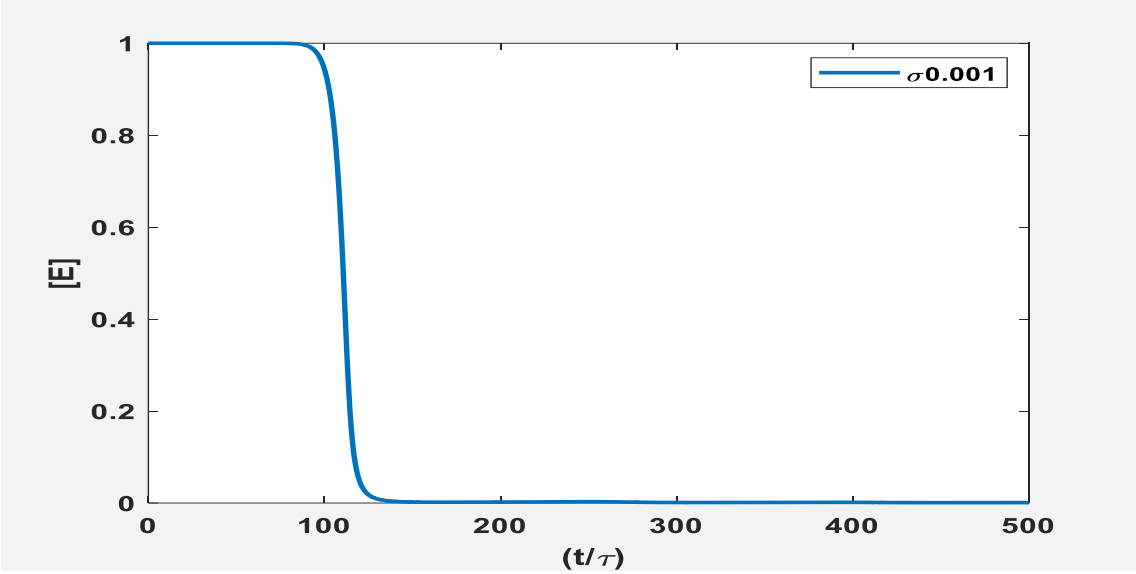

b)

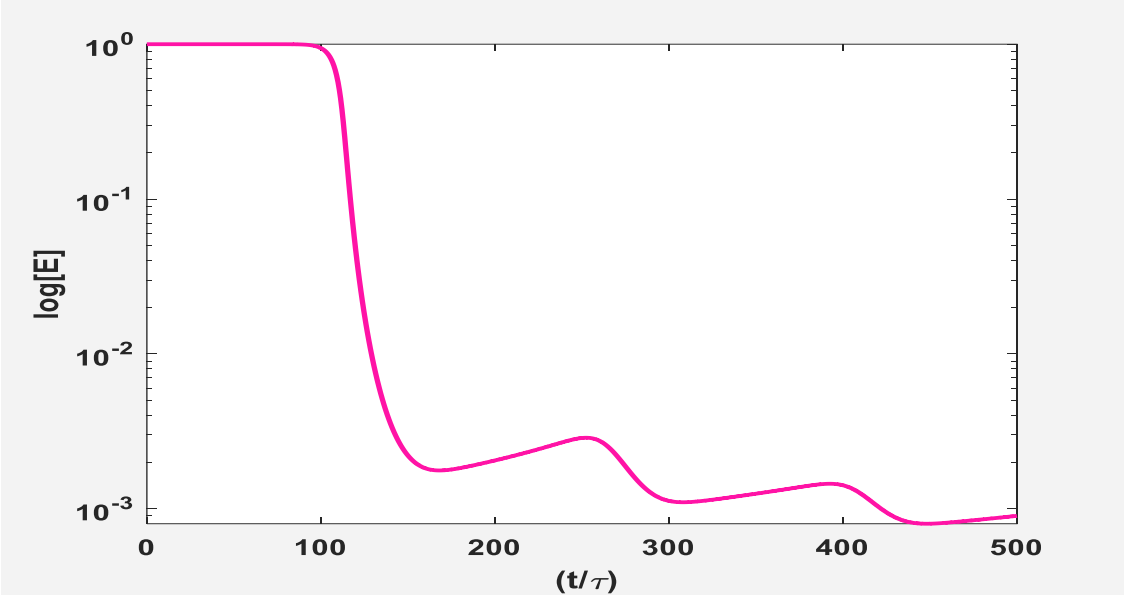

Figure 4.21: Concentration of enzyme in a) linear scale and b) semi-log scale. Loading cycle with a frequency of 200 Hz with a distribution width of 0.5ms at representative position $z = \frac{1}{2}$. Notice that a sharp decrease in the concentration is observable at time 100 τ (3.85 ms) to reach values near zero (less than 0.01) at 134.8 τ(4.7 ms). From the semi-log Figure, one can better visualize that the concentration of the enzyme exhibits valleys (low concentration) and hill (peak concentration).

The concentration of enzyme starts to drop at 98.14 τ (3.43 ms) (Figure 4.21), reaching a first valley at 161.6 τ with scaled concentration 1.8×10^{-3}. The hill that follows occurs at time 256.5 τ with concentration 2.8×10^{-3}. A second valley is observed at 298.5 τ and concentration 1.1×10^{-3}. A hill follows this at 395.7 τ with scaled concentration 1.4×10^{-3}, subsequently dropping until it reaches the last valley at time 441.6 τ with concentration 8×10^{-4}, which corresponds to the concentration value 3.6×10^{-7} M.

It is relevant to notice that the concentration of the enzyme does not reduce directly to zero after the loading of acetylcholine, but it reaches drastically low values. Still, a log-plot of this concentration, as illustrated in Figure 4.21, shows that the effect of loading cycles is noticeable on the concentration of the enzyme, in this case through three short, consecutive oscillations. This phenomenon can be seen from the relation between enzyme and acetylcholine concentrations given by equation 3.40:

$$[\mathrm{E}] = \frac{\kappa}{\kappa + [\mathrm{A}]}.$$

So as [A] oscillates between maxima and minima, [E] oscillates correspondingly.
The concentration of the enzyme would only be equal to zero if $\kappa = 0$ (which is never the case) or if the concentration of A tends to infinity. In any other case, the enzyme concentration may still be very low, but not zero.

a)

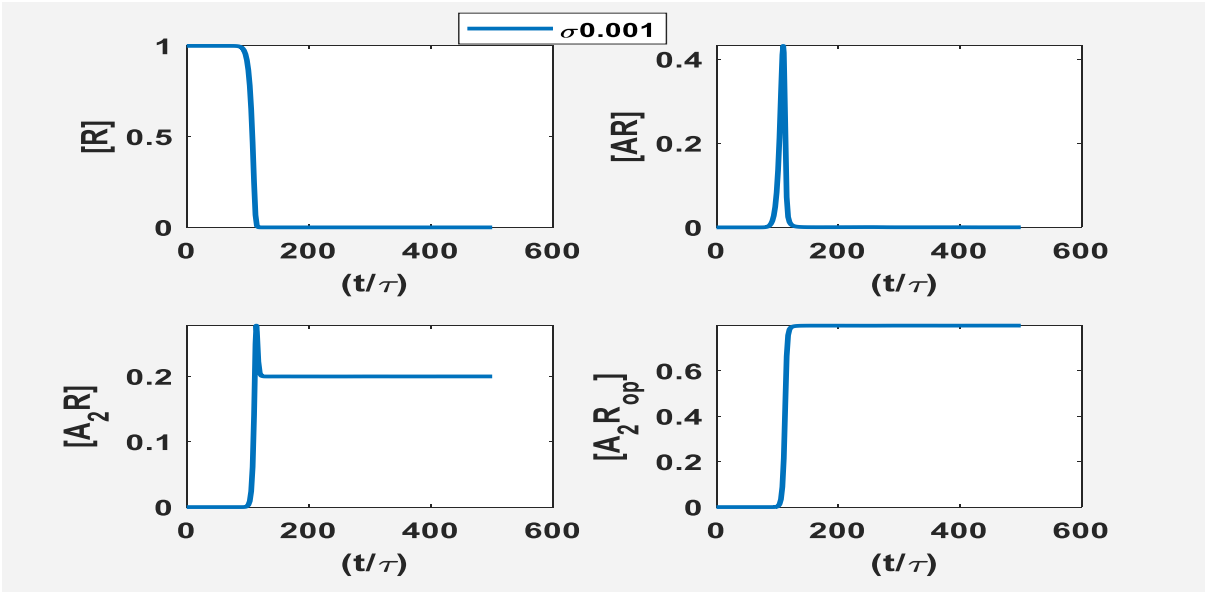
σ0.001
[R]
[AR]
[A2R]
[A2Rop]
(t/τ)

b)

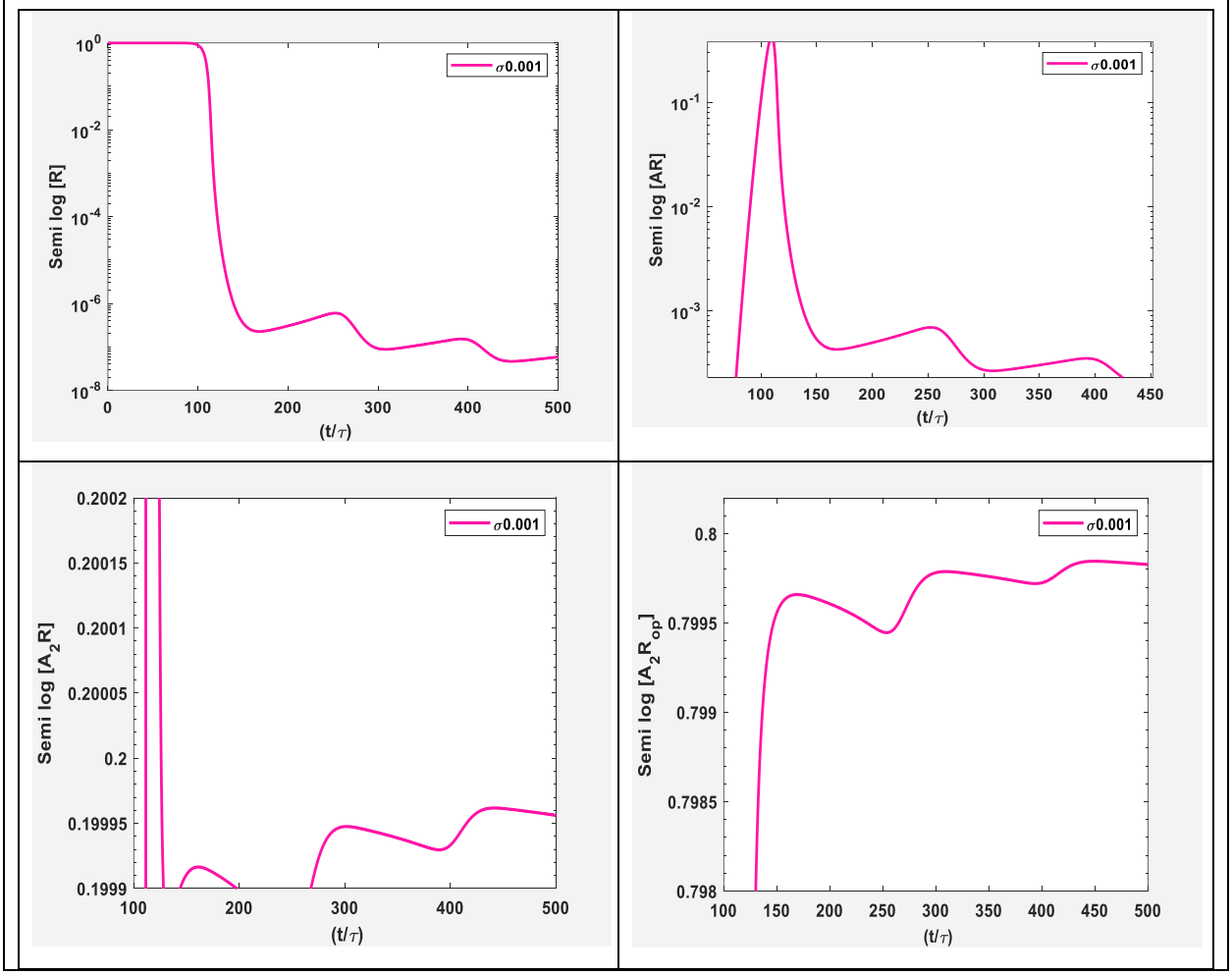
σ0.001
Semi log [R]
Semi log [AR]
Semi log [A2R]
Semi log [A2Rop]
(t/τ)

Figure 4.22: Concentration of receptors [R]and other species $[\mathrm{AR}]$, $[\mathrm{A_2R}]$, $[\mathrm{A_2R_{op}}]$. Loading cycle with a frequency of 200 Hz(5ms) with a distribution width of $0.5\mathrm{ms}$. a) The top left subplot above illustrates the concentration of the receptor [R] with respect to time. Initially, this concentration is set to one (1) as that all the receptor species concentrations have an initial value of zero. b) Semi-log concentration of receptors $[\mathrm{R}]$ and other species $[\mathrm{AR}], [\mathrm{A_2R}], [\mathrm{A_2R_{op}}]$. The concentration of the receptors species exhibits small fluctuations concentration

In Figure 4.22 a), the [R] decrease in value is noticeable at 90τ, reaching almost zero at time 119 τ. At 119 τ, the concentration becomes less than 10^{-6}, with some subsequent short fluctuations. Since this behavior at low concentration values cannot be observed in full scale, Figure 4.22 b) is used to show it using a semi-log axis. These releases, though relatively small, occur between 200 τ and 300 τ, and between 300 τ and 450 τ.

In Figure 4.22 a), the concentration of the species $[\mathrm{AR}]$, initially equal to zero, starts to increase at approximately 88.9 τ,reaching a peak at 109.7 τ with a maximum instantaneous concentration of 0.4 or 1.32×10^{-12} M. After reaching this value, the concentration sharply decreases, reducing to approximately zero at around 125 τ .Using semi-log plot, as shown in Figure 4.22 b), such concentration slightly fluctuates with drastically low magnitude, showing the same periods mentioned for the receptors (between 200τ and 300τ, and between 300τ and 450τ).

The concentration of species$[\mathrm{A_2R}]$ is shown in the bottom left of Figure 4.22 a), is zero at the beginning. It starts to rise at 97.4 τ. A sharp peak occurs at 130.9 τ with a scaled concentration value equal to 0.27. As soon as $[\mathrm{A_2R}]$ reaches a peak, it decreases very fast, reaching a pseudo-steady state with a concentration of 0.2 (6.6×10^{-13} M) at 126.1 τ. This magnitude, though apparently constant, fluctuates with shallow magnitude. Such releases can be noticed in Figure 4.22 b), with periods like the ones mentioned for receptors and [AR].

In Figure 4.22 a), the concentration of $[\mathrm{A_2R_{op}}]$, like $[\mathrm{A_2R}]$, is initially equal to zero. It starts to rise at 99.9 (3.49 ms) until it reaches a scaled concentration value of 0.79 at time 100.3 τ

(3.51 ms). In Figure 4.22 b) the three releases, though relatively small, occur between 200 τ and 300 τ, and between 300 τ and 450 τ similarly to the one mentioned for the bounded species.

4.8 200 Hz Loading Case –the effect of σ with a width of 0.5 ms

Further investigation of synaptic transmission was performed by studying the role of the parameterσ on the dynamics of the system over three loading cycles at 200 Hz (corresponding to realistic rate in electric fish) and a width of 0.5 ms.

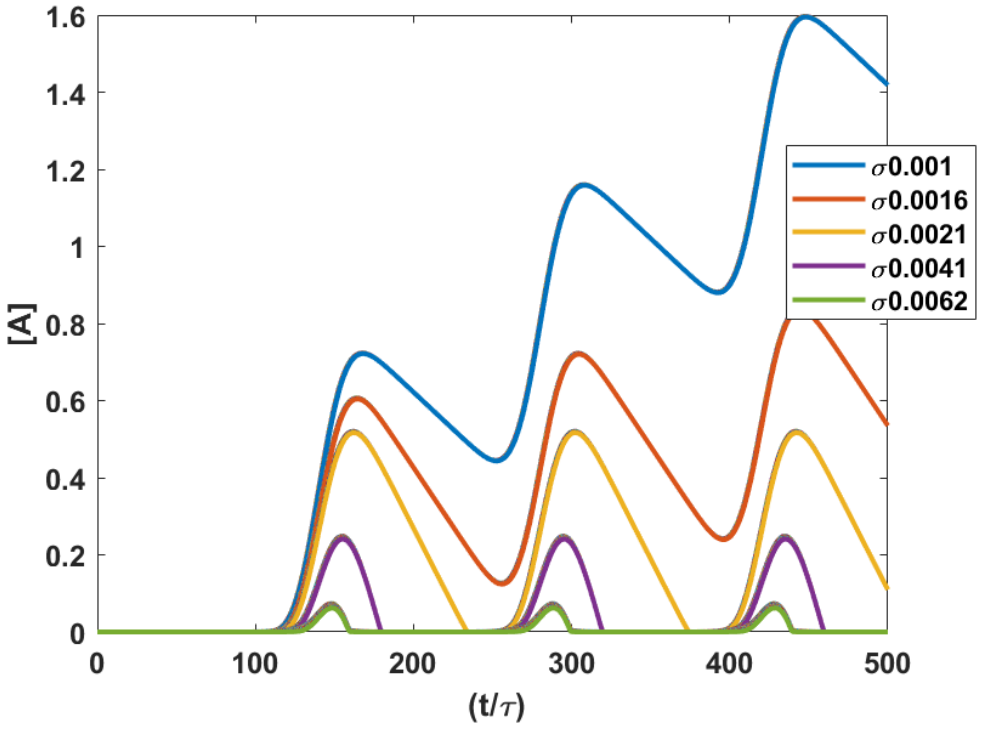

Figure 4.23: Concentrations of ACh for different values of σ at representative position $z = \frac{1}{2}$ for three loading cycles with a frequency of 200 Hz and a distribution width of 0.5ms. The value of σ drastically changes the dynamics of the process, with clearly distinguishable concentration of ACh.

Figure 4.23 shows the dynamics of acetylcholine with different values of σ. There is a distinguishable variation of acetylcholine as σ changes. The concentrations initially increase with

the release, but as soon as this release decreases, the reaction process causes consumption of acetylcholine, with subsequent reduction of its concentration. For lower values of σ, it is observed that ACh accumulates along time, while for higher values (σ>0.0021), its concentration vanishes from time to time, being completely consumed. New loading events generate an inflection on the concentration curve, with a subsequent increase of the concentration. The same behavior is observed for the three release cycles. With increasing σ, it can be noted that the maxima of ACh concentrations become lower with large σ, which is attributed to the reaction with the enzyme. However, in the presence of the enzyme, there is a build-up of ACh, which is only noticeable with lower σ.

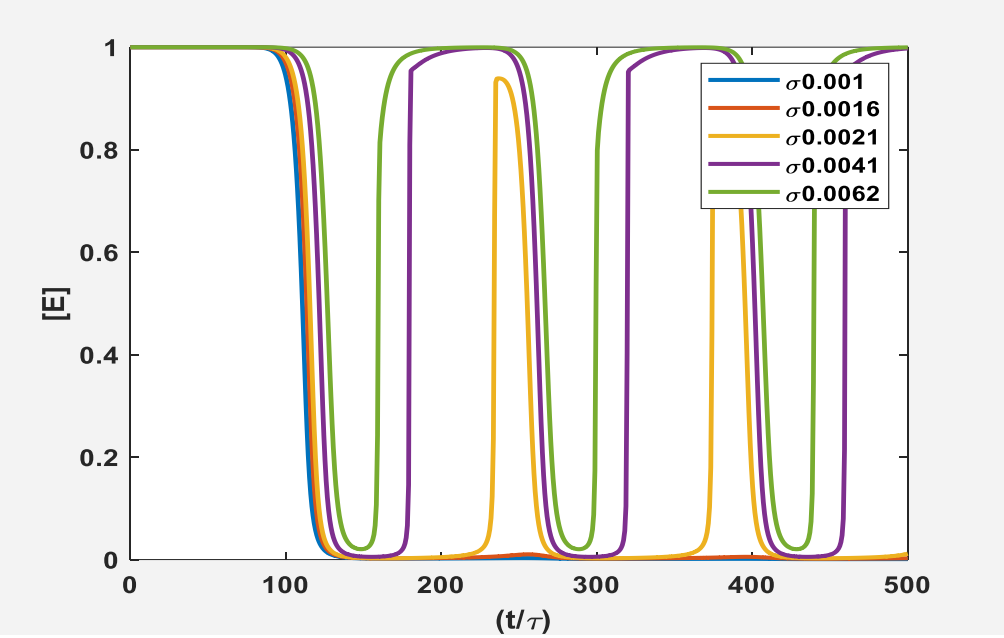

Figure 4.24: Shows enzyme concentration for different values of σ, for the same loading cycles as in Figure 4.23 at 200 Hz and a distribution width of 0.5ms at representative position $z = \frac{1}{2}$. Sharp edges can be observed for higher values of σ, indicating its high effect on the dynamics of the process.

As seen in Figure 4.24, the concentrations of the enzyme diminish directly to zero after the loading, which is the result of the reaction ACh with AChE. Importantly when σ is large (0.0041,0.0062), $[\mathrm{E}]$ increases again as soon as it reaches zero. It is relevant to mention that the reaction time with ACh becomes short when σ increases. Also, Figure 4.24 displays that the effect of loading cycles is noticeable on the concentration of the enzyme with continuous oscillations due to the relation between enzyme and acetylcholine, as discussed before.

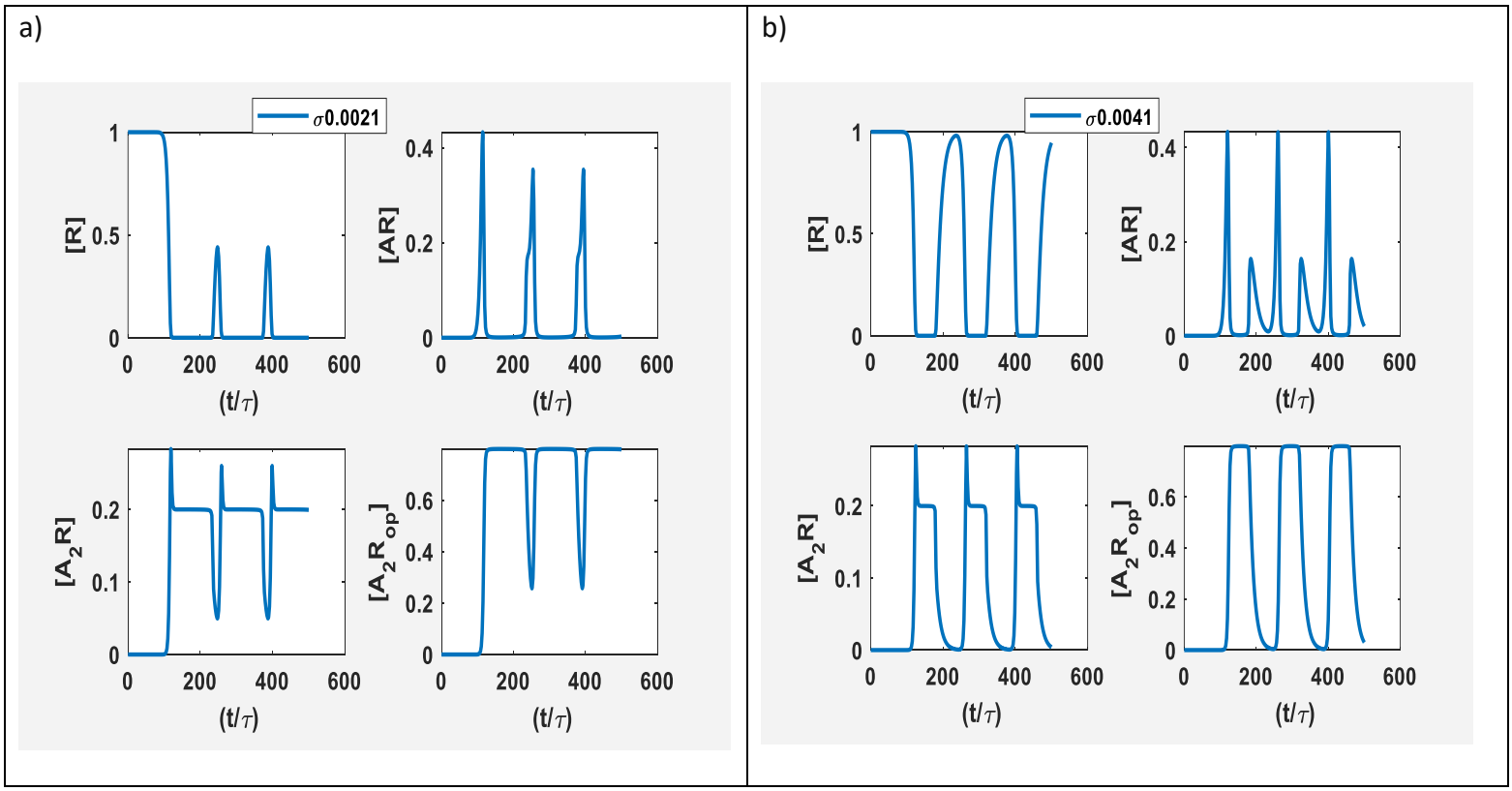

Figure 4.25: Receptors species concentration for a) $\sigma = 0.0021$ and b) $\sigma = 0.0041$. Using the same loading cycles as Figure 4.23 a frequency of 200 Hz and a distribution width of $0.5\mathrm{ms}$. For lower values of $\sigma = 0.0021$, it is observed that open receptors $[\mathrm{A_2R_{op}}]$ start to appear at 107τ or 3.75 ms with the duration of the plateau equals to $101.86\,\tau$ or 3.6ms while for $\sigma = 0.0041$, $[\mathrm{A_2R_{op}}]$ start at $114.7\,\tau$ or 4 ms with the duration of the plateau equals to $40.68\,\tau$ or 1.42ms.

In Figure 4.25 [R] decreases at 90 τ, monotonically reaching to almost zero at time 119 τ and increases again at 228 τ ,179.8 τ for σ=0.0021 and σ=0.0041, respectively. Besides, in Figure4.25 (a), [R]reaches a peak at 249 τ for σ=0.0021 with a maximum scaled concentration of 0.44. In contrast, when σ = 0.0041 Figure4.25 (b), [R] reaches a maximum concentration of 0.99 at around 230.9 τ. Importantly, it is noticed that when σ is small, [R] would not completely recover after the first loading. At this point, the results of intermediary species reveal that the concentration of the receptor [R] affects other species. When σ = 0.0041 (Figure4.25b), it is noticed that [AR] reaches a peak (0.45) and drops down to zero. After a duration of 42 τ, the concentration starts to grow again reaching almost one-fifth of [AR] maximum (0.16) In Figure 4.2(b), $[\mathrm{A_2R}]$ increases attaining a value of 0.28 at its maximum, then, decreases, reaching a pseudo-steady state with concentration 0.2. $[\mathrm{A_2R}]$ maintains its state with a period of 42 τ, then drops to zero.

Regarding the receptor species, interpretation of the results shown in Figure 4.25 is best achieved by analysing the concentration of open receptors $[\mathrm{A_2R_{op}}]$, since they enable a better understanding of firing signals at higher frequencies. For $\sigma = 0.0021$, one can notice that open receptors do not reach zero during the simulation. In contrast, simulation with $\sigma = 0.0041$ shows a complete closing of open receptors at each loading. Overall, it is found that for lower σ, $[\mathrm{A_2\ R_{op}}]$ is not zero.

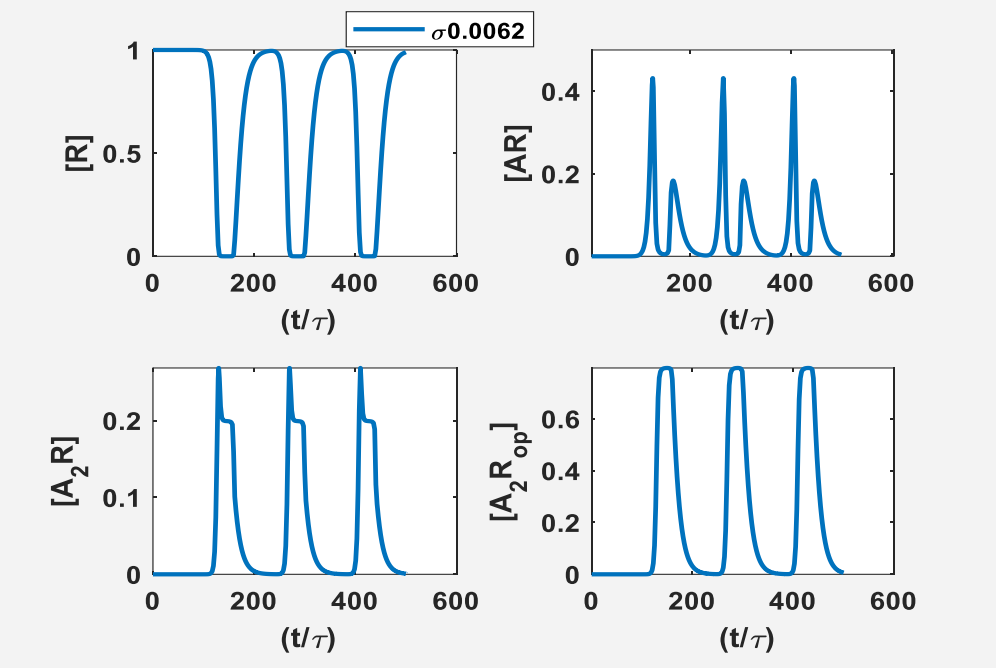

Figure 4.26: The concentration of receptors species at 200 Hz and a distribution width of 0.5ms. Here, $\sigma = 0.006$. The concentration of the open receptor appears at 119 τ with the duration of the plateau is equal to around 14.33 τ.

In Figure 4.26, the concentration of receptors species has a similar behavior as it is discussed before (Figure 4.25). Since open receptors enable a better understanding of high-frequency dynamics, the following discusses some properties extracted from Figure 4.26. Concerning [A_2R_{op}], the open receptors concentration appears to increase at 107τ, reaching a plateau of duration of 2.7τ. Also, increasing σ contributes to dropping [A_2R_{op}] down to zero during loading cycles (complete closing of open receptors).

Figure 4.27 shows the effect of choosing larger values of σ on the concentration of ACh.

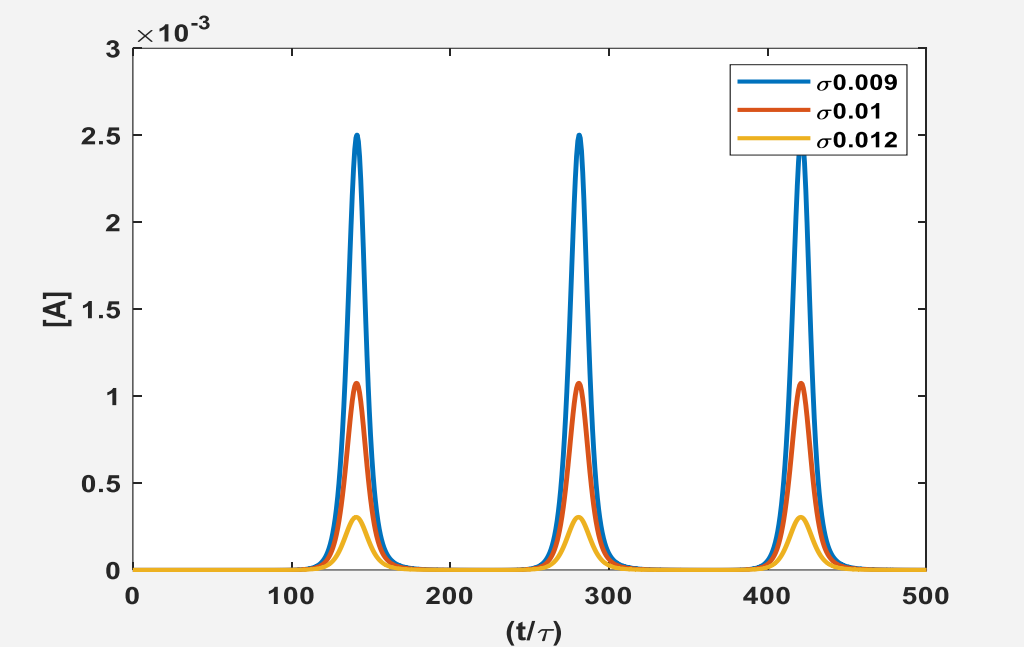

Figure 4.27: Concentration of ACh for σ 0.009, 0.01 and 0.012 at representative position $z = \frac{1}{2}$. Loading cycles with a frequency of 200 Hz and a distribution width of 0.5ms. For the simulation of the reaction-diffusion process with larger σ, the concentration of ACh shows steeper curves that exhibit abrupt linear decay.

Table 4.10. summarizes the results observed in the Figure 4.27, regarding the peak concentration values for the different values of σ investigated.

Table 4.10. Summary of results for acetylcholine concentration at higher values of σ.

σ	Scaled Concentration at Peaks
0.009	0.00245
0.01	0.001
0.012	0.002

Figure 4.27 illustrates the concentrations of acetylcholine with larger values of σ. The reaction between a high concentration of enzyme and acetylcholine concentrations causes high consumption of acetylcholine, with subsequent reduction of its peaks. For large values of σ, it is observed that ACh cannot reach a maximum larger than 2.5×10^{-3} $(10^{-3}M)$ as displayed in table 4.8. For example, when σ is higher than 0.009, ACh concentration vanishes from time to time rapidly, being completely consumed (steeper slope).

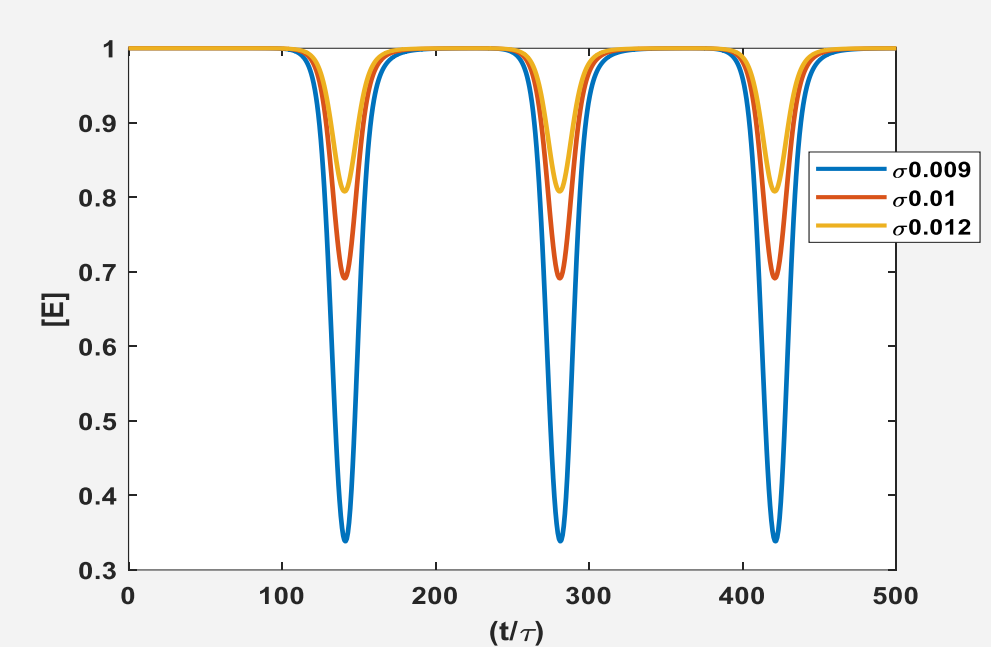

Figure 4.28: Concentration of enzyme for σ 0.009, 0.01 and 0.012 at representative position $z = \frac{1}{2}$. Loading cycles with the frequency of 200 Hz and a distribution width of 0.5ms.

Figure 4.28 illustrates the concentrations of the enzyme using the same loading cycles and larger values of σas Figure 4.27. [E] reduces at 107.8 τ with a concentration of 0.99 when enzyme reacts with ACh concentration. It is noticed that enzyme concentrations are never reaching zero when σ is large. This behaviour proves the relationship between E and A, which is stated as, $\mathrm{E} = \frac{\kappa}{\kappa+\mathrm{A}}$. This equation gives that when the concentration of ACh increases, E decreases. The recovery time (time until enzyme concentration is 99% recovered) for the different values of σ is summarized in table 4.11. Thus, when A increases E decreases.

Table 4.11 - Summary of results obtained for enzyme concentration with σ equals to 0.009, 0.01 and 0.012.

σ	Upside down peak concentration	Time	Recovery time
0.009	0.33	141.8 τ (4.9ms)	179.7(6.4ms)
0.01	0.69	141.8 τ (4.9ms)	179.7(6.4ms)
0.012	0.81	141.8 τ (4.9ms)	179.7(6.4ms)

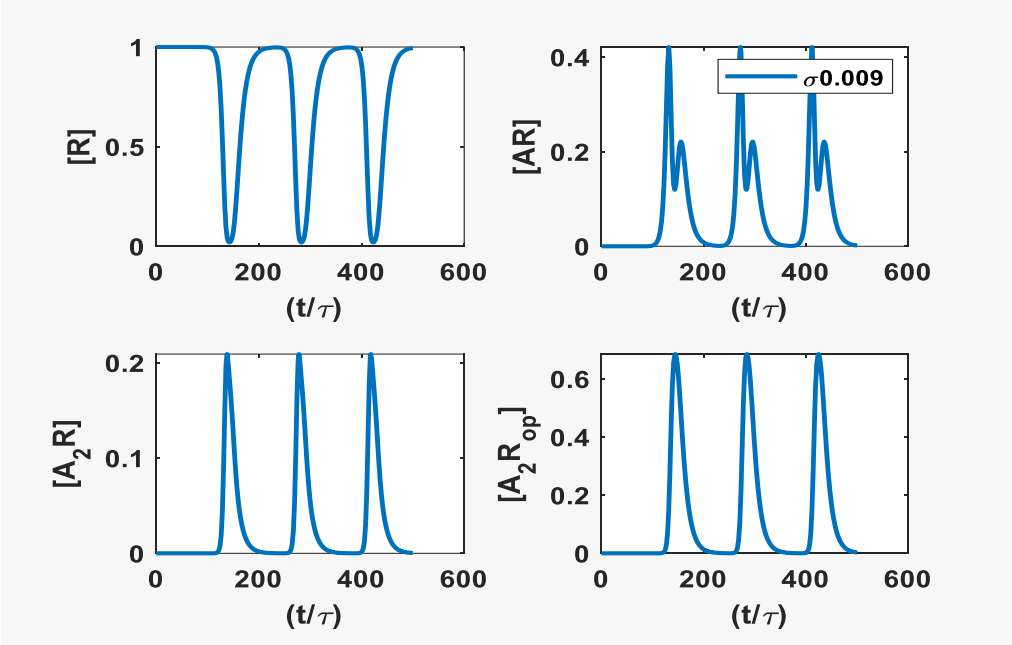

Figure 4.29: The concentration receptor species with $\sigma = 0.009$. Loading cycles with a frequency of 200 Hz and a distribution width of 0.5 ms. For this value of σ, one can clearly observe that the open receptors $[A_2R_{op}]$ (shown in the bottom right Figure) reaches a value of zero.

In Figure 4.29 shows the reaction dynamics of the receptor species using σ =0.009 at the 200 Hz loading cycles. The concentration of receptors species behaves similarly as it is discussed before (Figure 4.26), but $[A_2R]$ decreases sharply after it reaches a peak. At this point, the distinctive feature of $[A_2R]$ cannot be observed as seen in the previous section (Figure 4.25,4.26)

By Increasing the value of σ, it is possible to investigate the opening and closing receptors dynamics at a high frequency. For such a purpose, open receptors $[A_2R_{op}]$ dynamics were investigated with $\sigma = 0.009$ in Figure 4.29. $[A_2R_{op}]$ increases sharply, reaching a maximum scaled concentration of 0.65 at 144.4 τ and then monotonically reaching zero, indicating that $[A_2R_{op}]$ closes at certain higher values of σ , which is a desirable effect.

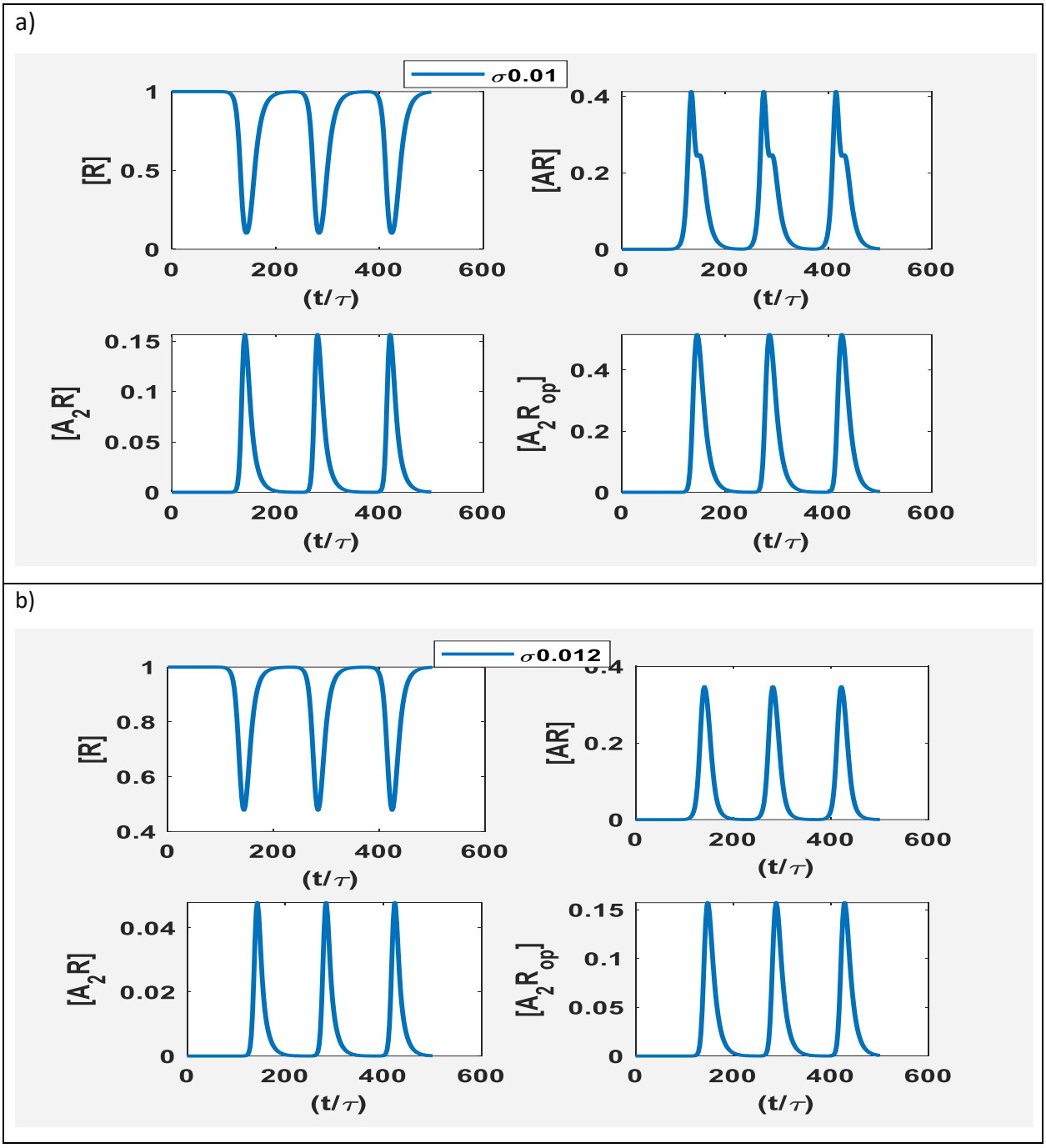

Figure 4.30: The concentration of receptor species a) $\sigma = 0.01$ and b) $\sigma = 0.012$. loading cycles with a frequency of 200 Hz and a distribution width of 0.5 ms. For σ=0.01, $[A_2\ R_{op}]$ has a maximum concentration (0.45) while For σ=0.012, the maximum concentration of $[A_2R_{op}]$ is 0.15.

Further investigation on the range of high frequency is illustrated in Figure 4.30, which shows the concentration of receptor species evaluated at $\sigma = 0.01$ and $\sigma = 0.012$.

It is noted that the same behaviour of the dynamics receptors occurs when σ equals to 0.01 and σ= 0.012, as mentioned in Figure4.29. However, with such a high value of σ, a significant difference in the concentration of $[\mathrm{AR}]$ and $[\mathrm{A_2R}]$ can be observed in Figure 4.30. Particular attention should be paid to [AR], which has different structures compared to previous results. When σ= 0.01, [AR] starts increasing, reaching a maximum. As soon as it reached the maximum, it drops to 0.25. After attaining one-fifth of its maximum, [AR] decreases again to zero. Whereas, this structure is not observed in the case of $\sigma = 0.012$, [AR] drops directly to zero.

In addition, it is seen that at $\sigma < 0.01$, a short peak in $[A_2R]$ follows a higher one at each loading cycle. This is not observed for the case where $\sigma \geq 0.01$, as illustrated in the Figure 4.29. The existence of such a double-peaks effect could be of interest for experimental investigation.

Higher values of σ were also tested to observe up to which point it is possible to observe the opening and closing receptors. In Figure 4.30, $\sigma = 0.012$ proved to be a limiting value, since evaluating values of σ higher than σ= 0.012, the acetylcholine starts to be completely consumed by enzyme; consequently, no opening receptors can be observed.

4.9 200 Hz Loading Case – Investigation of loading with a width of 0.2 ms

To better visualize the opening and closing of receptors, we examined how the width of each loading event affects the dynamics of the process. Figure 4.31 shows the loading cycles with a width 0.2 ms.

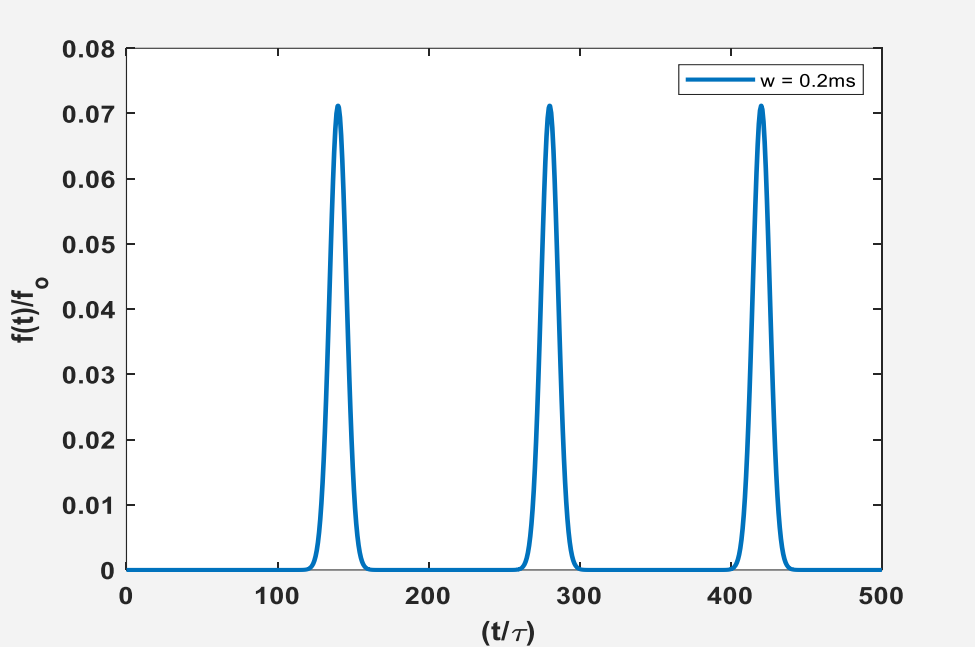

Figure 4.31: Three loading cycles with a distribution width of 0.2 ms (46 τ) and a period of 5ms.

Figure 4.31 shows the three ACh release cycles for a frequency of 200 Hz. Three Gaussian-shaped fluxes events are shown a distribution width of 0.2ms. It can be observed that the three peak inflows fall on 140.8 τ, 280.6 τ, and 420.4 τ, which corresponds to 5, 10, and 15 ms.

The corresponding concentration obtained for the acetylcholine with these conditions is shown in Figure 4.32.

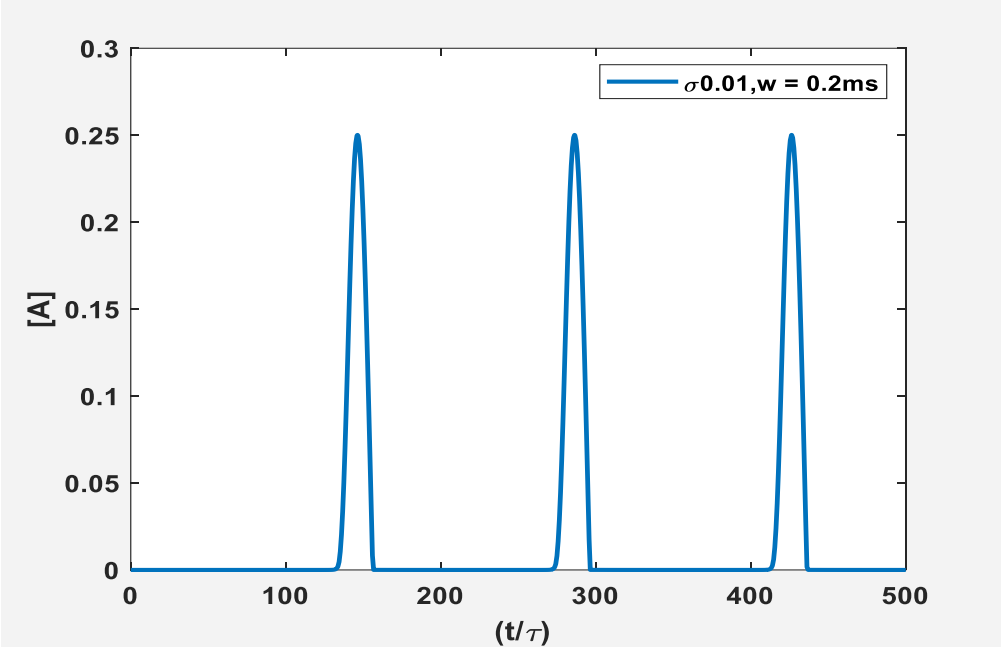

Figure 4.32: Concentration of ACh at a representative position $z = \frac{1}{2}$. Loading cycles with a frequency of 200 Hz and a distribution width of $0.2\ \mathrm{ms}$ with a period of 5ms. The ACh concentration clearly differs from the 200 Hz loading cycle with a width of 0.5 ms (Figure4.23).

For the previous scenario (Figure4.23), concentration builds-up, accumulating with the simulation time. However, in Figure 4.32, the concentration curves are distinguishable with no accumulation of ACh. The peak concentrations reach approximately 0.24, corresponding to 0.1M, and width equals 23τ.

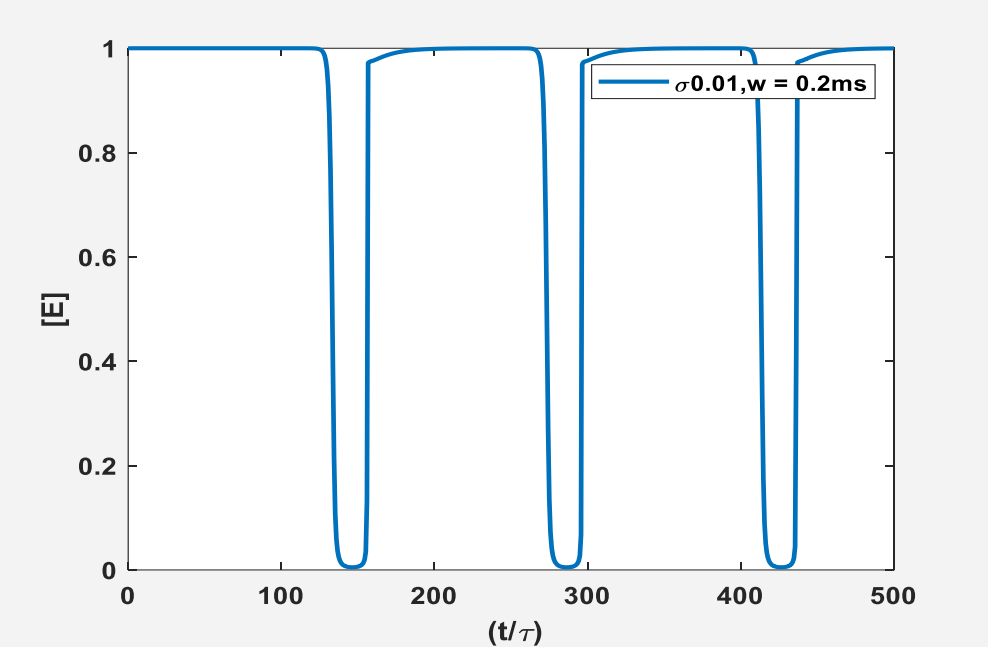

Figure 4.33: Concentration of the enzyme at representative position $z = \frac{1}{2}$. Loading cycles with a frequency of 200 Hz (5 ms), and a distribution width of 0.2 ms. As a result of changing the distribution width, the enzyme concentration is affected.

Figure 4.33 illustrates that the enzyme concentration is affected by changing the distribution width as ACh concentration affected in Figure 4.32. This behaviour confirms the interaction between ACh and enzyme, as previously mentioned. A detailed analysis of the result from Figure 4.33 reveals that the concentration of enzyme decreases until it reaches a minimum concentration 0.005 (corresponding to $2.6 \times 10^{-6}\ M$). This value is reached 146 τ(5.2 ms).

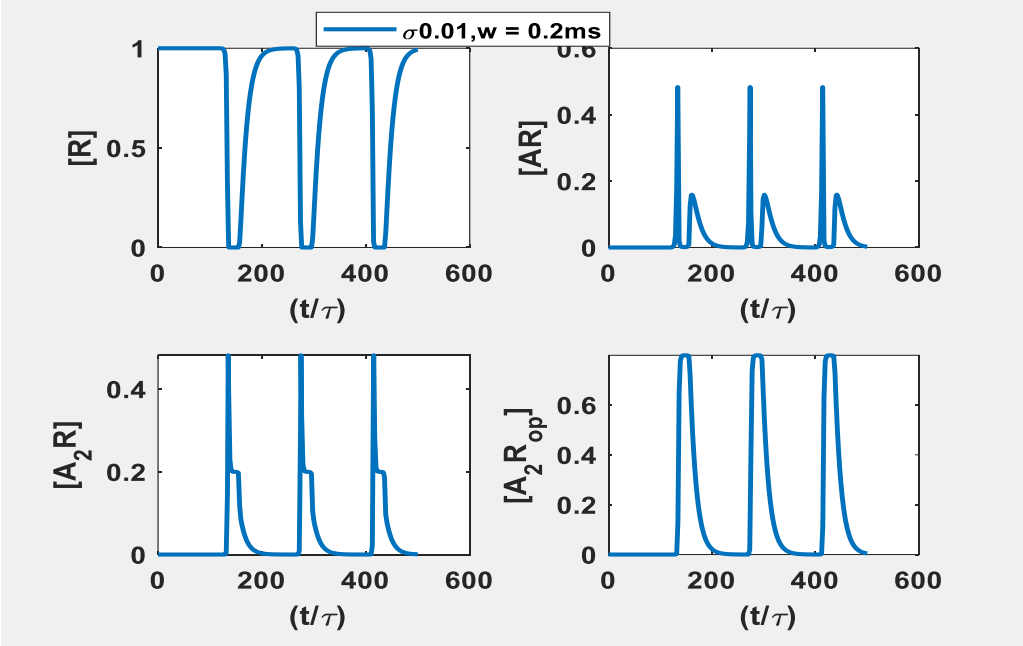

Figure 4.34: Concentration of receptors species and loading cycles with a frequency of 200 Hz and a distribution width of 0.2 ms. Attention should be given to the dynamics of open receptors. There are three clearly distinguishable peaks, the first one starting to raise at 133 τ, which corresponds to 4.7 ms. It reaches the maximum concentration value (0.8) at 147 τ (5.2 ms).

Figure 4.34 displays the same receptor dynamics as discussed before. The most prominent difference in this scenario, when compared with the distribution width of 0.5 in Figure 4.30, is that, with a shorter width (0.2 ms compared to 0.5 ms on the previous test), more open receptors are observed, as seen in the bottom right plot of Figure 4.34. Peaks are higher in magnitude and shorter in time when compared with 0.5 ms test cases. This behavior is already expected since a reduced loading width with the same release causes higher loading peaks. Such a difference in the magnitude of loading peaks is reflected in the concentration of open receptors.

4.10 500 Hz Loading Case – Reaction-diffusion process σ = 0.01 with a width of 0.5 ms

The investigation of a broad range of high frequencies is important to better understand the bioelectrical phenomenon of electric organ discharge (EOD) of *Eigenmannia*, since they may fire electric signals at different frequencies. Besides the value of $200\ \mathrm{Hz}$ already mentioned above, we also chose to investigate a loading cycle with a frequency of $500\ \mathrm{Hz}$.

Since high frequencies may cause superposition of concentrations in between each cycle, it was necessary to establish an optimum set of parameters which reproduces results that can be analysed. In this regard, it was chosen to fix σ, since it has a drastic effect on the dynamics of the reaction-diffusion process. The value chosen for it is 0.01. These values were not arbitrarily set, but it was seen that smaller values of σ would not allow the observation for cycles of opening and closing receptors $[\mathrm{A_2R_{op}}]$.

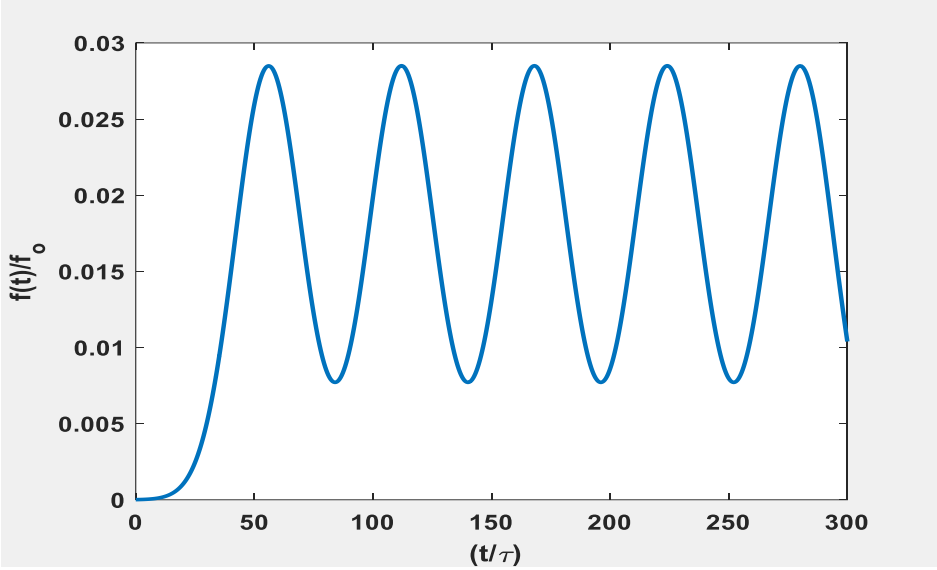

Figure 4.35: Illustrates the loading cycles $\mathrm{f(t)}$ for the period of 2 ms (500 Hz). The loading consists of 5 Gaussian-shaped fluxes of acetylcholine with the distribution width of $0.5\ \mathrm{ms}$. There is a slight superposition of the loading cycles, which prevents the flux from returning to zero in between each loading.

Figure 4.35 shows five ACh release cycles for a frequency of 200 Hz. Three Gaussian-shaped fluxes events are shown with a distribution width of 0.2ms. It can be observed that the five peak inflows fall on 56.1 τ, 112.6 τ, and 168.4 τ, 224.4 τ , 280 τ which corresponds to 2, 4,6,8 and 10 ms with a distribution width of 0.5ms.

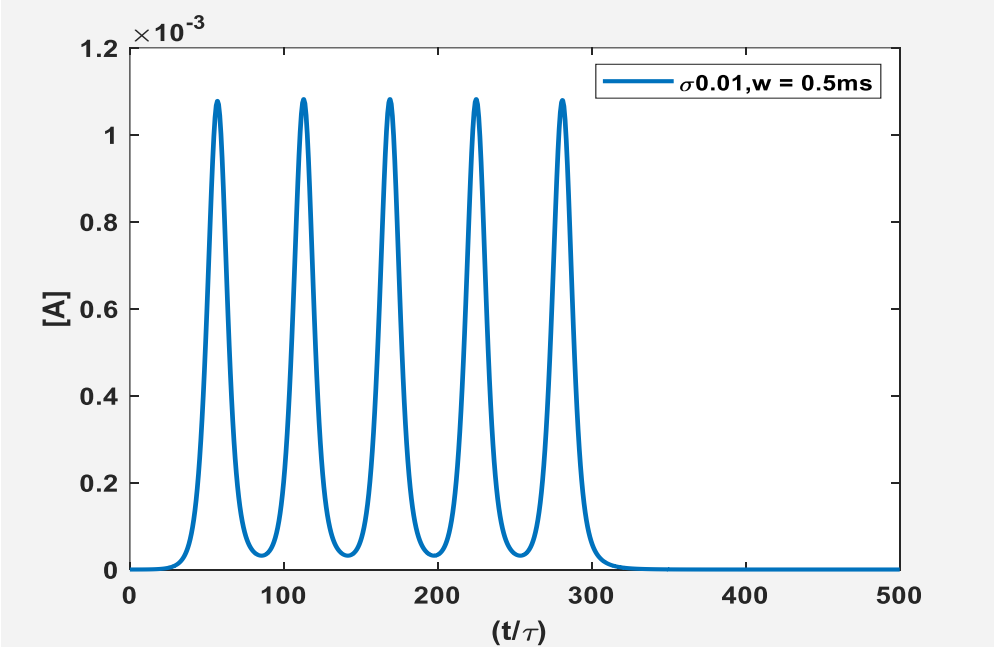

Figure 4.36: Shows the results obtained for the concentration of acetylcholine at representative position $z = \frac{1}{2}$ generated by a loading cycle 500 Hz with a distribution width of 0.5 ms and $\sigma = 0.01$.

With these simulation conditions, we can see in Fig. 4.36 the concentration of acetylcholine with shorter period of release 2ms at 500Hz. A builds-up, accumulating along the simulation time compared to the 200hz case. Besides, ACh concentration does not reach zero which means that a superposition of Gaussian curves prevents the concentration from vanishing. Thus, ACh concentration is not completely consumed. It is also noticeable that the decay is steeper. This fact is attributed to the high value of σ (0.01).

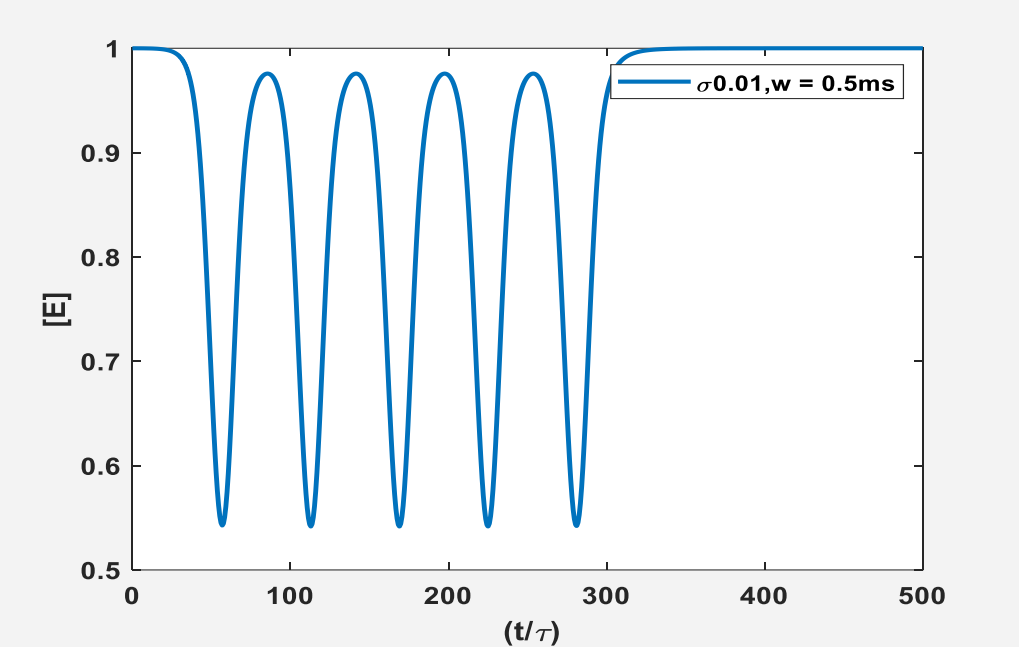

Figure 4.37: The enzyme concentration for loading cycles at a frequency of 500 Hz with a distribution width of 0.5 ms.and $\sigma = 0.01$ at representative position $z = \frac{1}{2}$.

Figure 4.37 shows that the enzyme concentration does not reach zero at 500 Hz. It almost reaches 50% of the initial concentration. In this case, the period of release is short (2ms), which means the ACh does not have enough time to react with the enzyme completely before the next loading. Also, Figure 4.37 shows that the enzyme is not completely consumed after each peak, though it reaches values slightly higher than 50% of the initial concentration. By the end, the enzyme is entirely recovered, reaching 1. This concentration profile is expected, since the loading consists of a low concentration of ACh (slightly higher than 1×10^{-3}, as observed in the previous Figure). Thus, ACh is the limiting reactant.

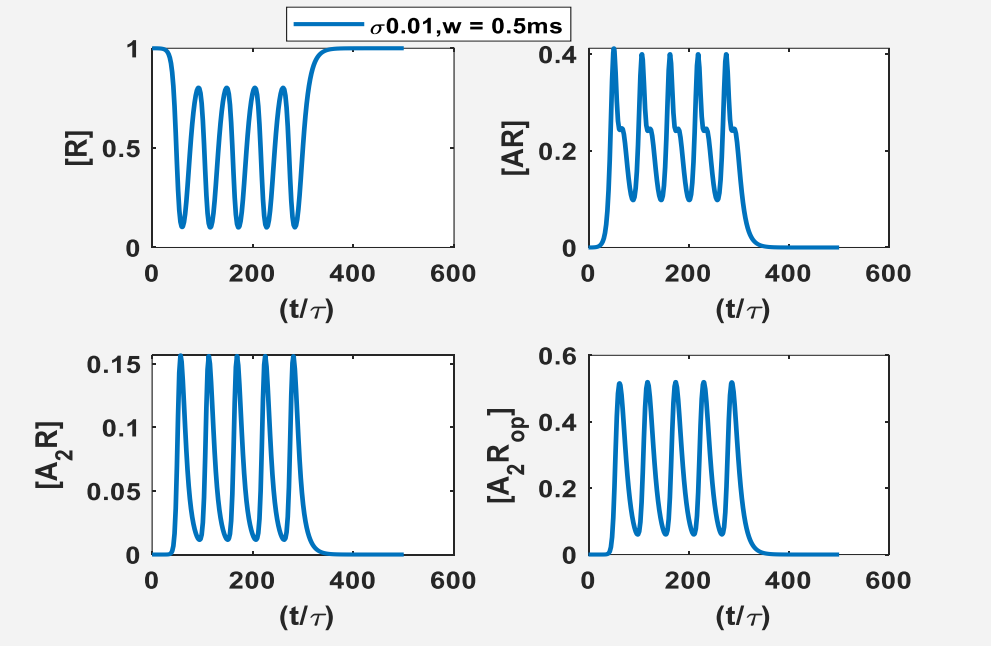

Figure 4.38: The concentration receptors species for loading cycle at frequency of 500 Hz with a distribution width of 0.5ms and $\sigma = 0.01$. Concentration of $[A_2R_{op}]$ peaks, all with a maximum value around 0.5. Each peak has an approximate width of 1.7ms.

In the present case (Fig. 4.38), the receptors [R] are not completely consumed (do not reach zero). However, the interval between the peaks is not enough for the recovery of the concentration to the initial value. This generates a visible fluctuation of the concentration, reducing when the peak of ACh reaches the post-synaptic membrane and increasing when the ACh concentration decreases. This behaviour differs considerably from the previous case (200 Hz and width 0.2) since the receptors had enough time to recover and were wholly consumed.

In the concentration of [AR], it is possible to note the slight formation of a secondary peak just after a high peak is formed. Though the decreasing concentration almost masks it, it is still noticeable by a short shift of the concentration curve. This "shoulder" is not seen in the previous case (Figure 4.34) where two distinct peaks were observed. Therefore, using this loading cycle and distribution width causes a superposition of the higher and lower peak observed in the 200 Hz and width 0.2.

In $[A_2R_{op}]$, there is slight superpositions of the peaks. The first peak starts at44 τ with an initial concentration of 0.02. It reaches the maximum value at 61 τ and concentration 0.5. The concentration rapidly decreases, reaching the first “valley” at 93.3 τ and with concentration 0.07.

It was observed that different receptors closing periods would be obtained by changing the simulation properties. For low frequencies, such as 200 Hz, it is possible to observe a higher interchange of open and close receptors. This can better correspond with the investigation of electric fish firing rates, since it is necessary to obtain as many open receptors as possible at higher frequency rates, such as 200 Hz and 500 Hz.

4.11 500 Hz Loading Case – Investigation of Reaction-diffusion process with $\sigma = 0.01$ and a width of 0.2ms

A similar investigation was conducted with a 500 Hz loading cycle with a width of 0.2 ms. The loading contains five peaks and is shown in Figure 4.39

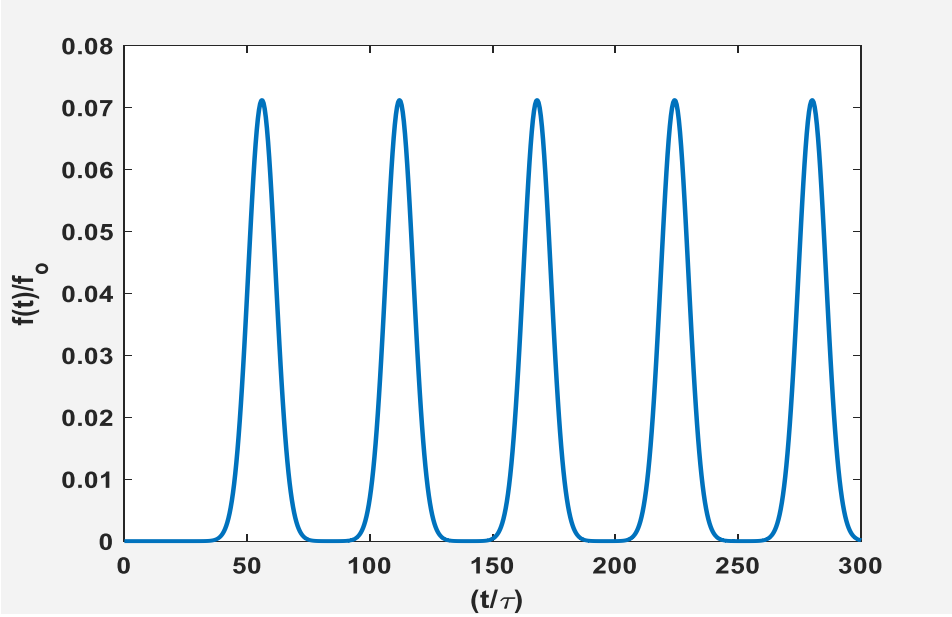

Figure4.39: Five loading events with a period of 2 ms(500Hz) and width a distribution width of 0.2 ms (46τ).

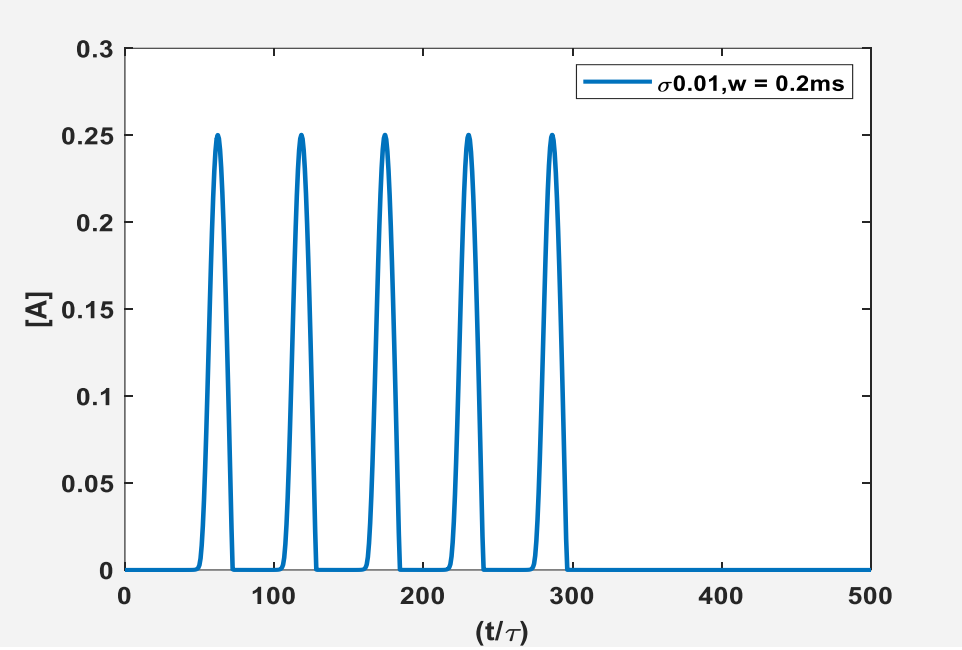

Figure 4.40: The concentration of ACh at representative position $z = \frac{1}{2}$. Loading cycle with frequency $500\ \mathrm{Hz}$ with a distribution width of $0.2\ \mathrm{ms}$ and $\sigma = 0.01$. Note that the maximum of ACh concentration increases compared to Figure 4.36, reaching 0.24 at 61.2 τ or 5.2ms

We can see that the same behavior for ACh occurs shorter release period with a narrow distribution. [A] accumulates along the simulation time, with subsequent growth of its peaks (0.24 or 0.1M). In this case, ACh concentration is completely consumed compared to Figure 4.36 due to narrower distribution width.

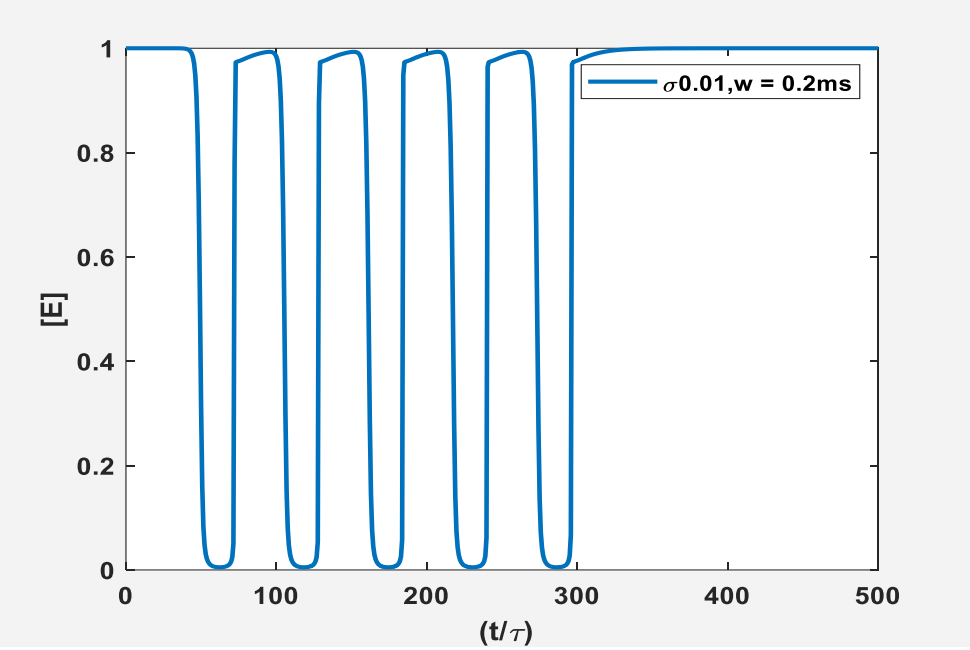

Figure 4.41: Concentration of the enzyme at representative position $z = \frac{1}{2}$. Loading cycle with frequency $500\ \mathrm{Hz}$ with a distribution width of $0.2\ \mathrm{ms}$ and $\sigma = 0.01$

Figure 4.41 shows the enzyme concentration reaches almost zero. The concentration of enzyme decreases, and it reaches approximately 5×10^{-4}, at $59\,\tau$. It can be added that such concentration values are negligible and may be considered approximately zero and the recovery of enzyme concentration occurs within a time 13 τ between acetylcholine loading, reaching its initial concentration.

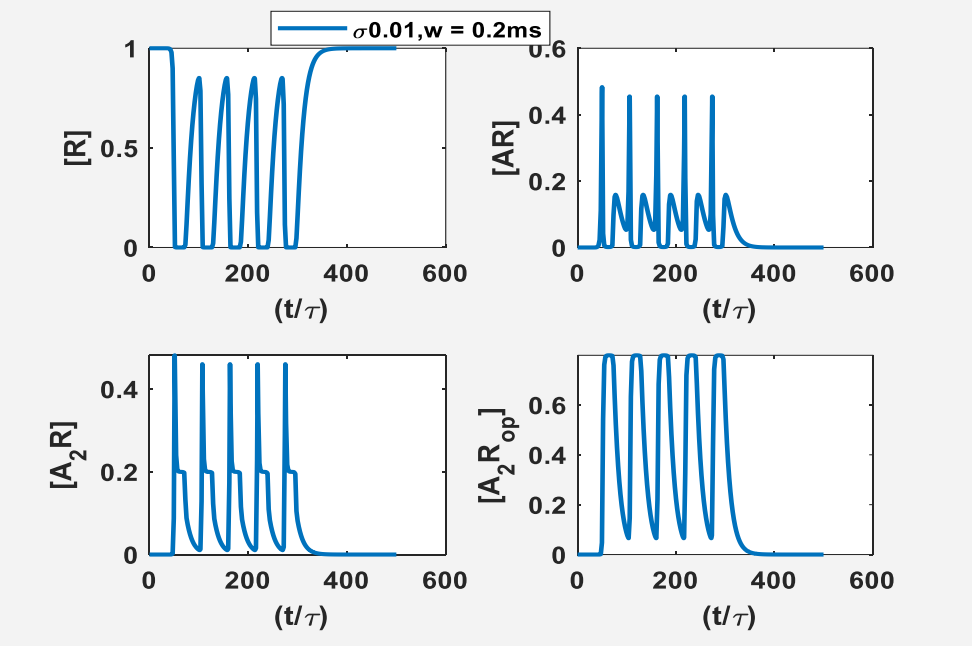

Figure 4.42: The receptors species concentration for $\sigma = 0.01$, loading cycle with the frequency of 500 Hz and a distribution width of 0.2 ms. One can observe that the open receptors do not completely close. Each peak exhibits a short plateau, decreasing to concentration values slightly lower than 0.2 units but increasing again, preventing the open receptors from closing.

We investigated the effects of the width of Gaussian loading input at 500 Hz. Figure 4.42 shows that the kinetics of receptors is similarly generated as seen before (Figure 4.38). For a reduced width (0.2 ms), one would expect that the open receptors would reach zero. However, we found that the concentration of open receptors never reaches zero at 500 Hz. The percentage of the opening receptor is around 6%.

Overall, the observed concentrations of ACh and $[\mathrm{A}_2\ \mathrm{R}_{\mathrm{op}}]$for loading width equal to 0.2 ms showed higher peaks with a narrower width. This can be observed in Figures 4.40 and Figure 4.42, bottom right. These results can be attributed to the same effect mentioned in the previous section (with 200 Hz), i.e., maintaining the areal concentration per release with a shorter width means a higher release peak, reflected on a higher concentration of species ACh and bounded receptors, such as $[\mathrm{A}_2\ \mathrm{R}_{\mathrm{op}}]$.

A last test has been implemented; we reduced the distribution width to 0.1ms in a single signal loading. The effect of narrower width (0.1ms) on ACh concentration is illustrated in Figure 4.43.

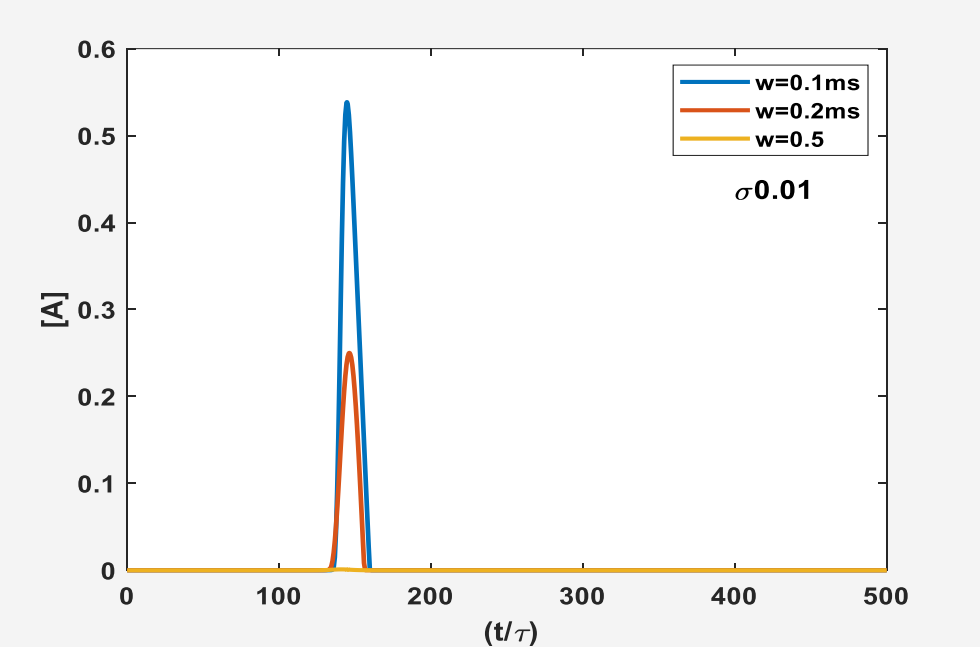

Figure 4.43: The concentration of ACh at representative position $z = \frac{1}{2}$ using a single loading event with different distribution width $0.1, 0.2, 0.5$ ms. Note that the maximum of ACh concentration increases, when the width of Gaussian cycle is decreased.

Figure 4.43 shows the effect of changing the distribution width on the concentration of ACh. One may notice the growth of the maximum of ACh concentration peaks with the same subsequent effect on the dynamics of the receptors. Additional reduction of the loading width (for instance, 0.1 ms) produced results like those obtained with the width 0.2 ms, as illustrated in Figure 4.40. Thus, the simulated kinetic results for loading width of 0.2 ms and 0.5 ms are as expected, indicating that our model performs correctly, reasonably mimicking the MNJ process in this regime.

5 Conclusion and Outlook

In this thesis we studied the opening of AChR receptors resulting from the periodic release of ACh in the frequency range 200Hz to 500Hz. Previous work had focussed on single releases of ACh [27, 35, 36]. In this study, we simulated the release of ACh and the kinetics of receptors (especially the open receptors) varying a set of relevant parameters. The effects of changes, in the concentration of enzyme (AChE), input flux, and concentration of receptors, on the emission of acetylcholine in the synaptic cleft and the subsequent influence on the receptor dynamics are discussed.

We considered the importance of the breakdown of ACh by AChE, which has a very high catalytic activity. For a given firing rate, we had to optimize the concentration of the enzyme (AChE). Subsequently, the mechanism is limited to a range of frequencies whose maximum is close to 500Hz.

In fact, the fundamental process of transmission of signals includes ACh's complex activity in diffusion through the synaptic cleft and its reactions with receptors. The receptors are in different states, unbound receptors R, single bound receptors AR, double-bound closed A_2R , and double-bound open receptors A_2R_{op}.

We have developed a one-dimensional model with cylindrically shaped cleft using a numerical method applied to solve the reaction-diffusion equation. We present the dynamics of the reaction-diffusion of acetylcholine and acetylcholine receptors in the neuromuscular junction in the presence of activating enzyme. The dynamics of the reaction-diffusion of acetylcholine in response to the determined range of parameters, the input concentration of acetylcholine (F), the ratio of initial receptors concentration to input acetylcholine concentration (γ) and the ratio (σ) of initial enzyme concentration $[\mathrm{E}_{\mathrm{tot}}]$ to the [A] concentration scale have been studied. We find that the enzyme has a significant impact on consuming ACh molecules from the cleft.

We presented the simulation results of the increasing reaction kinetics, which are associated with the consumption of ACh by AChE in the synaptic cleft with the analysis of the ACh decay and the subsequent effects on the receptor populations as a function of time.

Results show that the parameter σ has a significant effect on the slope of the linear part of the A(t) decay in the pseudo-steady state regime. The value of the slope of that linear part is -Kσ where K is the regeneration rate of enzyme, and it is confirmed analytically for different σ values. During the linear decay of [A], the receptor species $[\mathrm{R}, \mathrm{AR}, \mathrm{A_2R}, \mathrm{A_2\ R_{op}}]$ exhibited plateau values in the so-called pseudo-steady state regime, and the duration of the plateau scales as the inverse of σ . ACh reaches the post-synaptic terminal rapidly. Consequently, the binding of ACh molecules to AChR has practically no effect on ACh concentration in the synaptic cleft. We then presented two examples of acetylcholine concentration in the synaptic cleft at high-frequencies 200 Hz and 500 Hz. Importantly, adjusting only one parameter (σ) in this work enables a drastic effect on the production of open receptors at frequencies up to 500 Hz. Results show that in the first example at 200 Hz a non- zero population of open and close receptors can be easily obtained as acetylcholine is emitted, while in the second example at 500 Hz the population of open receptors would not close completely, which match low ACh concentration simulations when σ equals to 0.01 (the most favorable value). Joós. et al [7]. found that the receptors do not need to completely close to allow for electrocyte firing [7]. In this paper, the impact of a constant leak of the Na^+ is investigated. In our work the percentage of open receptors is around 6% at 500 Hz. Based on Ref [7], the system can fire at those frequencies. It is interesting to note the AChR not closing fully would add a cost of maintaining EODs as already modeled and investigated by Joós. et al., 2018 [7]. Our results indicate that 500 Hz is close to the maximum at which an effective synaptic transmission can occur.

One crucial observation regarding such dynamics is that by changing the concentration of enzyme (through the parameter σ), different concentration profiles can be obtained with non-zero open receptors. Thus, one of the limitations of this firing mechanism is the enzyme concentration. In this model, 500 Hz appears to close the maximum frequency at which *Eigenmannia* can fire. Future studies could consider more realistic distributions of, ACh, enzyme, and receptors, and a more complex geometry of the cleft. The effect of the thickness of the synaptic cleft could also be addressed.

For low values of σ (lower than 0.01), the single bound receptor [AR] exhibits a higher peak followed by a secondary peak at each loading. When σ becomes higher than 0.01, the lower peak disappears, probably collapsing into the higher one and forming a single peak. In the case $[\mathrm{A_2R}]$, one can observe the formation of a peak followed by a shoulder when σ is lower than 0.01. Above this value, the shoulder is not observable, only the peak due to the loading of ACh.

It would be interesting to have experimental investigations focussing on an in-depth study of intermediate species [AR], $[\mathrm{A_2R}]$ with an asymmetric distribution of ACh in the presynaptic membrane and modeling the chemical reaction processes using a more realistic NMJ geometry. Overall, this model, although with a simple one-dimensional geometry, reflects the essential observed features of synaptic transmission in *Eigenmannia*, and predicts an operational frequency range in accord with observation using parameter values obtained from the literature.

Appendix I

Analytical solution of the pure diffusion problem

In order to verify the validity of the numerical method for diffusion, it is useful to consider the situation where all reactions are inactivated ((no reaction with the receptors ($\gamma = 0$) or with the enzyme). We are interested in finding the analytical solution $A(z,t)$ of the following boundary-value problem, defined on the domain $0 \leq z \leq 1$ with time-dependent boundary condition:

$$\frac{\partial[\mathrm{A}]}{\partial \mathrm{t}} = \frac{\partial^2[\mathrm{A}]}{\partial \mathrm{z}^2}. \tag{6.1}$$

$$\left.\frac{\partial[\mathrm{A}]}{\partial \mathrm{z}}\right|_{\mathrm{z}=0} = -\frac{\mathrm{f(t)}}{\mathrm{f_0}} \equiv \phi(\mathrm{t}). \tag{6.2}$$

$$\left.\frac{\partial[\mathrm{A}]}{\partial \mathrm{z}}\right|_{\mathrm{z}=1} = 0\,. \tag{6.3}$$

At t=0 ,

$$[\mathrm{A}(\mathrm{z},0)] = 0; \phi(0) = 0.$$

First, let

$$\Psi(\mathrm{z},\mathrm{t}) \equiv -\frac{\phi(\mathrm{t})(1-\mathrm{z})^2}{2}. \tag{6.4}$$

Then

$$\left.\frac{\partial \Psi}{\partial \mathrm{z}}\right|_{\mathrm{z}=0} = \phi(\mathrm{t}); \quad \left.\frac{\partial \Psi}{\partial \mathrm{z}}\right|_{\mathrm{z}=1} = 0. \tag{6.5}$$

At t=0 ,

$$\Psi(\mathrm{z},0) = 0.$$

Let,

$$[A(z,t)] \equiv \Psi(z,t) + \alpha(z,t). \tag{6.6}$$

In terms of α, the equation to solve is

$$\frac{\partial \alpha}{\partial t} = \frac{\partial [A]}{\partial t} - \frac{\partial \Psi}{\partial t} = \frac{\partial^2 [A]}{\partial z^2} + \frac{\dot{\phi}(t)(1-z)^2}{2}$$
$$= \frac{\partial^2 \alpha}{\partial z^2} + \frac{\partial^2 \Psi}{\partial z^2} + \frac{\dot{\phi}(t)\,(1-z)^2}{2}. \tag{6.7}$$

$$\frac{\partial \alpha}{\partial t} = \frac{\partial^2 \alpha}{\partial z^2} - \phi(t) + \frac{\dot{\phi}(t)(1-z)^2}{2}. \tag{6.8}$$

$$\left.\frac{\partial \alpha}{\partial z}\right|_{z=0} = \left.\frac{\partial [A]}{\partial z}\right|_{z=0} - \left.\frac{\partial \Psi}{\partial z}\right|_{z=0} = \phi(t) - \phi(t) = 0. \tag{6.9}$$

$$\left.\frac{\partial \alpha}{\partial z}\right|_{z=1} = 0; \alpha(z,0) = 0. \tag{6.10}$$

We reduced the problem to an equation of diffusion with a time-dependent source term S(z, t) and homogeneous Neumann boundary conditions. We expend in the cosine Fourier series (which satisfies the Neumann boundary conditions):

$$\alpha(z,t) = \sum_{n=0,\dots} \hat{\alpha}_n(t) \cos(n\pi z). \tag{6.11}$$

$$S(z,t) \equiv -\phi(t) + \frac{\dot{\phi}(t)(1-z)^2}{2} = \sum_{n=0,\dots} \hat{S}_n(t) \cos(n\pi z). \tag{6.12}$$

Substitute in the differential equation

$$0 = \sum_{n=0,\dots} \left[\frac{d\hat{\alpha}_n(t)}{dt} + n^2\,\pi^2 \hat{\alpha}_n(t) - \hat{S}_n(t)\right] \cos(n\pi z). \tag{6.13}$$

Hence,

$$\frac{d\hat{\alpha}_n(t)}{dt} = -n^2\,\pi^2 \hat{\alpha}_n(t) + \hat{S}_n(t).$$
$$\Longrightarrow \hat{\alpha}_n(t) = \exp\left(-n^2\pi^2 t\right) \hat{c}_n + \int_0^t d\tau \hat{S}_n(\tau) \exp\left(-n^2\pi^2(t-\tau)\right). \tag{6.14}$$

Here $\hat{c}_n$ are the Fourier coefficients of α at time 0.

Since $\alpha(z,0)=0, \hat{c}_n=0$. Thus, Eq.6.6 is given as :

$$[A(z,t)] = -\frac{\phi(t)(1-z)^2}{2} + \sum_{n=0,\dots} \int_0^t d\tau \hat{S}_n(\tau) \exp\left(-n^2\pi^2(t-\tau)\right) \cos(n\pi z). \tag{6.15}$$

To find the cosine Fourier expansion coefficient of the source term $S(z,t)$:

$$\sum_{n=0,\dots} \hat{S}_n(t) \cos(n\pi z) = -\phi(t) + \frac{\dot{\phi}(t)(1-z)^2}{2}. \tag{6.16}$$

$$\Rightarrow \quad \hat{S}_0(t) = \int_0^1 dz[-\phi(t) + \frac{\dot{\phi}(t)(1-z)^2}{2}] = -\phi(t) + \frac{\dot{\phi}(t)}{6}. \tag{6.17}$$

$$\hat{S}_n(t) = 2\int_0^1 dz \cos(n\pi z)\left[-\phi(t) + \frac{\dot{\phi}(t)(1-z)^2}{2}\right]; n = 1,2,\dots \tag{6.18}$$

$$\hat{S}_n(t) = \dot{\phi}(t)\int_0^1 dz \cos(n\pi z)\,(1-z)^2 = \frac{2\,\dot{\phi}(t)}{n^2\pi^2}. \tag{6.19}$$

By putting Eq. (6.17,6.19) in Eq.6.15

$$[A(z,t)] = -\frac{\phi(t)(1-z)^2}{2} + \int_0^t d\tau\left(-\phi(\tau) + \frac{\dot{\phi}(\tau)}{6}\right) + 2\sum_{n=1,\dots}\int_0^t d\tau\, e^{\left(-n^2\pi^2(t-\tau)\right)}\frac{\dot{\phi}(t)}{n^2\pi^2}\cos(n\pi z). \tag{6.20}$$

We can simplify the last term by integration by parts in Eq.6.21 , We get:

$$[A(z,t)] = -\frac{\phi(t)(1-z)^2}{2} - \int_0^t d\tau\phi(\tau) + \left(\frac{\phi(t)}{6}\right) + 2\sum_{n=1,\dots}\frac{\cos(n\pi z)}{n^2\pi^2}\quad[\phi(t) - n^2\pi^2\int_0^t d\tau\, e^{\left(-n^2\pi^2(t-\tau)\right)}\phi(\tau). \tag{6.21}$$

$$= -\int_0^t d\tau\phi(\tau) + \left(\frac{\phi(t)}{6}\right)(6z - 3z^2 - 2) + 2\phi(t)\sum_{n=1,\dots}\frac{\cos(n\pi z)}{n^2\pi^2} - 2\sum_{n=1,\dots}\cos(n\pi z)\int_0^t d\tau\, e^{\left(-n^2\pi^2(t-\tau)\right)}\phi(\tau). \tag{6.22}$$

The third term sum can be expressed in terms of the poly-logarithm:

$$\sum_{n=1,\dots} \frac{\cos(n\pi z)}{n^2\pi^2} = \frac{(\,\mathrm{Li}_2(e^{i\pi z}) + \mathrm{Li}_2(e^{-i\pi z})}{2\pi^2}. \tag{6.23}$$

where the poly-logarithm function is defined as

$$\mathrm{Li}_n(x) \equiv \sum_{k=1,\dots} \frac{x^k}{k^n}.$$

The final manipulation consists in recognizing that the summation over n in the last term can be achieved in terms of Jacobi elliptic function of the third kind.

$$\theta_3(x,q) \equiv \sum_{n=-\infty}^{\infty} q^{n^2} e^{2nix} = 1 + 2\sum_{n=1,\dots} q^{n^2}\cos(2x). \tag{6.24}$$

Then,

$$2\sum_{n=1,\dots} \cos(n\pi z)\int_0^t d\tau\, e^{\left(-n^2\pi^2(t-\tau)\right)}\phi(\tau) = \int_0^t d\tau\,\phi(\tau)\;\theta_3\left(\frac{\pi z}{2}, e^{-\pi^2(t-\tau)}\right) - \int_0^t d\tau\,\phi(\tau). \tag{6.25}$$

Therefore,

$$[A(z,t)] = \frac{\phi(t)}{6}(6z - 3z^2 - 2) + \phi(t)\frac{(\,\mathrm{Li}_2(e^{i\pi z}) + \mathrm{Li}_2(e^{-i\pi z})}{\pi^2} - \int_0^t d\tau\,\phi(\tau)\;\theta_3\left(\frac{\pi z}{2}, e^{-\pi^2(t-\tau)}\right). \tag{6.26}$$

We choose a delta-function release of the form:

$$\phi(t) = -\delta(t - t).$$

Where T is the time at which the release occurs

For $t > T$,

$$[A(z,t)] = \theta_3\left(\frac{\pi z}{2}, e^{-\pi^2(t-\tau)}\right). \quad (6.27)$$

The following graph compares the numerical solution and the analytical one. This reveals the A field's time-evolution in two places, $z = \frac{1}{4}$ (upper curve), and $z = \frac{3}{4}$ (lower curve). The release was set to happen at $T = 1$. We implemented the delta-release as follows

$$-\phi(t) = \begin{cases} \frac{1}{\Delta t}, \text{if } |t-1| \leq \frac{\Delta t}{2} \\ 0, \text{otherwise.} \end{cases}$$

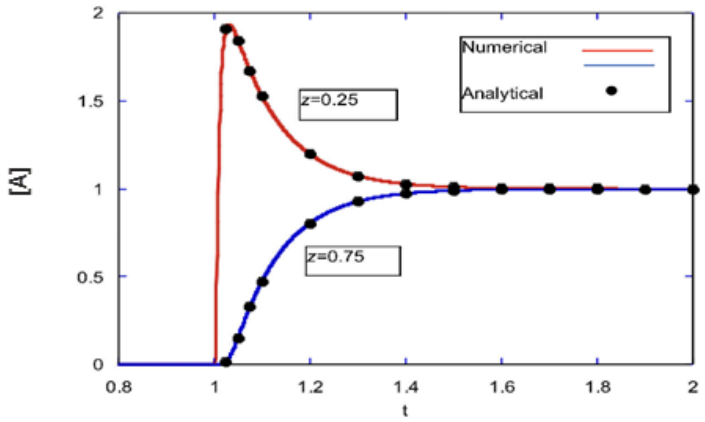

Here, Δt is the numerical time step (qual to 0.001 in this example). We have used Mathematica to evaluate the Jacobi elliptic function. We can reasonably conclude that the agreement is very satisfactory

Appendix II

Analytical treatment of the pseudo steady state.

The receptors species $[\mathrm{R}, \mathrm{AR}, \mathrm{A}_2\ \mathrm{R}, \mathrm{A}_2\ \mathrm{R}_{\mathrm{op}}]$ exhibit plateau values slightly before and during the linear decay of [A]. This regime is named the pseudo-steady state regime where the reaction rates of the receptor species are close to equilibrium state. We offer here an analytical treatment of this region.

A typical curve looks like this.

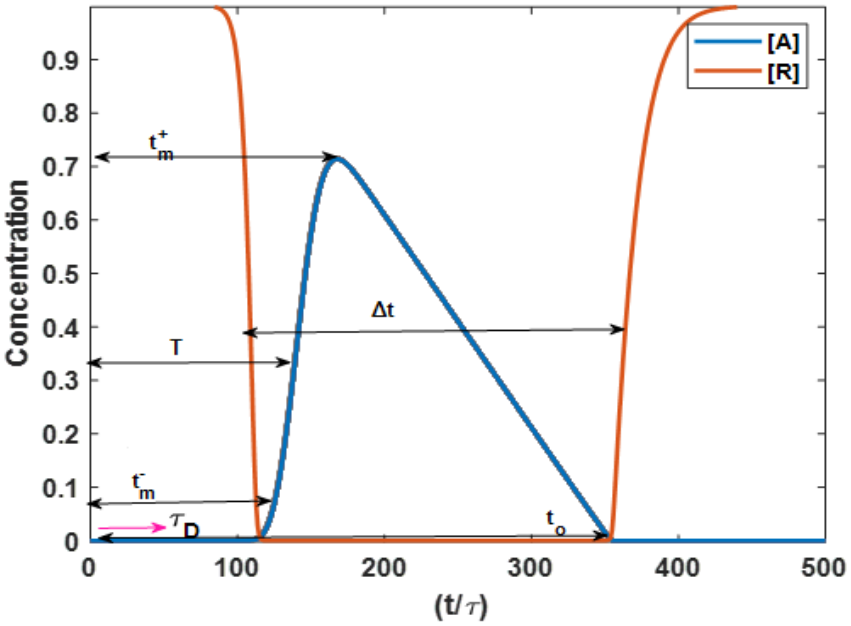

Figure 6.1: Typical curves of ACh and receptor concentrations.

A typical unbound receptor concentration starts to decrease and goes to zero at about the same time when A starts to increase as illustrated in Figure 6.1. In other words, A reaches the receptors very rapidly (diffusion happens relatively quickly). The starting point is the diffusion reaction equation for [A]:

$$\frac{\partial[\mathrm{A}]}{\partial \mathrm{t}} = \frac{\partial^2[\mathrm{A}]}{\partial \mathrm{z}^2} - \frac{\mathrm{K}\sigma[\mathrm{A}]}{\kappa + [\mathrm{A}]}. \tag{6.1}$$

In the pseudo-steady state regime, [A] is much larger than κ .It is acceptable to neglect κ in the denominator, so we get

$$\frac{\partial[\mathrm{A}]}{\partial \mathrm{t}} = \frac{\partial^2[\mathrm{A}]}{\partial \mathrm{z}^2} - \mathrm{K}\sigma. \tag{6.2}$$

The boundary conditions are given:

$$\left.\frac{\partial[\mathrm{A}]}{\partial \mathrm{z}}\right|_{\mathrm{z}=0} = -\frac{f(t)}{f_0}. \tag{6.3}$$

$$\left.\frac{\partial[A]}{\partial z}\right|_{z=1} = -2K_R\gamma[A(1)]R - K_{AR}\gamma[A(1)][AR] + K_{-R}\gamma[AR] + 2K_{-AR}\gamma[A_2R]. \tag{6.4}$$

Integrating (6.2) over the length of the cleft, we get

$$\frac{d\overline{[A]}}{dt} = -\left.\frac{\partial[A]}{\partial z}\right|_{z=0} + \left.\frac{\partial[A]}{\partial z}\right|_{z=1} - K\sigma. \tag{6.5}$$

where $\overline{[A]}$ is the spatial average of $[\mathrm{A}]$. Since $[\mathrm{A}]$ is homogenous to a reasonable degree of accuracy, we can set $\overline{[A]} \cong [A]$.

Since receptors have reached chemical equilibrium, on the right-hand side of Eq.6.4 is 0

$$\frac{d\overline{[A]}}{dt} = \frac{f(t)}{f_0} - K\sigma. \tag{6.6}$$

Now we solve this analytically, by integrating with respect to time starting at $t = \tau_D$. Here, τ_D is an initial delay time after which [*A*] starts to build up under the effect of the loading function. We assume [A] is still very small at the end of the delay .We take $[A] = 0$ at $\mathrm{t} = \tau_\mathrm{D}$.

.

$$[A] = -\mathrm{K}\sigma(\mathrm{t} - \tau_\mathrm{D}) + \int_{\tau_\mathrm{D}}^{t} \frac{f(t)}{f_0}\, dt. \tag{6.7}$$

When t is much larger than $T + w$, the loading function has approximately stopped growing . We take the upper limit in the integral to ∞:

$$t \gg T + w: [A] = -K\sigma t + \int_{\tau_D}^{\infty} \frac{f(t)}{f_0} dt' + K\sigma\, \tau_\mathrm{D}. \tag{6.8}$$

$$[A(t)] = -K\sigma\mathrm{t} + \mathrm{B}. \tag{6.9}$$

$$B = \int_{\tau_D}^{\infty} \frac{f(t)}{f_0} dt' + K\sigma\, \tau_\mathrm{D}. \tag{6.10}$$

Here, B is a constant. If $\tau_D \ll T - w$, the lower limit can be set to $-\infty$,thus,

$$B = 1 + K\sigma\, \tau_\mathrm{D}. \tag{6.11}$$

We then obtain the linear decay observed on the plot. The linear decay transits to an exponential one when [A] can be neglected in the denominator of equation 6.1 . This occurs close to time t_o when [A] is close to zero in our linear decay approximation:

$$[\mathrm{A}] \cong 0 = B - K\sigma t_o. \tag{6.12}$$

$$t_o = \frac{\mathrm{B}}{K\sigma} = \frac{1}{K\sigma} + \quad \tau_{\mathrm{D}}\,. \tag{6.13}$$

At $t = T$, the loading function is at its maximum $f'(t) = 0$ and hence the second derivative of [A] is zero from equation (6.2).

$$\frac{\partial^2[\mathrm{A}]}{\partial \mathrm{t}^2} = 0. \tag{6.14}$$

Then we have inflection point at T. When [A] is at its maximum

$$\frac{\partial[\mathrm{A}]}{\partial \mathrm{t}} = 0. \tag{6.15}$$

Or

$$\frac{f(t)}{f_0} = \frac{1}{\sqrt{2\pi w^2}}\ exp\left(\frac{-(t-T)^2}{2w^2}\right) = K\sigma. \tag{6.16}$$

There are two solutions for equation 6.16 $t_{m\pm}$ symmetrically located with respect to T.

(at t_{m+} and t_{m-}). The maximum of [A] occurs at t_{m+} while the pseudo-steady state regime starts at t_{m-}.

To find the maximum, the first derivative goes to 0.

$$\frac{\partial[\mathrm{A}](t_{m+})}{\partial \mathrm{t}} = 0. \tag{6.17}$$

Then,

$$\frac{f(t_{m^+})}{f_0} = \frac{1}{\sqrt{2\pi w^2}}\ exp\left(\frac{-(t_{m^+}-T)^2}{2w^2}\right) = K\sigma. \tag{6.18}$$

Then

$$t_{m^+} = T + \left[-2w^2 \log(\sqrt{2\pi w^2}K\sigma)\right]^{\frac{1}{2}}. \tag{6.19}$$

$$[A_m] = -K\sigma\, t_{m^+} + \frac{1}{\sqrt{2\pi w^2}} \int_{\tau_D}^{t_{m^+}} exp\left(\frac{-(t'-T)^2}{2w^2}\right) dt' + K\sigma\, \tau_D. \tag{6.20}$$

We assume that the pseudo-steady state regime is initiated at t_{m-} given by

$$t_{m^-} = T - \left[-2w^2 \log\left(\sqrt{2\pi w^2}K\sigma\right)\right]^{\frac{1}{2}}. \tag{6.21}$$

$$t_{m^-} = T - \sqrt{2}\, w \left[\log \frac{1}{K\sigma\sqrt{2\pi w^2}}\right]^{\frac{1}{2}}. \tag{6.22}$$

A solution exists if

$$\sigma < \log \frac{1}{K\sigma\sqrt{2\pi w^2}}.$$

For an estimate of the duration of the pseudo-steady state regime

$$\Delta t = t_0 - t_{m^-} = \frac{1}{K\sigma} - T + \sqrt{2}\, w \left[\log \frac{1}{k\sigma\sqrt{2\pi w^2}}\right]^{\frac{1}{2}} + \tau_D. \tag{6.23}$$

Here $\sqrt{2}\, w \left[\log \frac{1}{k\sigma\sqrt{2\pi w^2}}\right]^{\frac{1}{2}}$ is weakly dependent on σ,so

$$\Delta t \cong \frac{1}{K\sigma} + \text{constant}. \tag{6.24}$$

The curves of [*A*] for different values of σ are extrapolated to [*A*]=1 at the same value of time. This time is the delay time τ_D as is seen from equations 6.9 and 6.11. This gives a way to estimate τ_D empirically.

Appendix III

Stability analysis for steady sate for a single loading

In the true steady state regime, we have $[A]_o = 0$, $[R]_o = 1, [AR]_o = 0, [A_2R]_o = 0, [A_2R_{OP}]_o = 0$. We perform a linear stability analysis, which will involve the receptor kinetics. We introduce the deviations from the steady state:

$$\delta[A] = [A] - [A]_o.$$
$$\delta[R] = [R] - [R]_o.$$
$$\delta[AR] = [AR] - [AR]_o.$$
$$\delta[A_2R] = [A_2R] - [A_2R]_o$$
$$\delta\left[A_2R_{op}\right] = \left[A_2R_{op}\right] - \left[A_2R_{op}\right]_o$$

Close to the steady state regime, the concentration [A] is approximately homogeneous, so that linearizing the enzyme kinetics about the steady state,

$$\frac{\partial\delta[A]}{\partial t} \cong -\frac{K\sigma\delta[A]}{\kappa}. \qquad (7.1)$$

Assuming a fluctuation $\delta[A]$ about the steady state of the form $\delta[A]$~exp(ωt), we get directly one mode with ω =-Kσ/κ. Its numerical value for the reference state is -3.07 so that this mode is decaying rapidly.

Other modes are found by the boundary condition at *z*=1 and the receptor kinetics. The boundary condition is

$$\left.\frac{\partial[A]}{\partial z}\right|_{z=1} = \gamma(-2K_R R[A(1)] - K_{AR}[A(1)][AR] + K_{-R}[AR] + 2K_{-AR}[A_2R]) \cong 0. \qquad (7.2)$$

We introduce the deviations from the steady state, and we linearize about the steady state

$$0 = \gamma[-2K_R\delta[A] + K_{-R}\delta[AR] + 2K_{-AR}\delta[A_2R]]. \tag{7.3}$$

$$\frac{\partial\delta[R]}{\partial t} = -2K_R\delta[A] + K_{-R}\delta[AR]. \tag{7.4}$$

$$\frac{\partial\delta[AR]}{\partial t} = 2K_R\delta[A] - K_{-R}\delta[AR] + 2K_{-AR}\delta[A_2R]. \tag{7.5}$$

$$\frac{\partial\delta[A_2R]}{\partial t} = -2K_{-AR}\delta[A_2R] - K_{op}\delta[A_2R] - K_{cl}\delta[A_2R] - K_{cl}\delta[AR] - K_{cl}\delta[R]. \tag{7.6}$$

By putting equations (7.3,7.4,7.5,7.6) above in a matrix form:

$$\frac{\partial}{\partial t}\begin{pmatrix} 0 \\ \delta R \\ \delta AR \\ \delta A_2R \end{pmatrix} \equiv G = \begin{pmatrix} -2K_R\gamma & 0 & \gamma K_{-R} & 2\gamma K_{-AR} \\ -2K_R & 0 & K_{-R} & 0 \\ 2K_R & 0 & -K_{-R} & 2K_{-AR} \\ 0 & -K_{cl} & -K_{cl} & -2K_{-AR} - K_{cl} - K_{op} \end{pmatrix}\begin{pmatrix} \delta A \\ \delta R \\ \delta AR \\ \delta A_2R \end{pmatrix}. \tag{7.7}$$

We set the dynamics of the fluctuations $\delta A \approx \exp(\omega t)$ etc...

$$G = \begin{pmatrix} -2K_R\gamma & 0 & \gamma K_{-R} & 2\gamma K_{-AR} \\ -2K_R & -\omega & K_{-R} & 0 \\ 2K_R & 0 & -\omega - K_{-R} & 2K_{-AR} \\ 0 & -K_{cl} & -K_{cl} & -\omega - 2K_{-AR} - K_{cl} - K_{op} \end{pmatrix}\begin{pmatrix} \delta A \\ \delta R \\ \delta AR \\ \delta A_2R \end{pmatrix}. \tag{7.8}$$

The discriminant of the above matrix must be zero in order to have a non-trivial solution.

We have three solutions

$\omega = 0$

and

$$\omega = \left(-K_{-AR} - \frac{K_{cl}}{2} - \frac{K_{op}}{2}\right) \pm [-2K_{cl}K_{-AR} + \left(\frac{K_{cl}}{2} + \frac{K_{op}}{2} + K_{-AR}\right)^2]^{\frac{1}{2}}. \quad (7.9)$$

It is easy to prove that the quantity under the square root is always positive so that ω is real. Moreover, a simple examination of Eq. (7.9) shows that ω <0. Then, the steady state is stable and $[A]$ approaches its steady state as a sum of three exponentially decaying functions (including the enzyme mode -Kσ/κ). However, two of these exponentially decaying modes are fast. For large time, only one decay mode survives.

From Eq 7.9, we use reference values:

$$\omega = -0.0835, -1.519.$$

ω are real and negative values. Overall, the mode corresponding to the smallest value of ω will survive at late times, as seen in the Figure 4.9

Bibliography

[1] Güth, R., Pinch, M., Samanta, M. P., Chaidez, A., & Unguez, G. A. ,“Sternopygus macru-rus electric organ transcriptome and cell size exhibit insensitivity to short-term electrical inactivity”. Journal of Physiology-Paris, 110(3), 233-244. (2016).

[2] Assad, C., Rasnow, B., Stoddard, P. K., & Bower, J. M. , “The electric organ discharges of the gymnotiform fishes: II. *Eigenmannia*”. Journal of Comparative Physiology A: Sensory, Neural, and Behavioral Physiology, 183(4), 419–432. doi: 10.1007/s003590050268.(1998).

[3] Markham, M. R. , “Electrocyte physiology: 50 years later”. Journal of Experimental Biology, 216(13), 2451–2458. doi: 10.1242/jeb.082628.(2013).

[4] Lewis, J. E., Gilmour, K. M., Moorhead, M. J., Perry, S. F., & Markham, M. R., “Action Potential Energetics at the Organismal Level Reveal a Trade-Off in Efficiency at High Firing Rates”. Journal of Neuroscience, 34(1), 197–201. doi: 10.1523/jneurosci.3180-13.2014.(2013).

[5] Ban, Y., Smith, B. E., & Markham, M. R. , “A highly polarized excitable cell separates sodium channels from sodium-activated potassium channels by more than a millimeter”. Journal of Neurophysiology, 114(1), 520–530. doi: 10.1152/jn.00475.2014. (2015)

[6] Emde, G. V. D., “Capacitance detection in the wave-type electric fish *Eigenmannia* during active electrolocation”. Journal of Comparative Physiology A: Sensory, Neural, and Behavioral Physiology, 182(2), 217–224. doi: 10.1007/s003590050172. pp.217-24,(1998).

[7] Joós , B., Markham, M. R., Lewis, J. E., & Morris, C. E. A , “model for studying the energetics of sustained high frequency firing”. Plos One, 13(4). doi: 10.1371/journal.pone.0196508.(2018).

[8] Stamper, S. A., Fortune, E. S., & Chacron, M. J., “Perception and coding of envelopes in weakly electric fishes”. Journal of Experimental Biology, 216(13), 2393–2402. doi: 10.1242/jeb.08232. pp.2393–402. (2013).

[9] Boucher, P.A., Joós, B., & Morris, C. E. , “ Erratum to: Coupled left-shift of Nav channels: modeling the Na^+ loading and dysfunctional excitability of damaged axons”. Journal of Computational Neuroscience, 33(2), 321–321. doi: 10.1007/s10827-012-0415-7. pp. 301–19.(2012).

[10] Kondev, J., Phillips, R., & Theriot, J., “Physical Biology of the Cell”. New York: Garland Science.pp.685-695.(2012).

[11] Milo, R., & Phillips, R., “Cell Biology by the Numbers”. New York, NY: Garland Science. pp 326-327.(2016).

[12] Nelson, P. C., & Goodsell, D., “Biological Physics: energy, information, life”. New York: W.H. Freeman and Company. pp.379-382.(2014).

[13] Fletcher, A. , “Action potential: generation and propagation”. Anaesthesia & Intensive Care Medicine, 17(4), 204–208. doi: 10.1016/j.mpaic.2016.01.006.(2016)

[14] Wang, Bo, et al. “Firing Frequency Maxima of Fast-Spiking Neurons in Human, Monkey, and Mouse Neocortex.” Frontiers in Cellular Neuroscience, vol. 10, doi:10.3389/fncel.2016.00239.(2016a).

[15] Ford, Marc C., et al. “Tuning of Ranvier Node and Internode Properties in Myelinated Axons to Adjust Action Potential Timing.” Nature Communications, vol. 6, no. 1,doi:10.1038/ncomms9073.(2015).

[16] Pereda, A. E. ," Electrical synapses and their functional interactions with chemical synapses". Nature Reviews Neuroscience, 15(4), 250–263. doi: 10.1038/nrn3708.(2014).

[17] Yamagata, Y. , "New Aspects of Neurotransmitter Release and Exocytosis: Dynamic and Differential Regulation of Synapsin I Phosphorylation by Acute Neuronal Excitation In Vivo". Journal of Pharmacological Sciences, 93(1), 22–29. doi: 10.1254/jphs.93.22.(2003).

[18] Prinston, J. E., Emlaw, J. R., Dextraze, M. F., Tessier, C. J., Pérez-Areales, F. J., Mcnulty, M. S., & Dacosta, C. J. , "Ancestral Reconstruction Approach to Acetylcholine Receptor Structure and Function". Structure, 25(8). doi: 10.1016/j.str.2017.06.005.(2017).

[19] Falk, M. M., Baker, S. M., Gumpert, A. M., Segretain, D., & Buckheit, R. W. , " Gap Junction Turnover Is Achieved by the Internalization of Small Endocytic Double-Membrane Vesicles". Molecular Biology of the Cell, 20(14), 3342–3352. doi: 10.1091/mbc.e09-04-0288.(2009).

[20] Janeczek, Monica, et al. “Variations in Acetylcholinesterase Activity within Human Cortical Pyramidal Neurons Across Age and Cognitive Trajectories.” Cerebral Cortex, vol. 28, no. 4, Jan, pp. 1329–1337., doi:10.1093/cercor/bhx047.(2017).

[21] Ribrault, C., Sekimoto, K., & Triller, A., "From the stochasticity of molecular processes to the variability of synaptic transmission". Nature Reviews Neuroscience, 12(7), 375–387.doi: 10.1038/nrn3025.(2011).

[22] Thomsen, M., Sørensen, G., & Dencker, D. “Physiological roles of CNS muscarinic receptors gained from knockout mice”. Neuropharmacology, 136, 411-420. (2018).

[23] Thesleff, S. “Functional aspects of quantal and non-quantal release of acetylcholine at the neuromuscular junction”. In Progress in Brain Research ,Vol. 84, pp. 93-99. (1990).

[24] B. Katz, R. Miledi, “Release of acetylcholine from a nerve terminal by electric pulses of variable strength and duration”, Nature 207 :1097–1098. (1965).

[25] Gulyas AI1, Miles R, Hajos N, Freund TF, “Precision and variability in postsynaptic target selection of inhibitory cells in the hippocampal CA3 region” Eur J Neurosci. 1;5(12):1729-51. (1993).

[26] Hartzell HC, Kuffler SW, Yoshikami, "The number of acetylcholine molecules in a quantum and the interaction between quanta at the subsynaptic membrane of the skeletal neuromuscular synapse". Cold Spring Harb Symp Quant Biol.;40:175-86.(1976).

[27] Aidoo, A. Y., & Ward, K. , "Spatio-temporal concentration of acetylcholine in vertebrate synaptic cleft". Mathematical and Computer Modelling, 44(9-10), 952-962. doi:10.1016/j.mcm.(2006).

[28] B.R. Land, E.E. Saltpeter, M.M. Saltpeter, “Acetylcholine receptor site density affects the rising phase of miniature endplate currents”, Proc. Natl. Acad. Sci. 77:3736–3740. (1980).

[29] D. Bruns, R. Jahn "Real-time measurement of transmitter release from single synaptic vesicle" Nature, 377. (1995).

[30] Raymond C. “Physical Chemistry for the Biosciences”. Sausalito, CA: University Science, pp. 363-371. (2005).

[31] Berg JM, Tymoczko JL, Stryer L, “Biochemistry”, 5th edition, Section 8.4 “The Michaelis-Menten Model Accounts for the Kinetic Properties of Many Enzymes”, New York: W H Freeman. (2002).

[32] Atkins, P.W & Julio de.P. “Physical Chemistry for the Life Sciences".NY: W. H. Freeman and Company, pp.309-313. (2006).

[33] Quinn, Daniel M., “Acetylcholinesterase: Enzyme Structure, Reaction Dynamics, and Virtual Transition States.” Chemical Reviews, vol. 87, no. 5, pp. 955–979., doi:10.1021/cr00081a005.(1987).

[34] J.L. Smart, J.A. McCammon, “Analysis of synaptic transmission in the neuromuscular junction using a continuum finite element model”, Biophys. J. 75 :1679–1688. (1998).

[35] Khaliq A., Jenkins F, DeCoster M, Dai W,“A new 3D mass diffusion–reaction model in the neuromuscular junction” J Comp. Neurosci. 30:729–745 doi 10.1007/s10827-010-0289-5. (2011).

[36] Liu D, Wang Y, DeCoster MA “ Spectral Element Simulation of Reaction-Diffusion System in the Neuromuscular Junction”. J Appl Computat Math 2: 136. doi:10.4172/2168-9679.1000136.(2013).

[37] Omar A; Marwaha K; C. Bollu.,"Physiology, Neuromuscular Junction" ,StatPearls Publishing; Retrieved from https://www.ncbi.nlm.nih.gov/books/NBK470413/ (2019).

[38] Jia J, Sogabe T, Li S “A generalized symbolic Thomas algorithm for the solution of opposite bordered tridiagonal linear systems" Elsevier Journal of Computational and Applied Mathematics, 423-432. (2015).